

AFIT/GA/ENY/92J-01

AD-A256 566

2



A MODAL ANALYSIS AND MODELLING
OF A LIGHTLY DAMPED LARGE
SPACE STRUCTURE

THESIS

Scott E. George
Captain, USAF

AFIT/GA/ENY/92J-01

Approved for public release; distribution unlimited.

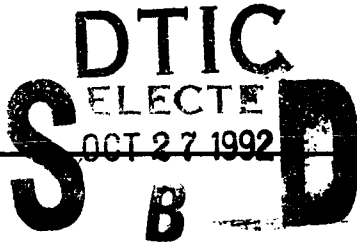
92-28243



REPORT DOCUMENTATION PAGE

Form Approved
OMB No 0704-0188

Public reporting burden for this collection of information is estimated to average 1 hour per response, including the time for reviewing instructions, searching existing data sources, gathering and maintaining the data needed, and completing and reviewing the collection of information. Send comments regarding this burden estimate or any other aspect of this collection of information, including suggestions for reducing this burden, to Washington Headquarters Services, Directorate for Information Operations and Reports, 1215 Jefferson Davis Highway, Suite 1204, Arlington, VA 22202-4302, and to the Office of Management and Budget, Paperwork Reduction Project (0704-0188), Washington, DC 20503.

1. AGENCY USE ONLY (Leave blank)		2. REPORT DATE June 1992	3. REPORT TYPE AND DATES COVERED Master's Thesis	
4. TITLE AND SUBTITLE A MODAL ANALYSIS AND MODELLING OF A LIGHTLY DAMPED LARGE SPACE STRUCTURE			5. FUNDING NUMBERS	
6. AUTHOR(S) Scott E. George, Captain, USAF				
7. PERFORMING ORGANIZATION NAME(S) AND ADDRESS(ES) Air Force Institute of Technology, WPAFB, OH 45433-6583			8. PERFORMING ORGANIZATION REPORT NUMBER AFIT/GA/ENY/92J-01	
9. SPONSORING / MONITORING AGENCY NAME(S) AND ADDRESS(ES) WL/FIBG Wright-Patterson AFB OH 45433			10. SPONSORING / MONITORING AGENCY REPORT NUMBER	
11. SUPPLEMENTARY NOTES				
12a. DISTRIBUTION / AVAILABILITY STATEMENT Approved for public release; distribution unlimited				
12b. DISTRIBUTION CODE				
13. ABSTRACT (Maximum 200 words) A large space structure (LSS) laboratory model exhibiting closely-spaced, low frequency vibration modes is modified to remove the passive damping treatment. An experimental modal analysis is performed on the resulting lightly damped structure using the frequency response function technique to characterize the flexible vibration modes below 20 Hz. The structure is modelled using MSC/NASTRAN finite element code and the results are compared to the experimental data. The model is reduced using Guyan reduction and modal reduction and the final 50 degree of freedom model is tuned to match measured data. The resulting reduced-order model is for use in active control research to be conducted at a later time.				
14. SUBJECT TERMS Large Space Structures, Modal Analysis Structural Vibrations, Finite Element Modelling			15. NUMBER OF PAGES 184	
			16. PRICE CODE	
17. SECURITY CLASSIFICATION OF REPORT Unclassified	18. SECURITY CLASSIFICATION OF THIS PAGE Unclassified	19. SECURITY CLASSIFICATION OF ABSTRACT Unclassified	20. LIMITATION OF ABSTRACT UL	

AFIT/GA/ENY/92J-01

A MODAL ANALYSIS AND MODELLING
OF A LIGHTLY DAMPED LARGE
SPACE STRUCTURE

THESIS

Presented to the Faculty of the School of Engineering
of the Air Force Institute of Technology
Air University
In Partial Fulfillment of the
Requirements for the Degree of
Master of Science in Astronautical Engineering

Scott E. George, B.S.
Captain, USAF

June 1992

Approved for public release; distribution unlimited.

Acknowledgements

In the performance of the work and the writing of this thesis, I have received a great deal of help from others. I deeply appreciate the assistance and patience I have received from my faculty advisors; Capt Howard Gans, Lt Col Ron Bagley, and Dr. Bradley Liebst. I would also like to extend a word of thanks to Mr. Jay Anderson of the AFIT labs and Mr. John Brohaus of the AFIT Fabrication Shop for their help in expediting the experimental part of this thesis.

A special thanks goes to my wife Velma, who made many sacrifices to support me during my completion of this work. By now, I must owe her a lifetime of returned favors.

Scott E. George

DTIC QUALITY INSPECTED

Accession For	
NTIS GRA&I	<input checked="" type="checkbox"/>
DTIC TAB	<input type="checkbox"/>
Unannounced	<input type="checkbox"/>
Justification	
By	
Distribution/	
Availability Codes	
Dist	Avail and/or Special
A-1	

Table of Contents

	Page
Acknowledgements.....	i
Table of Contents.....	ii
List of Figures.....	iv
List of Tables.....	v
Abstract.....	vi
I. INTRODUCTION.....	1
Background on the PACOSS program.....	2
Planned Research.....	4
II. THEORY.....	5
The Equation of Motion.....	5
The Transfer Function Matrix.....	9
Model Reduction.....	13
Guyan Reduction.....	14
Further Model Reduction.....	16
III. MODIFICATIONS TO THE DTA.....	20
Description of the DTA.....	20
The Ring Truss.....	22
The Box Truss.....	23
The Tripod.....	24
The Solar Arrays.....	25
IV. MODAL TESTING AND ANALYSIS.....	28
V. MODELLING AND MODEL REDUCTION.....	41
Real Eigenvalue Analysis.....	48

Frequency Response Analysis.....	51
The Second Model Reduction.....	53
Final Model Tuning.....	56
VI. CONCLUSIONS AND RECOMMENDATIONS.....	60
Bibliography.....	63
Appendix A. MEASUREMENT TABLES.....	65
Appendix B. GUYAN-REDUCED MODEL INFORMATION.....	88
Appendix C. MODEL REDUCTION UTILITIES.....	127
Appendix D. FINAL MODEL FREQUENCY RESPONSE FUNCTIONS...	142
Vita.....	178

List of Figures

Figure	Page
1. The Undamped Structure.....	21
2. Ring Truss Joint Block.....	23
3. Ring Truss Interface Block.....	24
4. Modified Tripod-Apex Interface.....	25
5. Solar Array Root with Modified Shear Strap.....	27
6. Measurement Points on the Modified Structure.....	29
7. Drive Point +97X, Showing Stinger and Force Gauge..	31
8. Modal Test 1 Drive Point FRF.....	33
9. Modal Test 2 Drive Point FRF.....	34
10. Modal Test 3 Drive Point FRF.....	35
11. Modal Test 4 Drive Point FRF.....	36
12. Modal Test 5 Drive Point FRF.....	37
13. Horizontal Measurement From Solar Array Blanket....	38
14. Mode Shape Plot From Curvefit Results.....	40
15. Finite Element Model of the Modified Structure.....	42
16. Solar Array Mast Showing QUAD4 Elements.....	44
17. Tripod Leg Interface Showing QUAD4 Elements.....	45
18. Solar Array Root Modelling.....	46
19. Solar Array Blanket Spreader QUAD4 Elements.....	48
20. Drive Point FRF Comparison - 182 DOF Model.....	53
21. Drive Point FRF Before Model Tuning.....	57
22. Drive Point FRF After Tuning (Magnitude).....	58
23. Drive Point FRF After Tuning (Phase).....	59

List of Tables

Table	Page
1. Modal Test Parameters.....	32
2. Real Eigenvalue Analysis.....	50
3. Distribution of DOFs in Final Model.....	56

Abstract

This study involves the modification to the PACOSS Dynamic Test Article to create a lightly damped representative large space structure with closely spaced, low frequency modes. An experimental modal analysis is performed to recharacterize the low frequency flexible vibration modes. A finite element model is created using MSC/NASTRAN to predict low frequency behavior using both real eigenvalue analysis and frequency response analysis. Then a reduced order model is created and fine-tuned to represent the dynamics of the structure for the identified low frequency modes.

A MODAL ANALYSIS AND MODELLING
OF A LIGHTLY DAMPED
LARGE SPACE STRUCTURE

I. INTRODUCTION

Space systems envisioned for the future for both military and civilian applications will be both large and lightweight. These characteristics lead to low frequency, closely-spaced flexible vibration modes (Morgenthaler, 1990). In addition, mission requirements for these systems may require precise pointing capability and rapid repositioning. Rapid repositioning requirements may cause the attitude control system to overlap the low frequency resonances of the structure, inducing substantial structural vibrations. If these vibrations are not attenuated rapidly, the performance of the system will be limited. Both active and passive measures can be implemented to attenuate the response of low frequency modes and to reduce settling time.

This thesis involves modification to a laboratory scale model of a large space structure to remove all passive damping measures. A recharacterization of the flexible modes is performed through modal testing with comparison to finite element modelling results. Finally, a reduced order model will be produced and fine tuned to adequately represent the

lightly damped structure.

This thesis research was necessary to set up further, planned research on this structure. Planned research at AFIT includes design of an entirely active control system for the lightly damped structure and the study of alternative passive damping methods. Therefore, one goal of this thesis was to modify the existing structure to create a lightly damped, realistic large space structure while retaining the attributes of low frequency, densely spaced flexible vibration modes. The other major goal of the thesis is to deliver an experimentally verified reduced order model that represents the structure's response to low frequency excitation.

Background of the PACOSS Program

In 1982 the Flight Dynamics Branch of Wright Laboratory issued a contract to Martin Marietta Astronautics Group to examine damping methods for an envisioned future space system and design a combined active and passive control system that could be applied efficiently to a realistic structure.

Under the Passive and Active Control of Space Structures (PACOSS) program, anticipated future space system missions were studied. A representative system article (RSA) model was designed to study the application of various damping techniques. The RSA was designed to contain substructures directly traceable to many of the future missions that were

researched (Gehling, 1985). The analytical studies of the RSA provided goals and guidance for passive damping design levels and strategies (Morgenthaler, 1990).

The RSA consisted of seven substructures; a ring truss, a box truss, a tripod, an equipment platform, an antenna, and two solar arrays. The ring truss was the main structural component of the RSA, serving as the central mounting point for other subassemblies. The box truss was designed to represent a support structure for a large reflector surface. The tripod represented the supporting structure of a secondary reflector of a Cassegrain system envisioned for use in space-based laser or radar systems. The antenna is a dish type communications antenna sized to be consistent with the overall RSA system. The equipment platform was designed to represent typical long, narrow truss structures. The solar arrays were designed to resemble the arrays used in the Solar Array Flight Experiment (SAFE) and were sized to provide power consistent with the rest of the RSA subsystem requirements (Morgenthaler, 1990).

The dynamic test article (DTA) was designed and constructed to have modal characteristics similar to the RSA (Morgenthaler, 1988). The DTA contained the same type of subassemblies as the RSA but was built to laboratory scale. The DTA served as an experimental platform to validate the passive and active damping techniques and demonstrate their

applicability to deployable systems (Morgenthaler, 1990).

The purpose of the PACOSS program was to demonstrate that passive and active measures could be combined to adequately damp low frequency, closely spaced modes. In addition, the Martin Marietta team concluded that predictable levels of passive damping could be designed and modelled (Gehling, 1990). The researchers also concluded that better methods of modal identification were required for structures with dense resonant modes and high damping.

Planned Research

At the termination of the PACOSS contract, the DTA (without the box truss), the active control system, and an MSC/NASTRAN finite element model were delivered to the Air Force Institute of Technology (AFIT) laboratories for further research. AFIT will begin research efforts with attempting to control the flexible vibrations below 12 Hz using exclusively active means. The structure will also be used to demonstrate alternative passive and passive/active damping strategies.

II. THEORY

Modal analysis is the process of obtaining a mathematical representation of the flexible dynamic properties of a structure (Ewins, 1985). During a modal test a structure is "discretized" by measuring its dynamic properties at a finite number of locations (Structural Measurement Systems, 1990). This enables the use of matrix methods to construct the equations of motion for the structure. A mathematical model of the structure can be created using finite element methods and analytical predictions of dynamic response can be compared to measured responses. The mass and stiffness properties in the model can be modified until a good representation of measured dynamic behavior is generated.

The Equation of Motion

The dynamic motion of the discrete degrees of freedom of the structure is described by the following matrix differential equation (Meirovich, 1986):

$$[M] \{\ddot{x}(t)\} + [C] \{\dot{x}(t)\} + [K] \{x(t)\} = \{F(t)\} \quad (1)$$

where

[M] is the mass matrix (N x N)

[C] is the damping matrix (N x N)

[K] is the stiffness matrix (N x N)

{x} is the displacement vector (N x 1)

$\{\dot{x}\}$ is the velocity vector ($N \times 1$)
 $\{\ddot{x}\}$ is the acceleration vector ($N \times 1$)
 $\{F\}$ is the vector of external forces ($N \times 1$)
 N is the number of degrees of freedom

This equation assumes that the damping is viscous in nature. This is not always the case and other damping models exist, but in this thesis the damping in the structure is small and the distinction is not significant.

To determine the response of the structure to periodic loading, we begin by noting that a periodic function may be represented by a Fourier series of sinusoids (Ewins, 1985). The response to periodic, dynamic loading can be determined by representing the external load as a summation of sinusoids. Therefore, we can determine the response to a single sinusoidal excitation with the understanding that the analysis applies for any periodic loading. Equation (2) defines the vector of external forces as sinusoidal with a frequency, ω (in radians per second).

$$\{F(t)\} = \{F\} e^{i\omega t} \quad (2)$$

Then the resulting motion can be assumed to be steady-state and sinusoidal and the equation of motion can be written

$$-\omega^2 [M] \{x\} + i\omega [C] \{x\} + [K] \{x\} = \{F\} \quad (3)$$

where $\{F\}$ is an $N \times 1$ vector containing the amplitudes of the external forces. If the applied forces, frequency of excitation, and mass, damping, and stiffness characteristics are known, the displacements of the structure's degrees of freedom can be determined.

A popular method of solving the equation of motion involves finding the unforced response of the structure (where $\{F\}=\{0\}$). If a coordinate transformation can be found that decouples the equations of motion, then the forced response can be determined by applying the same coordinate transformation to the forced problem. The unforced, or homogeneous, solution to the equation of motion can be found numerically from the complex eigenvalue problem,

$$-(\omega_n^k)^2 [M] \{\phi_k\} + (i\omega_n^k) [C] \{\phi_k\} + [K] \{\phi_k\} = \{0\} \quad (4)$$

where $\{\phi_k\}$ is the k th mode shape (or eigenvector) and ω_n^k is the corresponding k th natural frequency (or eigenvalue). If N degrees of freedom are represented in the structure and the eigenvalues are distinct, then there will be N linearly independent mode shapes.

If the structure exhibits proportional damping (that is, if the damping matrix can be written as a linear combination of the mass and stiffness matrices) the following orthogonality conditions hold (Cook, 1989).

$$\begin{aligned}
[\Phi]^T [M] [\Phi] &= [m] \\
[\Phi]^T [C] [\Phi] &= [c] \\
[\Phi]^T [K] [\Phi] &= [k]
\end{aligned}
\tag{5}$$

$[\Phi]$ is the $N \times N$ modal matrix. It has columns which are the N mode shape vectors, $\{\phi_k\}$. $[m]$, $[c]$, and $[k]$ are the modal mass, damping, and stiffness matrices and they are diagonal. It can be shown (Meirovitch, 1986) that if the columns of $[\Phi]$ are each solutions to the eigenvalue problem of equation (4), then the orthogonality conditions will be true. The system of equations (3) can be decoupled by using the following coordinate transformation:

$$\{x(t)\} = [\Phi] \{\eta(t)\} \tag{6}$$

where $\{\eta\}$ is a generalized displacement vector represented in modal coordinates. Substituting equation 6 into equation 3,

$$-\omega^2 [M] [\Phi] \{\eta\} + i\omega [C] [\Phi] \{\eta\} + [K] [\Phi] \{\eta\} = \{F\} \tag{7}$$

Premultiplying equation 7 by $[\Phi]^T$ and using the orthogonality relations of equation 5 yields

$$-\omega^2 [m] \{\eta\} + i\omega [c] \{\eta\} + [k] \{\eta\} = [\Phi]^T \{F\} \tag{8}$$

Since $[m]$, $[c]$, and $[k]$ are all diagonal, the equations are decoupled and can be solved separately. It should be noted that the orthogonality conditions in equation (5) apply only if the structure exhibits proportional damping. Although

proportional damping cannot be assumed in this thesis, it will be assumed that the lightly damped nature of the structure will allow damping forces to be neglected in comparison to inertial forces and restoring forces. Under this assumption, the eigenvalue problem becomes

$$(-\omega_k)^2 [M] \{\phi_k\} + [K] \{\phi_k\} = \{0\} \quad (9)$$

The Transfer Function Matrix

The development in this section follows somewhat the development in reference 2 (Ewins, 1985).

The equation of motion, equation (3), can be written using the Laplace Transform in the following form (with zero initial conditions)

$$[B(s)] \{X(s)\} = \{F(s)\} \quad (10)$$

where

$$[B(s)] = s^2 [M] + s [C] + [K] \quad (11)$$

and s is the Laplace variable. $[B(s)]$ is known as the system matrix.

The homogenous problem can be written as

$$[B(s)] \{X(s)\} = \{0\} \quad (12)$$

Equation 12 is the eigenvalue problem in terms of the

Laplace variable. This equation is equivalent to equation (4). The eigenvalues are the complex values of the Laplace variable where the determinant of $[B(s)]=0$. The k th eigenvalue is written

$$p_k = \sigma_k + i\omega_k \quad (13)$$

for $k=1,2,\dots,N$. σ_k is the damping rate (or decay) and ω_k is the modal frequency of the k th mode. The corresponding k th eigenvector is $\{\phi_k\}$.

In Laplace form, the forced response of the structure is written (again, for zero initial conditions)

$$\{X(s)\} = [H(s)]\{F(s)\} \quad (14)$$

where

$$[H(s)] = [B(s)]^{-1} \quad (15)$$

$[H(s)]$ is called the transfer matrix or receptance matrix and its elements are transfer functions between the respective degrees of freedom (Ewins, 1985). Because $[B(s)]$ is made up of elements which are quadratic in s , $[H(s)]$ will have elements which are the ratio of two polynomials in s . Because $[H(s)]$ is the inverse of $[B(s)]$, the determinant of $[B(s)]$ will be the denominator of every element of $[H(s)]$. Since the model has N degrees of freedom, the determinant of $[B(s)]$, or

the characteristic polynomial, will be of order $2N$. If the structure is a resonant system, that is, if there are no eigenvalues lying on the real axis, then the roots (eigenvalues) are complex and there will be N pairs of complex conjugate eigenvalues.

If there are no repeated roots, $[H(s)]$ can be written in partial fraction form as follows:

$$[H(s)] = \sum_{k=1}^N \left[\frac{[r_k]}{s-p_k} + \frac{[r_k^*]}{s-p_k^*} \right] \quad (16)$$

where p_k^* denotes the complex conjugate of the k th eigenvalue and

$$[r_k] = \begin{bmatrix} r_{11}^k & r_{12}^k & \dots & r_{1N}^k \\ r_{21}^k & \ddots & & \vdots \\ \vdots & & \ddots & \vdots \\ r_{N1}^k & \dots & \dots & r_{NN}^k \end{bmatrix} \quad (17)$$

$[r_k]$ is called the matrix of residues for the k th eigenvalue.

Equation (17) represents the transfer function in partial fraction form. It can now be written completely in terms of modal parameters. Recalling that the k th eigenvector, $\{\phi_k\}$, is a solution to the homogeneous equation corresponding to the k th eigenvalue, the k th residue matrix can be written

$$[r_k] = \{\phi_k\}\{\phi_k\}^T \quad (18)$$

Therefore, the transfer function matrix can be written in modal parametric form as follows:

$$[H(s)] = \sum_{k=1}^N \left[\frac{\{\phi_k\}\{\phi_k\}^T}{s-p_k} + \frac{\{\phi_k^*\}\{\phi_k^*\}^T}{s-p_k^*} \right] \quad (19)$$

Note that the kth eigenvalue and the kth eigenvector appear in every column of $[H(s)]$. Therefore, once all N eigenvalues and eigenvectors are known, all N^2 elements of $[H(s)]$ can be generated. So, to build an N degree of freedom model, only N transfer functions are required. In practice, only positive frequencies are used, so the measured functions are called frequency response functions (FRFs) and the transfer function matrix is written

$$[H(\omega)] = \sum_{k=1}^N \left[\frac{\{\phi_k\}\{\phi_k\}^T}{i\omega-p_k} + \frac{\{\phi_k^*\}\{\phi_k^*\}^T}{i\omega-p_k^*} \right] \quad (20)$$

In modal analysis, the elements of $[H(\omega)]$ are measured, and the modal parameters are estimated by curvefitting the FRFs in the region of resonant frequencies. In this thesis, Rational Fraction Least Squares (RFLS) polynomial curvefitting was used. The RFLS method uses linear combinations of complex polynomials to estimate each frequency response function

(Richardson and Formenti, 1982).

Model Reduction

To produce a model of the structure's dynamic properties up to 15 Hz that will be appropriate for use in active control, it is necessary to reduced the number of degrees in the finite element model to a size more appropriate for a state space control algorithm. The number of degrees of freedom represented in the finite element model is on the order of 10,000. Since the modal test measures responses at only 143 degrees of freedom, it is desirable to reduced the model to these degrees of freedom plus the degrees of freedom represented by the active control actuators and feedback accelerometers. This will allow direct comparison of model results with modal test results. It will also be necessary to produce a model using about 50 degrees of freedom for use in planned research in active control of the structure.

Model reduction can be accomplished using a variety of methods. Freed and Flanigan discuss and compare results of four common methods (Freed, 1991). Since Guyan reduction is readily available in finite element programs and is generally more stable than other methods (Freed, 1991), it will be reviewed here.

Guyan Reduction

The basic assumption underlying Guyan reduction is that the inertial properties at each degree of freedom have a lesser impact on the dynamic response of the structure than do the elastic restoring forces. If the most significant mass properties are retained in a smaller subset of degrees of freedom, the remaining degrees of freedom can be neglected in the analysis without an adverse impact on accuracy.

The following development explains Guyan reduction as it is implemented in MSC/NASTRAN (MacNeal, 1972).

The displacement vector of unconstrained points can be partitioned as follows:

$$\{x_f\} = \begin{Bmatrix} x_a \\ x_o \end{Bmatrix} \quad (21)$$

where the "a" subscript denotes the degrees of freedom to be retained for analysis, the "o" subscript refers to omitted degrees of freedom and "f" denotes the unconstrained (or free) degrees of freedom.

Using the partitioned displacement vector the static equation of motion can be written

$$\begin{bmatrix} \overline{K_{aa}} & K_{ao} \\ K_{ao}^T & K_{oo} \end{bmatrix} \begin{Bmatrix} x_a \\ x_o \end{Bmatrix} = \begin{Bmatrix} F_a \\ F_o \end{Bmatrix} \quad (22)$$

Equation 22 can be solved for the displacement at the omitted degrees of freedom assuming there are no external forces acting on the omitted degrees of freedom.

$$\{x_o\} = [G_o] \{x_a\} \quad (23)$$

where

$$[G_o] = -[K_{oo}]^{-1} [K_{ao}]^T \quad (24)$$

The top partition of equation 22 can be written

$$[\overline{K}_{aa}] \{x_a\} + [K_{ao}] \{x_o\} = \{F_a\} \quad (25)$$

Substituting for $\{x_o\}$ in equation 25 yields a new static equation of motion,

$$[\overline{K}_{aa} + K_{ao} G_o] \{x_a\} = \{F_a\} \quad (26)$$

This equation can be rewritten in the following simpler form

$$[K_{aa}] \{x_a\} = \{F_a\} \quad (27)$$

where the following definition has been used

$$[K_{aa}] = [\overline{K}_{aa} + K_{ao} G_o] \quad (28)$$

The mass matrix is reduced by considering the inertial properties of the omitted degrees of freedom to be constrained to the retained degrees of freedom by the matrix $[G_o]$ as indicated by equation 23. The NASTRAN Theoretical Manual shows that structural matrices subject to multipoint constraints can be written in partitioned form and reduced to the independent degrees of freedom (Macneal, 1972) - in this case the retained degrees of freedom. The reduced mass matrix is shown to be given by

$$[M_{aa}] = [\overline{M}_{aa} + M_{ao}G_o + G_o^T M_{ao}^T + G_o^T M_{oo} G_o] \quad (29)$$

Using the mass and stiffness matrices from the Guyan reduction process (equations 28 and 29) in the generalized eigenvalue problem (equations 3), the problem is reduced to

$$-\omega^2 [M_{aa}] \{\phi_a\} + [K_{aa}] \{\phi_a\} = \{0\} \quad (30)$$

If a full order damping matrix is used in the model, it can be reduced using an analogous form of equation (29).

Further Model Reduction

The reduced model from the Guyan reduction process is adequate for efficient extraction of the system's eigenvalues and eigenvectors and for comparison to experimental results,

but the model must be reduced further to be directly manipulated to match experimentally determined dynamic properties. Also, a smaller model is desirable for use in an active control system.

The mass and stiffness matrices from the Guyan reduction can be used to form a reduced equation of motion,

$$[M_{aa}]\{\ddot{x}_a(t)\} + [K_{aa}]\{x_a(t)\} = \{F_a(t)\} \quad (31)$$

This equation of motion can be reduced further by retaining the first r eigenvectors (spanning the 20 Hz desired bandwidth) corresponding to the first r eigenvalues and using them in the following transformation

$$\{x_a\} = [\Phi_1]\{\eta_m\} \quad (32)$$

where $[\Phi_1]$ is an $a \times r$ modal transformation matrix.

Using this transformation in equation 31 yields

$$-\omega^2 [M_{aa}] [\Phi_1]\{\eta_r\} + [K_{aa}] [\Phi_1]\{\eta_r\} = \{F_a\} \quad (33)$$

Again, using the orthogonality relationships from the eigenvalue problem and premultiplying by $[\Phi_1]^T$ yields

$$-\omega^2 [m_{rr}]\{\eta_r\} + [k_{rr}]\{\eta_r\} = [\Phi_1]^T \{F_a\} \quad (34)$$

where $[m_{rr}]$ and $[k_{rr}]$ are r by r diagonal matrices. Equation

34 is a reduced system of r decoupled equations and can be easily solved.

The associated orthogonality conditions for this reduced system are

$$\begin{aligned} [\Phi_1]^T [M_{aa}] [\Phi_1] &= [m_{mm}] \\ [\Phi_1]^T [K_{aa}] [\Phi_1] &= [k_{mm}] \end{aligned} \quad (35)$$

Equation 34 represents a reduced r order equation but it is in modal coordinates. What is needed is a model that can be used in physical coordinates. This can be obtained by partitioning the modal matrix $[\Phi_1]$ into r retained degrees of freedom and $a-r$ deleted degrees of freedom as follows:

$$[\Phi_1] = \begin{bmatrix} \Phi_r \\ \Phi_d \end{bmatrix} \quad (36)$$

where $[\Phi_r]$ is an $r \times r$ modal matrix whose columns are the eigenvector components of retained degrees of freedom and $[\Phi_d]$ is an $(a-r) \times r$ matrix of the deleted eigenvector degrees of freedom.

$[\Phi_r]$ represents a matrix of eigenvectors represented in a desired set of physical degrees of freedom. This matrix can be used to find the r order mass and stiffness matrices corresponding to an r order equation of motion in physical coordinates.

Starting with the orthogonality conditions for an r order problem,

$$\begin{aligned} [\Phi_r]^T [M_{rr}] [\Phi_r] &= [m_{rr}] \\ [\Phi_r]^T [K_{rr}] [\Phi_r] &= [k_{rr}] \end{aligned} \quad (37)$$

Since $[m_{rr}]$, $[k_{rr}]$ and $[\Phi_r]$ are known from equation 34 and equation 36, equation 37 can be solved for the fully populated mass and stiffness matrices for the reduced model, yielding

$$\begin{aligned} [M_{rr}] &= [[\Phi_r]^T]^{-1} [m_{rr}] [\Phi_r]^{-1} \\ [K_{rr}] &= [[\Phi_r]^T]^{-1} [k_{rr}] [\Phi_r]^{-1} \end{aligned} \quad (38)$$

Equation 38 gives the desired matrices for the reduced model provided that $[\Phi_r]$ is invertible. As long as the retained degrees of freedom are chosen such that similar mode shapes can still be distinguished from one another, then $[\Phi_r]$ will be nonsingular and invertible.

III. MODIFICATIONS TO THE STRUCTURE

At the termination of the PACOSS program, the passively and actively damped DTA and active control system were delivered to the AFIT laboratories for further study. This thesis involves modification to the DTA to remove the passive damping from the structure and then a recharacterization of the flexible modes through modal testing. This section discusses the modifications made to the delivered structure.

Description of the DTA

The DTA, as delivered to AFIT, consisted of six major subassemblies; a ring truss, two solar arrays, a tripod, an antenna and an equipment platform. The passive damping design called for constrained layer viscoelastic damping treatments to be used on the surfaces of the solar array masts, the tripod legs, the antenna, and the equipment pod. The original design of the DTA, including drawings, is discussed in detail in the drawing package for the PACOSS contract (Morgenthaler, 1988). The damping design strategy is discussed in the PACOSS Final Report Volume 1 (Morgenthaler, 1990). The present research required reconstruction of the DTA as closely as possible, but without passive damping, while retaining its characteristics of closely spaced, low frequency modes. The modified DTA is shown in figure 1. The following sections



Figure 1. The Modified PACOSS Structure

give a brief description of each subassembly in the delivered condition and as modified for this research.

The Ring Truss

The ring truss is a circular truss constructed of 6061-T6 aluminum tubing bonded between solid aluminum joint blocks. The ring truss functions as the primary substructure in the system and was designed mainly to support gravitational loading of the entire DTA assembly and to represent the support for a primary mirror in a Cassegrain optical system (Morgenthaler, 1988). The ring truss contains the mounting points of the other substructures. No passive damping was designed into the ring truss and therefore no modification was necessary.

The main structural members are constructed of 3/4" O.D. x 0.083" wall tubing and additional support is obtained from 5/16" O.D. x 0.035" wall diagonal members. Figure 2 shows a typical joint block with diagonal and main members.

The six interfaces between sections of the ring truss are constructed of 1/4" aluminum plates. These interface plates have mounts for attachment to the tripod, mass simulators, and suspension cables. Figure 3 shows a typical interface plate. The solar arrays are attached to aluminum plates fixed to the outer diameter of the ring truss.

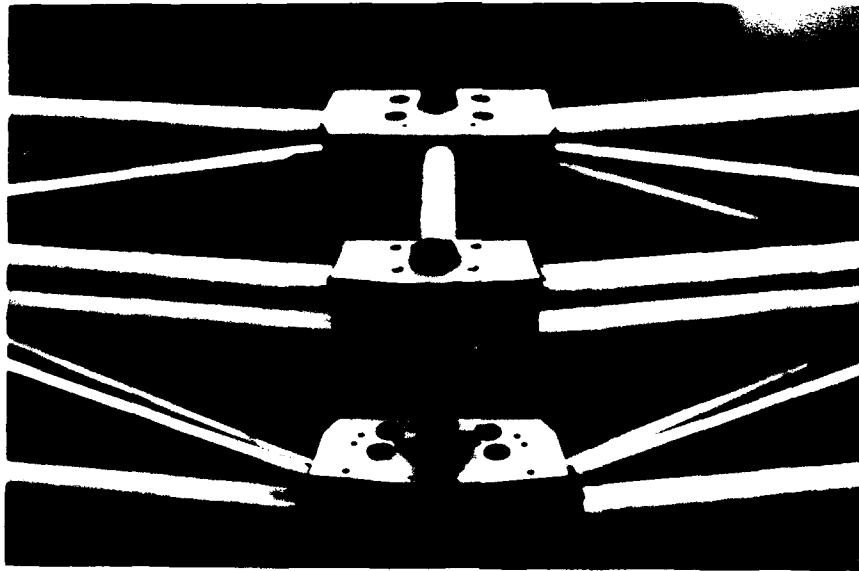


Figure 2. Ring Truss Joint Block

The Box Truss

The original DTA built at Martin Marietta included a box truss attached beneath the ring truss. The box truss was constructed of thin-walled aluminum tubing and tightly-bonded joint blocks in a similar manner to the ring truss. Passive dampind was designed into the box truss using extensional viscoelastic shear dampers. Passive modal damping in the box truss was reported to be greater than 5% (Gehling, 1990).

The box truss was not delivered to the AFIT laboratory. It was replaced by attaching three undamped mass simulators to the ring truss to represent the mass properties of the box truss.

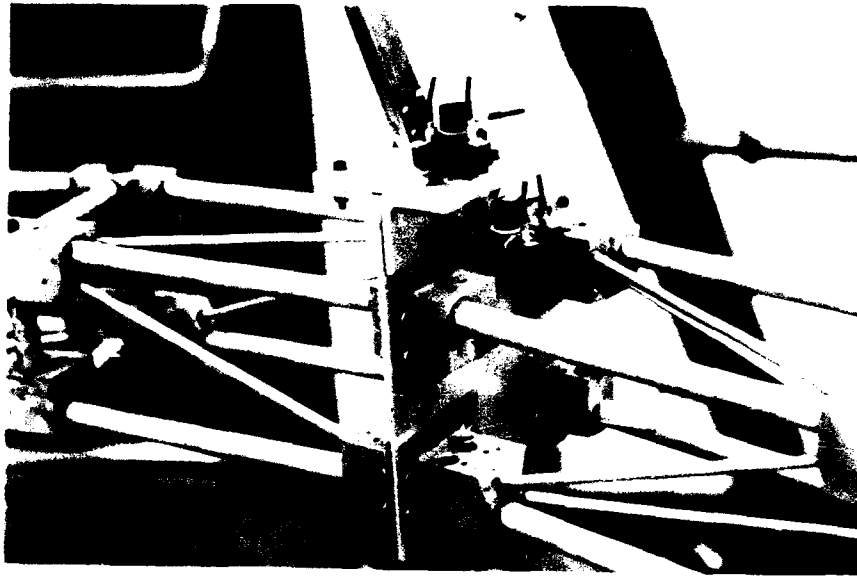


Figure 3. Ring Truss Interface Plate

The Tripod

The original tripod subassembly was designed for a fundamental frequency of less than 5.0 Hz and approximately 5% passive modal damping for modes with significant tripod participation (Morgenthaler, 1988). The tripod consists of three legs of 1" x 1/2" x 0.065" wall aluminum tubing topped by a 50 lb steel plate representing the secondary mirror of an optical system.

Passive damping was achieved by applying a constrained layer of acrylic core foam tape to the surfaces of the tripod legs and by placing rotational shear dampers in the interface between the tripod legs and the secondary plate.

The undamped tripod was constructed to the original

drawings without the constrained layer treatment. The rotational damper was redesigned as a rigid interface to the secondary plate. Figure 4 shows the modified tripod leg to secondary plate interface. This interface is stiffer than the original interface, but this effect is small compared to the high mass of the secondary plate.



Figure 4. Modified Tripod-Apex Interface

Solar Arrays

The solar arrays were designed to exhibit the typical low frequency behavior displayed by actual solar arrays and were built to dimensions necessary to produce power for the representative system (Morgenthaler, 1988). The solar arrays were delivered to AFIT with considerable passive damping.

Each solar array consists of a solar blanket constructed of 1/4" x 1/8" aluminum strips connected to a 1" x 1" x 0.095" aluminum mast via 1/4" plates. Passive damping in the original solar arrays was provided by constrained layer treatment on the mast surface, a viscoelastic shear strap between the solar array and supporting hardware, and the attachment of tuned mass damping devices to the solar blankets themselves.

The undamped arrays were rebuilt to the dimensions of the original drawings. The tuned mass dampers and their associated attachment hardware and the constrained layer treatment were not included. The viscoelastic shear straps were replaced by aluminum blocks of the same dimensions. These blocks provide a somewhat stiffer support than the viscoelastic shear straps, but they allow the solar array mounting hardware to be built to the original drawing requirements and the resulting impact to the dynamics of the solar arrays should be small. The new shear straps are shown in figure 5.

The omission of the tuned mass dampers from the solar blankets will have a tendency to increase the fundamental modes of the solar arrays. Other factors such as the preloading in the blankets during assembly, and the amount the arrays will sag under gravity may cause unknown differences from the original solar array.

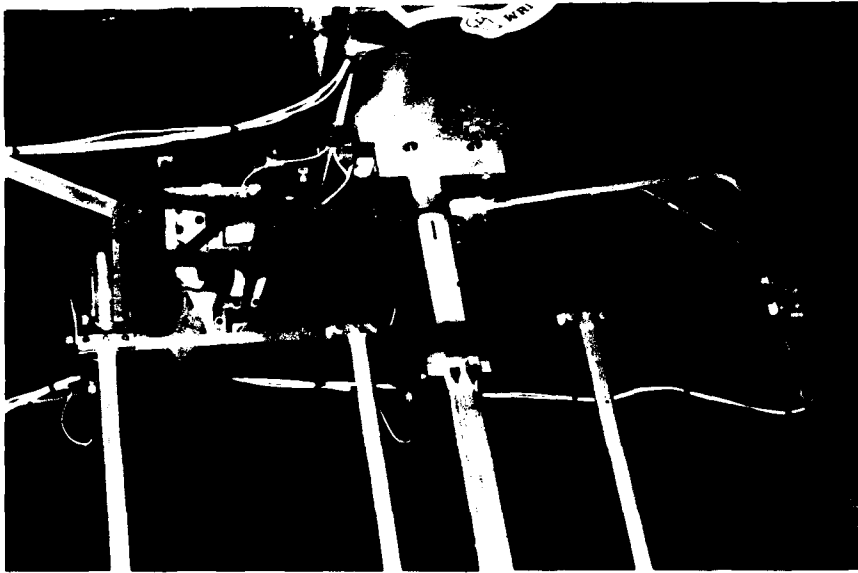


Figure 5. Solar Array Root with Modified Shear Strap

IV. MODAL TESTING AND ANALYSIS

After the structure was modified to eliminate the passive damping material, a redetermination of the low frequency vibration characteristics was necessary. To accomplish this, acceleration frequency response functions (FRFs) were generated by measuring accelerations at various points on the structure due to random sinusoidal force inputs. Using the measured FRFs, it is possible to determine the undamped structure's natural frequencies and mode shapes experimentally and generate a structural model based upon the results.

The structure was instrumented with Kistler model 8632A5 piezoelectric accelerometers using the same measurement points originally used by the Martin Marietta team, with the exception of those points on substructures that were removed from the structure. The undamped structure was instrumented at 143 degrees of freedom. The measurement numbers used by Martin Marietta were retained for this research. Therefore gaps exist in the numbering system where the equipment pod, antenna, and box truss measurements were taken. Included in Appendix A is a table showing the location of each measurement number, measurement point and direction, and corresponding MSC/NASTRAN grid number and direction. Also included in Appendix A is a table listing the serial numbers of the accelerometers used for each measurement. Figure 6

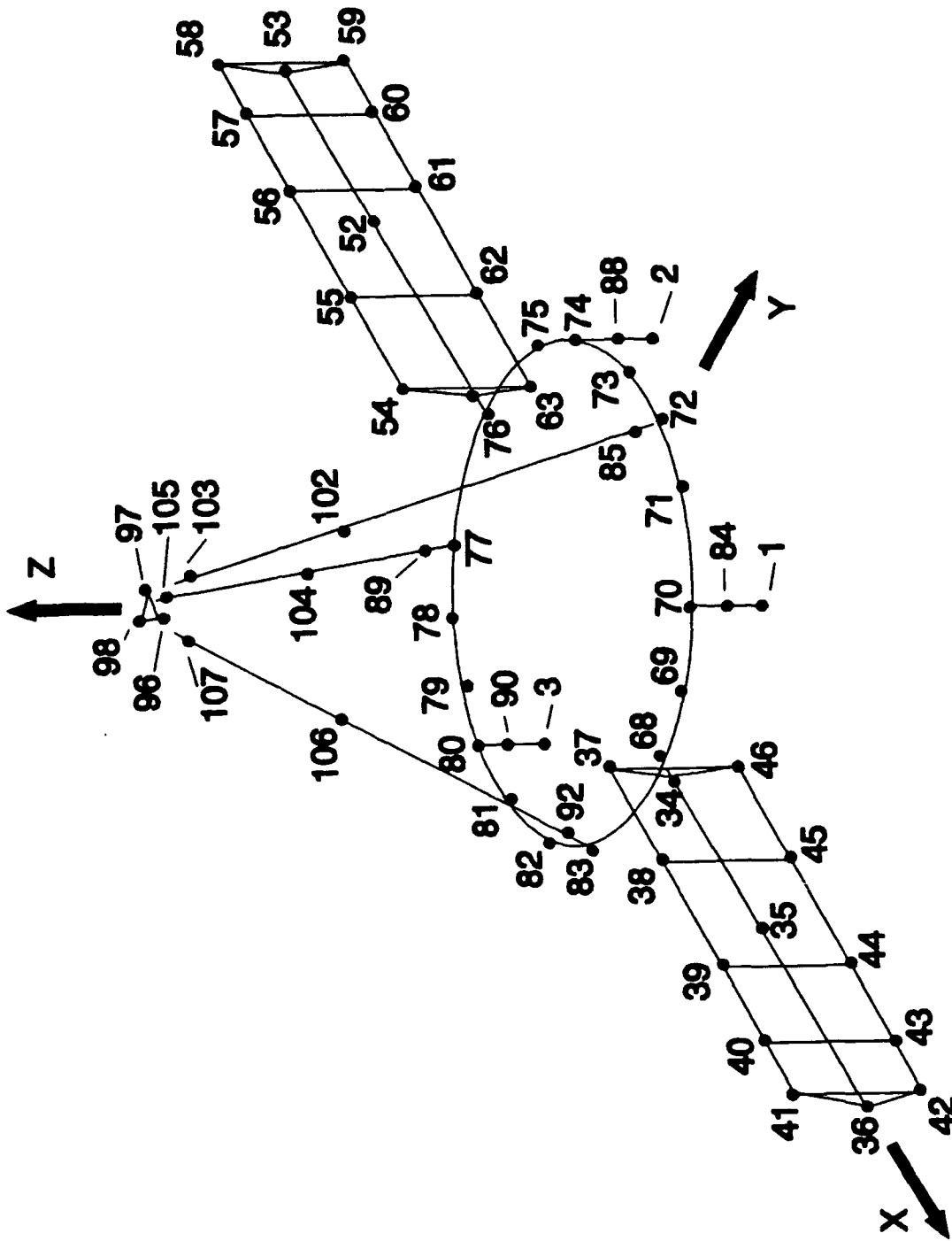


Figure 6. Measurement Points on the Modified Structure

below shows graphically the physical location of the measurement points on the structure. Not included are the measurement points on the suspension and ground. The suspension measurements are Z direction measurements located on the cable attachments to the suspension mechanisms. The ground measurements are located on the cases of the suspension devices and are used only to check for any vibrations transmitting through to the supporting structure. Detailed figures showing views of the installed positions of installed accelerometers after modification are included in Appendix A.

The structure is supported at three points by cable attachment to a CSA Engineering Zero Spring Rate Mechanism (ZSRM) support. The ZSRMs support the weight of the structure by supplying air pressure beneath pistons attached to the supporting cables. The pistons float on air bearings resulting in an extremely low stiffness support and very good isolation from the environment of the supporting structure. The finite element model indicates that the six rigid body suspension modes of the structure are all below 0.6 Hz which is well below the first flexible mode of the structure (predicted at 1.63 Hz).

Excitation of the structure was accomplished using an APS 40 lb shaker. The shaker was attached to the structure using a double-swivel stinger to eliminate coupling between the structure and the shaker suspension. The research conducted

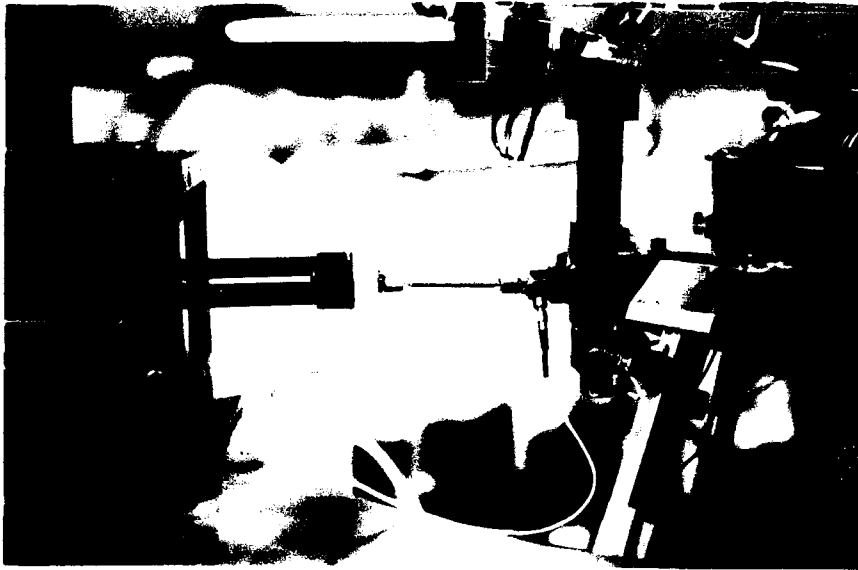


Figure 7. Drive Point +97X, Showing Stinger and Force Gauge

by Martin Marietta indicated that double-swivel type stingers provided the most flat power spectral density for frequencies up to 50 Hz and force levels up to 1 lb RMS (Gehling, 1990). The light weight of the structure's subassemblies required that the shakers be fixed to ground. The shakers were driven by a random input signal with a flat power spectrum over a frequency bandwidth of interest. The force was measured by a Kistler model 9712A5 force transducer. Three drive points were used to generate frequency responses. The +97X point on the secondary plate generally produced the highest quality data. Figure 7 shows the shaker attached to the +97X drive point. The +42Y and +42Z drive points on the tips of solar array 1 were used in an attempt to obtain good quality data on the behavior of the modes dominated by solar array motion.

A total of 5 sets of measurements were taken during the modal tests. Each set used a single random input and FRFs were collected three at a time using a four channel Tektronix Model 2642 Fourier Analyzer. Hanning windowing was used to eliminate leakage. Built-in filters were used to eliminate aliasing effects. Data acquisition frames were overlapped 50% to reduced the time required to collect FRFs. 30 to 40 averages were taken per FRF to ensure high quality data. The following table lists the parameters of the modal tests.

Table 1
Modal Test Parameters

<u>Test No.</u>	<u>Drive Pt.</u>	<u>Excitation Level (Lb RMS)</u>	<u>Frequency Band (Hz)</u>	<u>Resolution (Hz)</u>
1	+97X	0.25	0.0-20.0	0.025
2	+97X	0.25	0.0-20.0	0.0125
3	+42Y	0.125	0.0-20.0	0.0125
4	+42Z	0.125	0.0-20.0	0.0125
5	+42Y	0.125	0.0- 5.0	0.0125

The Martin Marietta team found that spectral resolution of at most 0.03125 Hz was necessary to extract modal parameters for the passively damped structure (Gehling, 1990). Therefore, spectral resolution was kept at about the same level or below during these modal tests. Force levels were kept low to avoid overloading the accelerometers. Typical force levels are listed in Table 1. Even with low force levels, responses were above the noise floor of the accelerometers at points with

high response.

Data quality was generally very good for the first, second, and third modal tests. Figures 8 through 12 show drive point FRFs for each of the five tests.

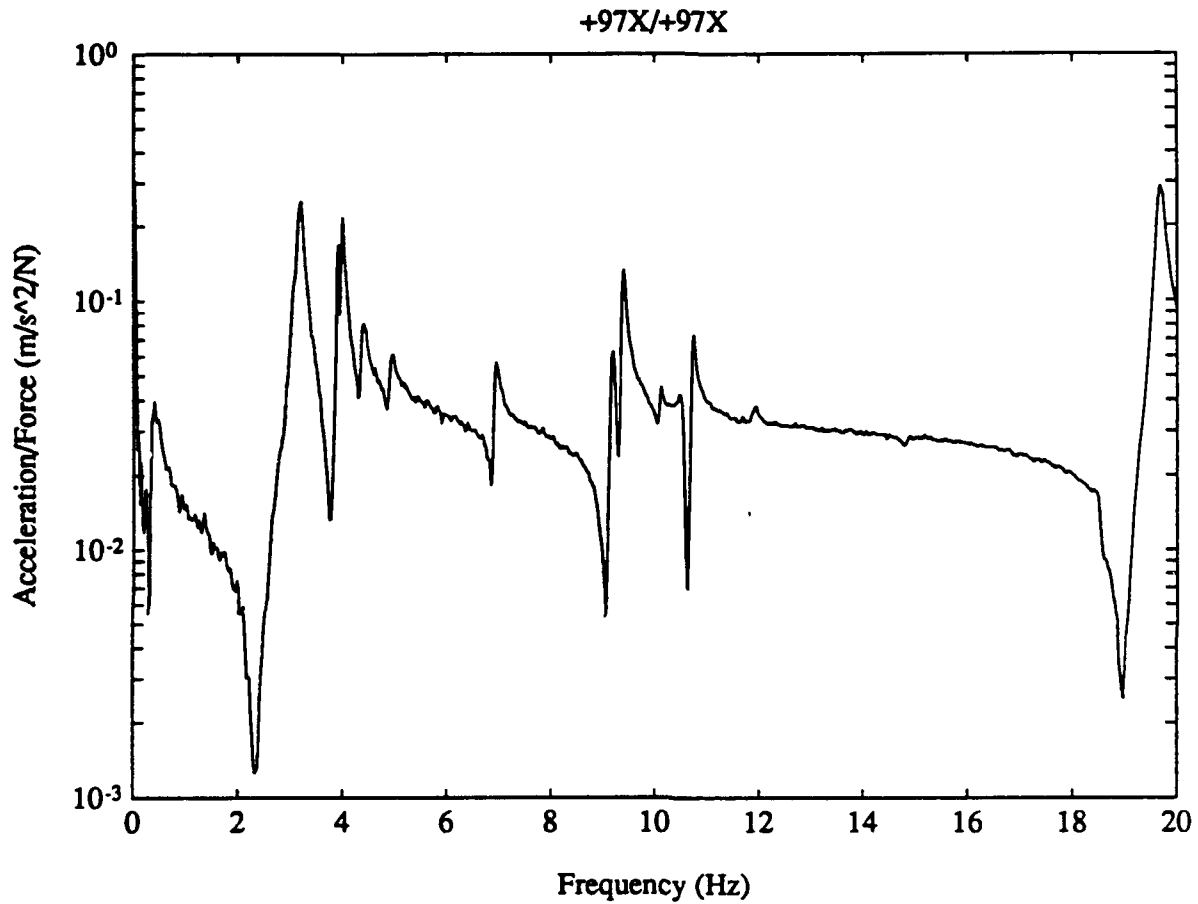


Figure 8. Modal Test 1 Drive Point FRF

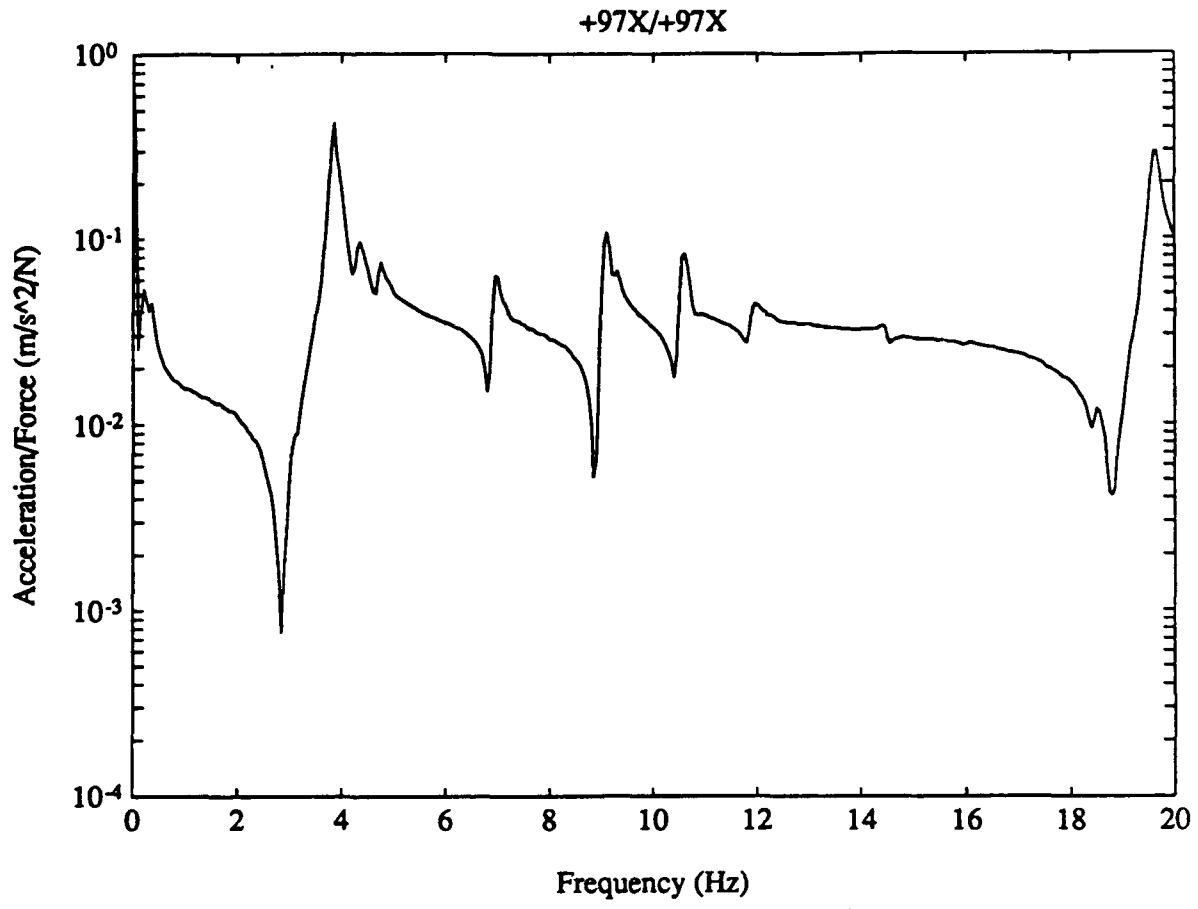


Figure 9. Modal Test 2 Drive Point FRF

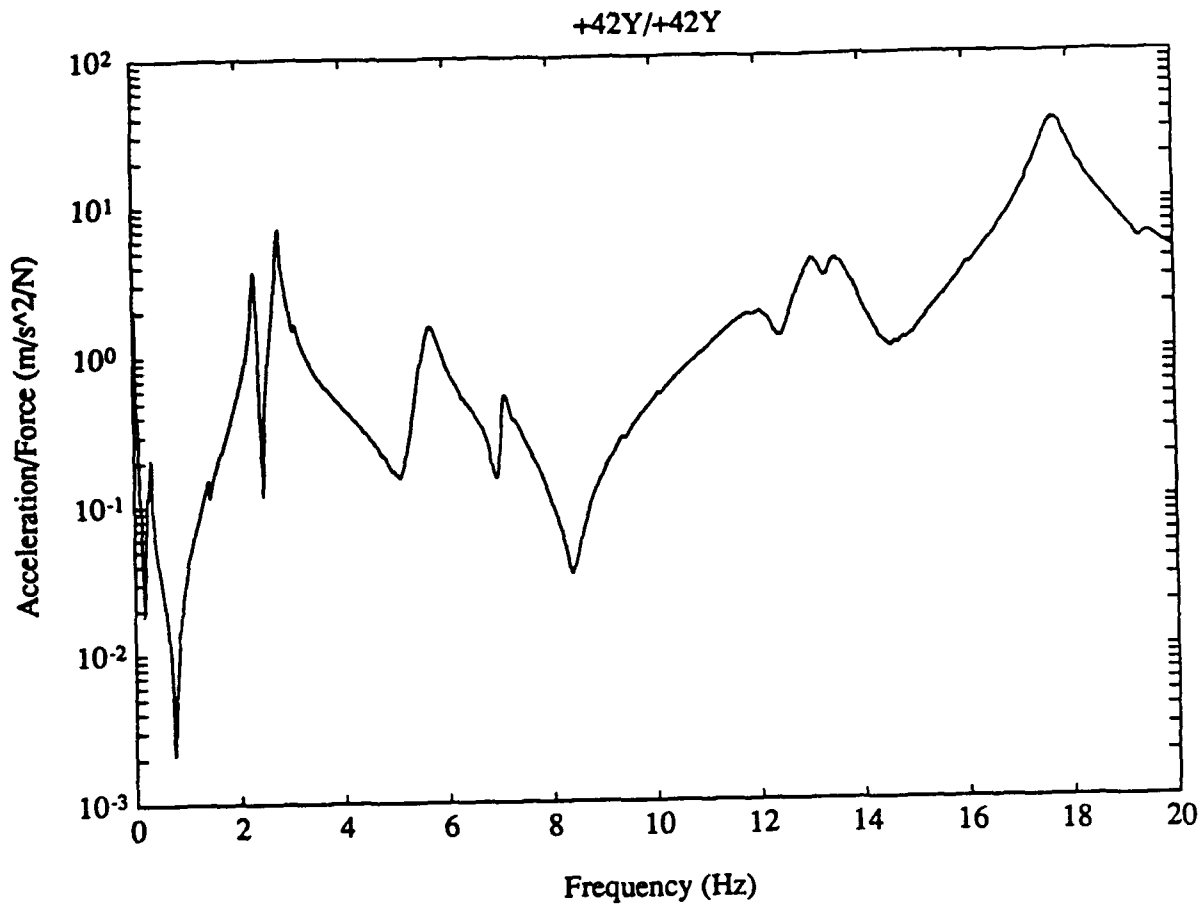


Figure 10. Modal Test 3 Drive Point FRF

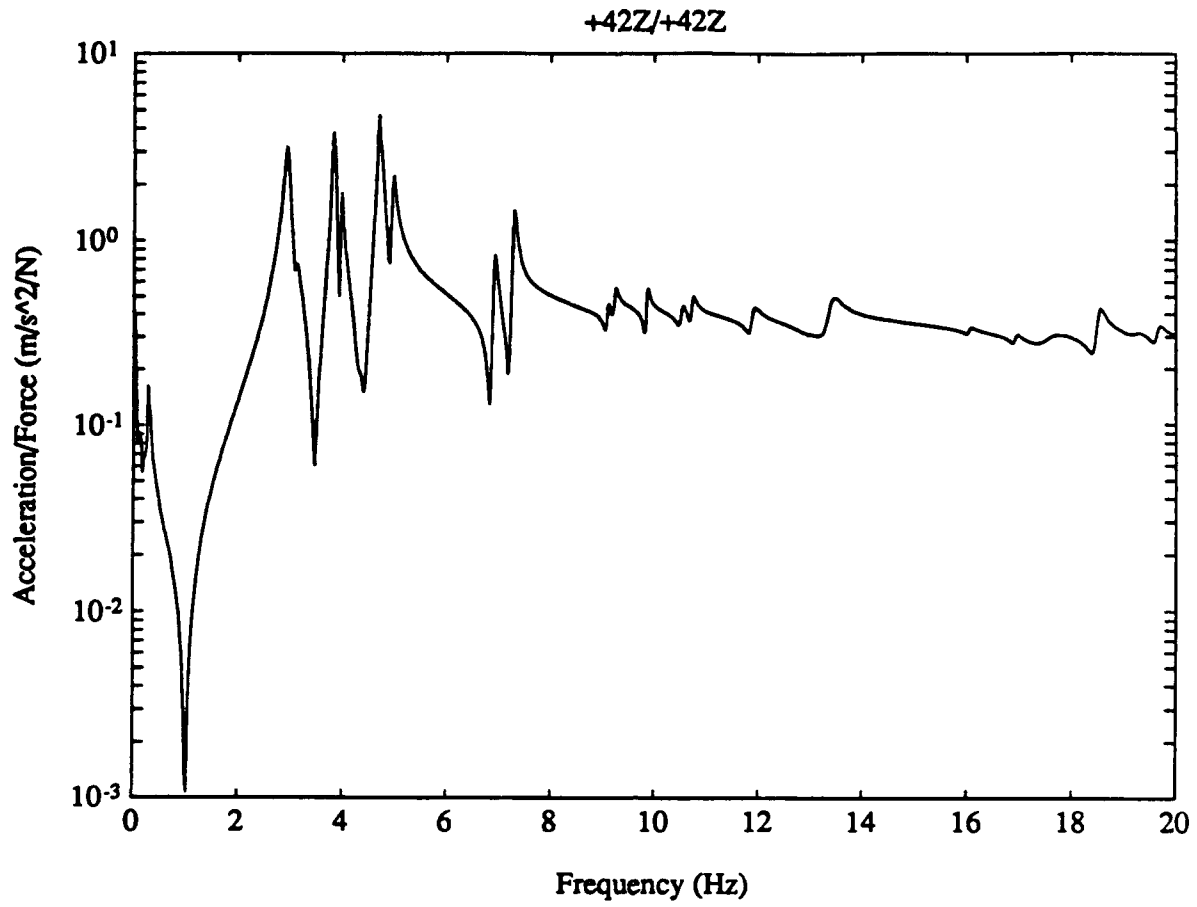


Figure 11. Modal Test 4 Drive Point FRF

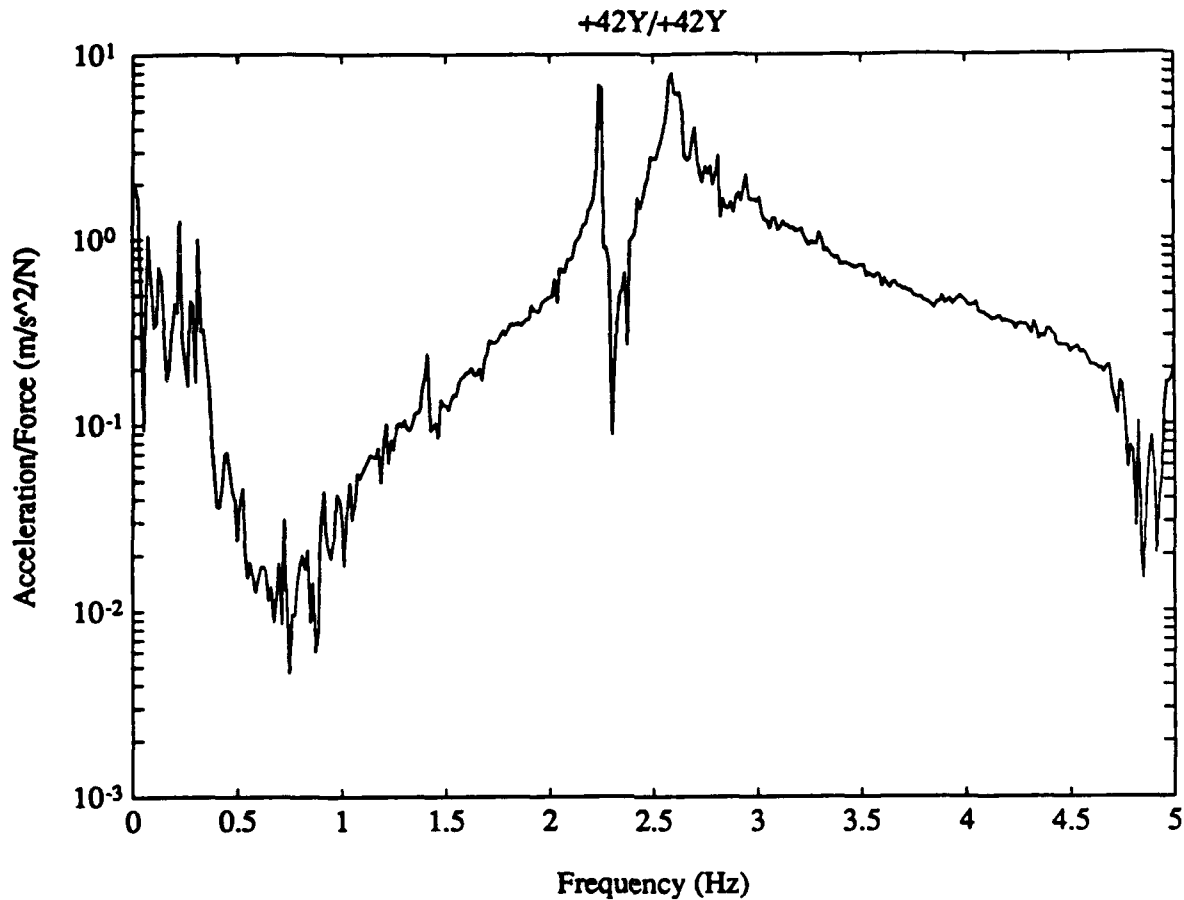


Figure 12. Modal Test 5 Drive Point FRF

Horizontal measurements (Y direction) on the solar array blankets generally were noisier than measurements at other locations. Also, in modal tests 3 and 5, where excitation is applied horizontally at the bottom of the outboard spreader on solar array 1, measurements were noisy at many locations. The Martin Marietta team experienced the same problem with the damped structure and concluded that it was a result of nonlinear behavior of the tuned mass dampers on the solar

array blankets (Gehling, 1990). It is possibly caused by nonlinear effects due to the accelerometer cables or coupling with the dynamics of the shaker armature. Or it is possible that the solar blanket members are thin enough that they are experiencing geometrically nonlinear bending. Figure 13 shows a typical FRF taken from a horizontal measurement on a solar array blanket.

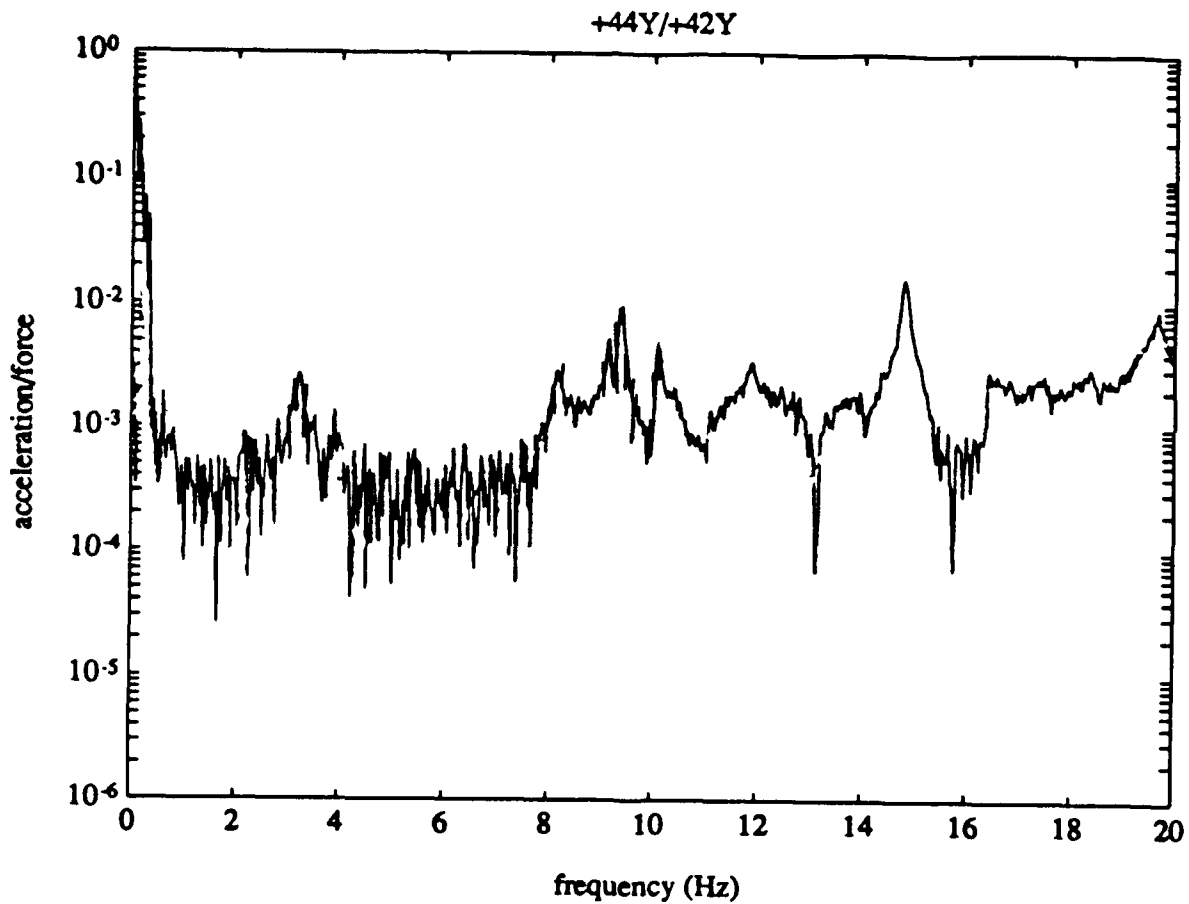


Figure 13. Horizontal Measurement From Solar Array Blanket

The experimental FRFs were analyzed using Structural Measurement Systems' STARModal modal analysis software running

on a personal computer. The STARModal system allows both single degree of freedom and multiple degree of freedom curve fitting techniques to be used on frequency domain FRF data to determine natural frequencies, modal damping factors, and mode shapes. Orthogonality products, FRF synthesis, forced response synthesis, and other modal analysis features are also available.

The FRF data in each of the modal tests was analyzed by curvefitting each apparent mode with a polynomial. Single-degree-of-freedom curvefits were used whenever curvefitting bands could be defined around a single apparent resonant frequency. In some instances, it was necessary to perform multiple-degree-of-freedom polynomial curvefits around peaks which were very closely spaced. In these cases, the number of peaks within the curvefitting band was kept to a minimum to reduce processing time.

In general, polynomial curvefitting produced very good reproduction of FRF data near resonant peaks. However, mode shape plots generated in STARModal using the modal parameters extracted from the curvefitting process were generally very poor. Figure 14 shows a typical mode shape plot generated from a modal test.

The poor quality of the mode shape plots is probably due to the closely spaced nature of the vibration modes. Even the light amount of damping present in the modified structure is

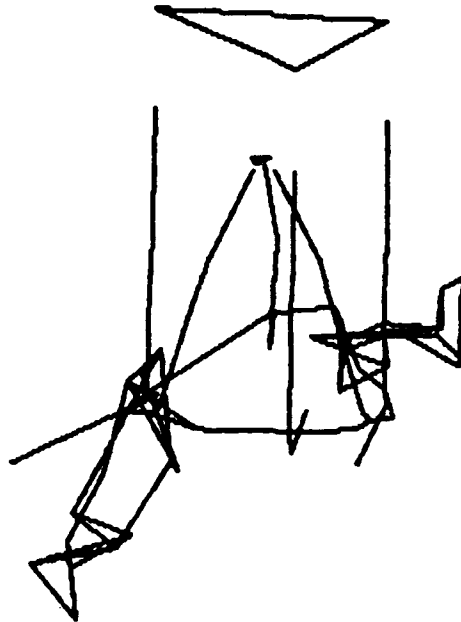


Figure 14. Mode Shape Plot From Curvefit Results

apparently able to couple the modes to an extent that the modal parameters cannot be extracted from one another. In other words, the transfer function matrix has essentially repeated poles. The occurrence of repeated poles violates an assumption necessary to guarantee that the transfer function matrix can be placed in terms of the modal parameters (Structural Measurement Systems, 1990).

V. MODELLING AND MODEL REDUCTION

The finite element model used in this thesis was originally developed by the Martin-Marietta researchers as part of the PACOSS contract. This model was written for MCS/NASTRAN and is described in Volume 3 of the PACOSS Final Report (Gehling and Morgenthaler, 1990).

The finite element model was modified in accordance with the structural changes made to the delivered test article as described in Chapter III. The grid point definition cards for all viscoelastic material and graphite epoxy constraining layer material were deleted and the tripod leg to top plate interface was changed to reflect the undamped design. The grid points and finite elements describing the tuned mass dampers on the solar array blankets were also deleted. The element connectivity in the solar array blankets was redefined to reflect the omission of the TMDs. The material property card for the shear strap was changed to properties of 6061-T6 aluminum. Additionally, all bulk data representing the equipment pod and antenna were removed and associated multipoint constraints were eliminated.

The resulting MSC/NASTRAN bulk data deck contains 2292 grid points and 1405 finite elements. The finite element model is shown in figure 15. Note that the concentrated mass elements representing the mass simulators do not appear.

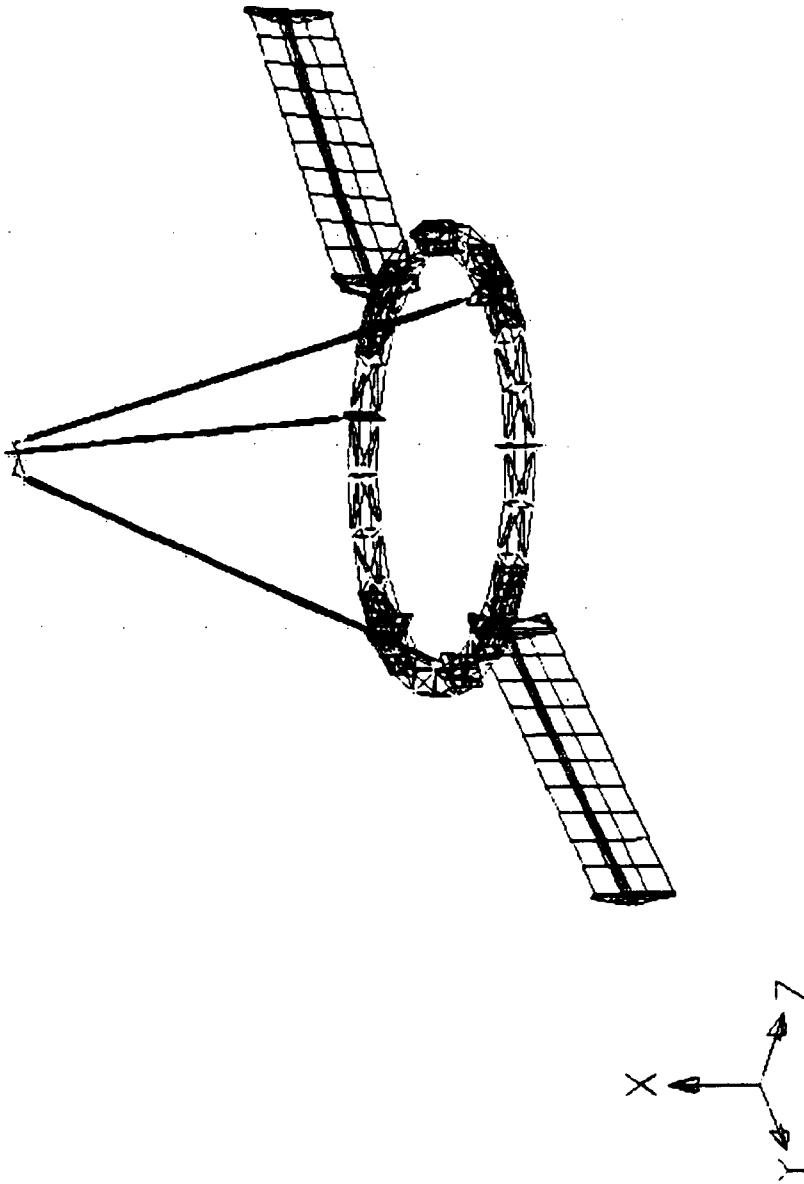


Figure 15. Finite Element Model of the Modified Structure

The model is made up of the following MSC/NASTRAN elements:

297 BAR elements which are primarily used to model the structural truss members of the ring truss.

134 BEAM elements which are used to model the solar array blanket members.

30 ELAS1 elements which represent the geometric stiffness of the cables supporting the structure.

11 ELAS2 elements which model the passive stiffness of the air bearing suspension and the springs in the mass actuators.

40 HEXA elements representing the solid inserts in the solar array roots and tips.

300 CONM2 elements used to model the concentrated mass structures of the ring truss joint blocks, actuator masses, box truss mass simulators, the secondary plate, accelerometers, and the overlapping of solar array blanket members.

56 PENTA elements used in modelling the solid inserts in the solar array roots and tips.

777 QUAD4 elements describing ring truss attachment plates for other substructures, ring truss section interfaces plates, solar array blanket spreaders, and the surfaces of the

solar array masts and tripod legs.

15 ROD elements modelling the material stiffness of the suspension cables.

45 TRIA3 elements used to model the ring truss interface plates and solar array blanket spreaders.

6 PLOTEL elements used to provide visibility to the secondary plate.

The hollow aluminum tubing of the tripod legs and the solar array masts are modelled using four QUAD4 elements in

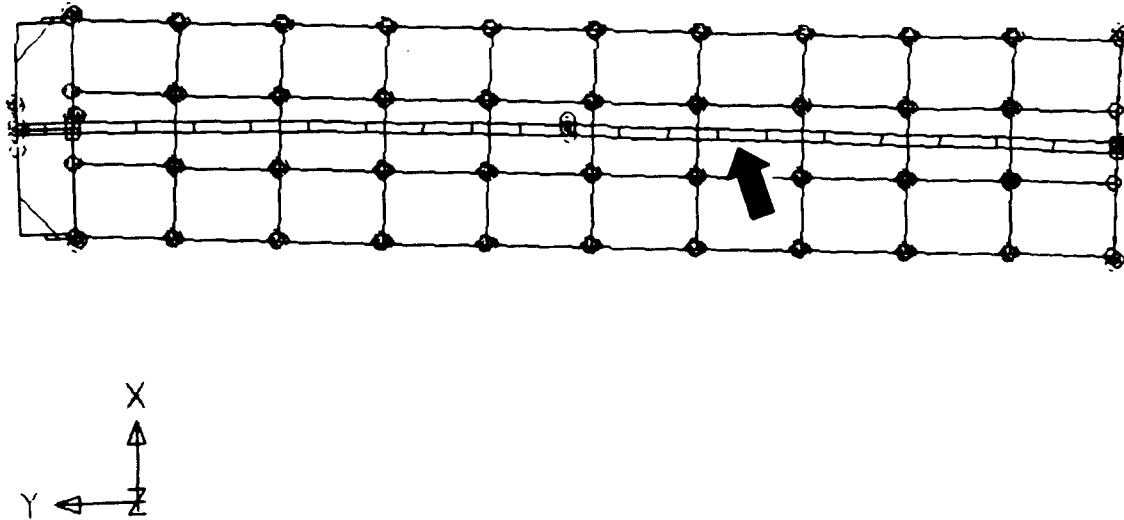


Figure 16. Solar Array Mast showing QUAD4 Elements

place of an equivalent beam type of element as seen in figures 16 and 17. This was necessary in the damped model to allow for different strain energy in different sides of the masts and tripod legs.

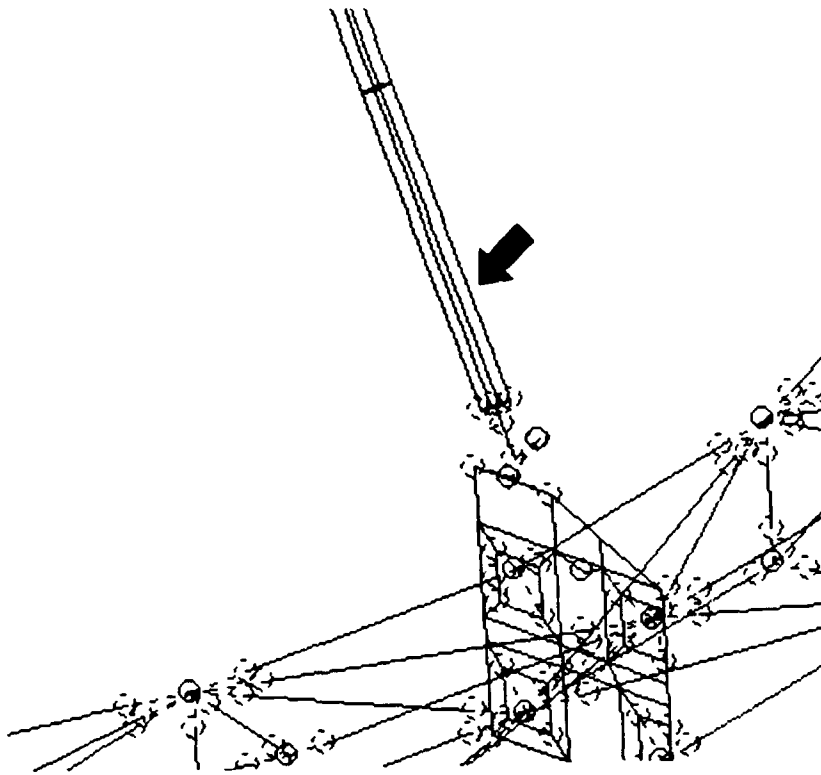


Figure 17. Tripod Leg Interface Showing QUAD4 Elements

The epoxy bonded solar array root assembly is modelled as a solid aluminum section of the same dimensions as the outside dimensions of the rectangular section tubing of the mast (figure 16). Analysis of this region by Martin-Marietta indicated that the modelling of this region was too stiff . The material properties were adjusted so that the assembly is

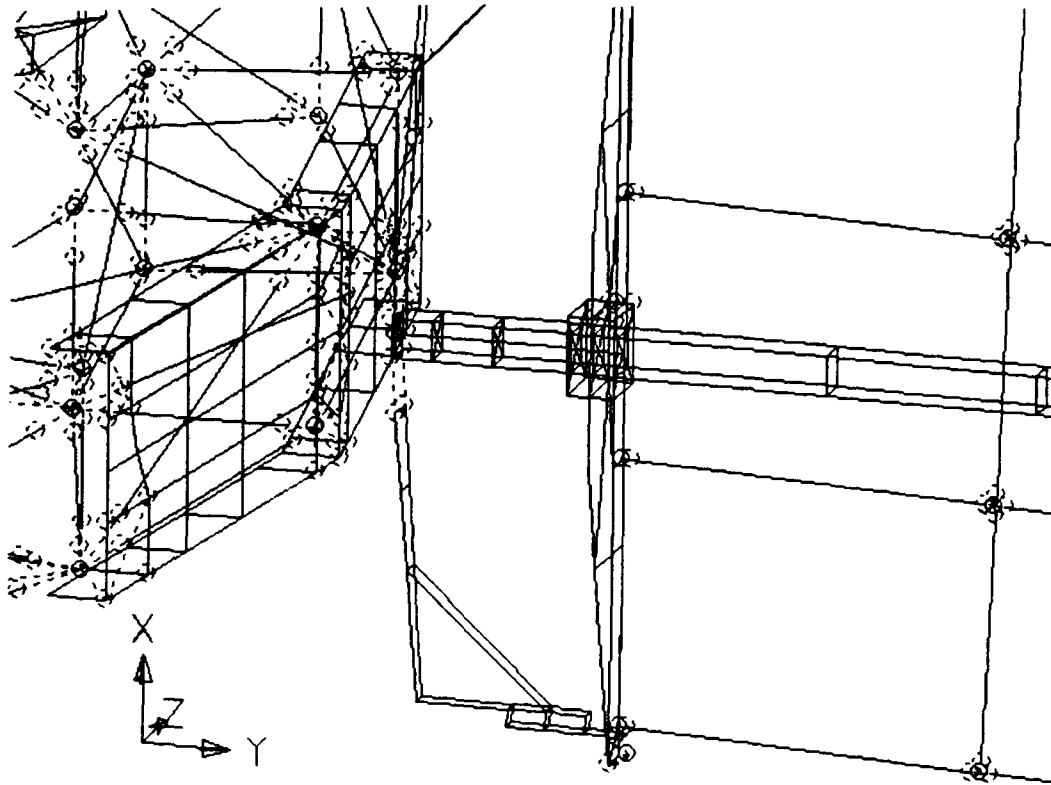


Figure 18. Solar Array Root Modelling

modelled with material 78 percent as stiff as a solid aluminum section (Gehling and Morgenthaler, 1990).

It is also important to note that the BEAM elements used in modelling the solar array blanket do not include cross-sectional warping coefficients or other BEAM element features and are therefore equivalent to BAR elements within MSC/NASTRAN. The nonzero rigid body modes of the structure are maintained by including the small amount of stiffness in the pneumatic suspension as ELAS1 elements connected between ground and the pistons in the suspension.

It should be noted that the MSC/NASTRAN output lists bad

geometry warning messages (User Warning Message 5491) for the following elements:

Solar Array 1:

Low Skew Angle: 7235, 7239, 7266, 7270

High Taper: 7247, 7248, 7249, 7251, 7252, 7278, 7279,
7280, 7282, 7283

Solar Array 2:

Low Skew Angle: 9235, 9239, 9266, 9270

High Taper: 9247, 9248, 9249, 9251, 9252, 9278, 9279,
9280, 9282, 9283

These elements are all QUAD4 plate elements representing the solar array blanket spreaders (figure 19). The warnings were disregarded because the QUAD4 element has been demonstrated to give good results for poor aspect ratios, skew angles, taper, and out of plane grid points (MacNeal, 1978). Also, the spreader plates are stiff relative to the rest of the solar array and small inaccuracies will not contribute appreciably to errors in computed mode shapes or natural frequencies. No difficulties were ever encountered in the behavior of the spreaders.

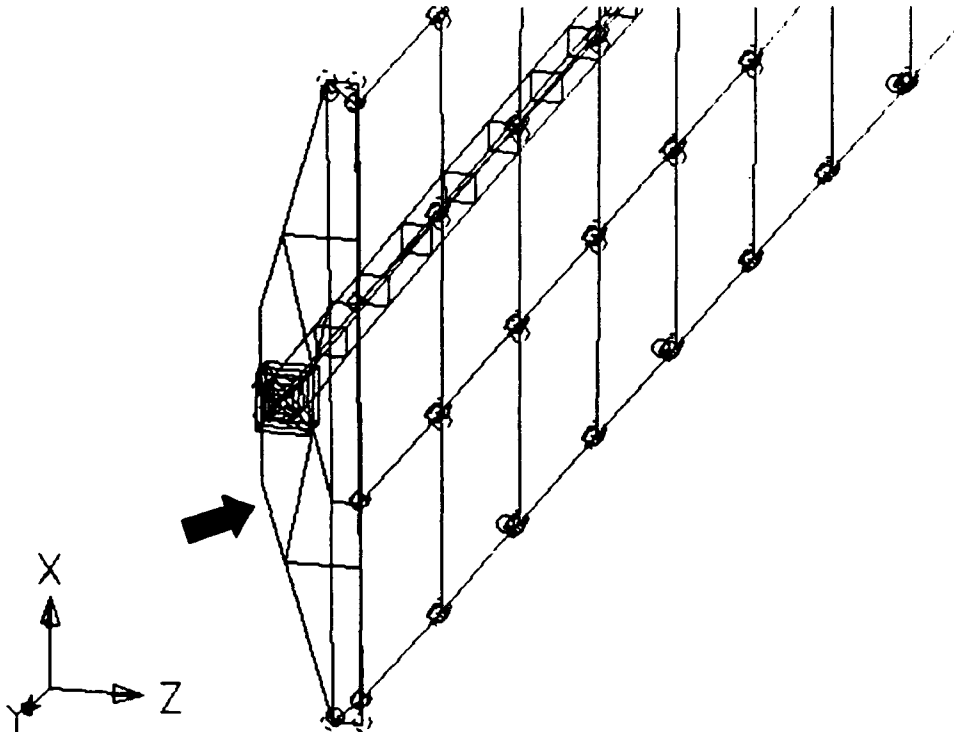


Figure 19. Solar Array Blanket Spreader QUAD4 Elements

Real Eigenvalue Analysis

The finite element model was used to determine analytical mode shapes and natural frequencies for a full order model. MSC/NASTRAN solution sequence 103 (normal modes) was run using the Sturm inverse power (SINV) eigensolution extraction method. 52 modes were reported below 20 Hz for the full order model.

After the modes were determined for the full order model, the model was reduced to 182 degrees of freedom using Guyan

(static) reduction and the normal modes solution was run again for the same frequency range. The set of retained degrees of freedom were selected to correspond to degrees of freedom measured by accelerometers during the the modal test so that a correlation could be made to the experimental data. Also degrees of freedom corresponding to the mass actuators and their respective attachment points on the ring truss and tripod so that the actuators would be represented in the final model. The degrees of freedom representing the suspension of the structure were included so that the rigid body modes of the structure would be present. Appendix B contains a table listing the 182 degrees of freedom retained in the Guyan reduction process. The table includes the degree of freedom number in the 182 DOF reduced model and the MSC/NASTRAN grid number and direction.

A normal modes solution was run on the Guyan-reduced model. Again, the Sturm inverse power method was used to extract the mode shapes and natural frequencies below 20 Hz. The Guyan-reduced model produced 48 modes in this region. Table 2 on the following page compares the 52 modes of the full order model to the 48 modes of the Guyan-reduced model.

Table 2

Real Eigenvalue Analysis Comparison

<u>Mode No.</u>	<u>Full F_n (Hz)</u>	<u>Reduced F_n (Hz)</u>	<u>Mode No.</u>	<u>Full F_n (Hz)</u>	<u>Reduced F_n (Hz)</u>
1	0.072	0.072	27	6.091	6.184
2	0.108	0.108	28	6.796	6.900
3	0.126	0.126	29	6.923	7.008
4	0.313	0.313	30	9.056	9.277
5	0.313	0.313	31	9.246	9.463
6	0.584	0.584	32	10.559	1.092
7	0.745	0.745	33	10.666	1.096
8	0.746	0.746	34	10.975	11.152
9	1.493	1.493	35	10.975	11.152
10	1.497	1.497	36	11.919	12.377
11	1.497	1.497	37	11.954	12.729
12	1.503	1.503	38	12.011	12.745
13	1.517	1.517	39	12.324	12.865
14	1.518	1.518	40	13.267	13.595
15	1.634	1.634	41	15.032	15.317
16	1.714	1.715	42	15.155	15.402
17	1.812	1.813	43	15.272	15.575
18	1.845	1.845	44	15.884	16.282
19	2.402	2.406	45	17.104	17.272
20	2.406	2.409	46	17.912	18.134
21	4.331	4.336	47	18.956	19.175
22	4.391	4.396	48	19.001	19.218
23	4.423	4.434	49	19.647	-----
24	5.416	5.432	50	19.649	-----
25	5.417	5.433	51	19.947	-----
26	6.090	6.183	52	19.968	-----

Generally, the natural frequencies of the Guyan-reduced model match very closely for low frequencies. For higher frequencies, the Guyan-reduced natural frequencies are slightly higher than corresponding full model resonances. The disparity increases with higher frequencies. Although, natural frequencies are shifted upward by the Guyan-reduction process, a comparison of mode shape plots from each model indicates that no modes were omitted in the Guyan-reduced model. Modes 49 through 52 of the full order model were shifted above 20 Hz by the reduction process and were not reported. Mode shape plots were obtained from the MSC/XL finite element pre- and postprocessor. The mode shapes for the 182 degree of freedom Guyan-reduced model are included in Appendix B.

Frequency Response Analysis

For comparison to the modal test data, a frequency response solution (MSC/NASTRAN solution sequence 111) was performed. Since the goal was to produce acceleration FRFs, a unit magnitude (1 Newton) frequency dependent force was applied to grid point 30003 in direction 1, corresponding to measurement point 97 in the +X direction. Acceleration response to this force allows direct comparison to the FRF's measured in the second modal test. Frequency resolution of 0.01 Hz was defined for the force over the desired bandwidth

of 0 to 15 Hz using a FREQ1 bulk data card. To provide a reasonable amount of damping, a TABDMP1 card was included defining 0.5% critical modal damping for all modes. The acceleration response was requested in magnitude and phase format for all points in the Guyan-reduced set. The executive and case control decks and selected bulk data cards pertaining to the frequency response solution are included in Appendix C.

The results of the solution were loaded from the MSC/NASTRAN results database into MSC/XL for postprocessing. The FRFs were saved as text files that could be read into PRO-MATLAB and directly compared to the corresponding FRFs measured in the second modal test. The magnitude plots of the 182 degree of freedom Guyan-reduced model are not included in the thesis for brevity. Figure 20 shows the drive point FRF comparison. The solid line denotes the measurement. The dashed line denotes the modelled response.

Figure 20 shows that the low frequency, closely-spaced modal characteristics of the structure are present in the model, but there is no clear matching between natural frequencies in the model versus natural frequencies in the experimental FRFs. Other FRFs produced by the 182 DOF model show similar results. After the model is reduced further, the mass and stiffness terms can be modified by hand to produce a final model with more fidelity to measured data.

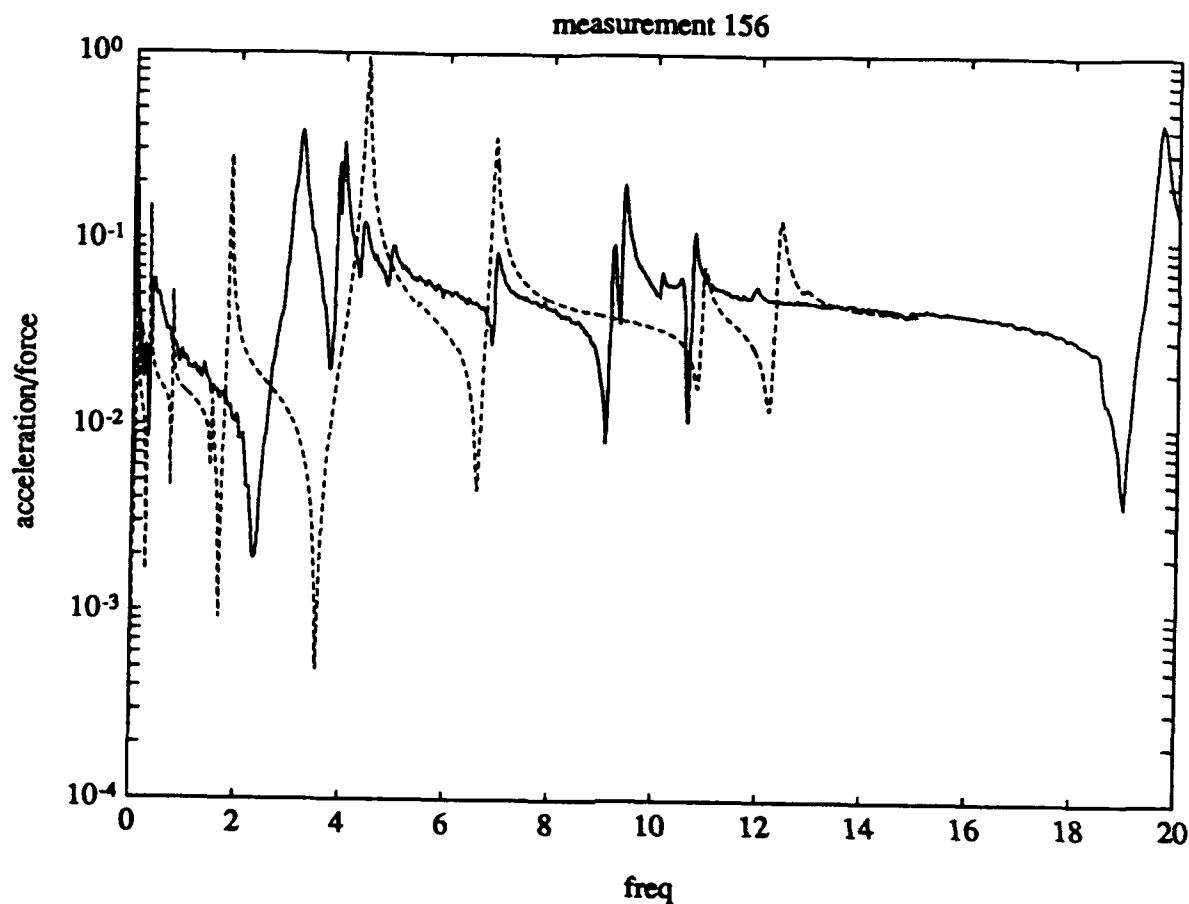


Figure 20. Drive Point FRF Comparison - 182 DOF Model

The Second Model Reduction

The model was reduced to 50 degrees of freedom using the method described in the theory section (Chapter II, pages 16-19, equations 31-36).

The mass and stiffness matrices from the 182 degree of freedom Guyan reduced model were extracted from MSC/NASTRAN and manipulated in PRO-MATLAB to obtain the 50 degree of freedom model. Appendix C contains a detailed explanation of

how this was done. Also included in Appendix C are the MSC/NASTRAN and PRO-MATLAB files that were used in the second model reduction.

The 50 degrees of freedom retained in the final model are listed in Appendix C. The following table shows how the final degrees of freedom are distributed among the components of the structure.

Table 3

Distribution of DOFs in Final Model

Solar Array 1:

<u>DOF</u>	<u>Grid/Dir</u>	<u>DOF</u>	<u>Grid/Dir</u>
1.	70004-1	6.	70009-3
2.	70004-3	7.	70014-3
3.	70016-1	8.	70008-3
4.	70016-3	9.	70012-3
5.	70015-3	10.	70006-3

Solar Array 2:

<u>DOF</u>	<u>Grid/Dir</u>	<u>DOF</u>	<u>Grid/Dir</u>
36.	90006-3	41.	90015-3
37.	90012-3	42.	90016-1
38.	90008-3	43.	90016-3
39.	90014-3	44.	90004-1
40.	90009-3	45.	90004-3

Ring Truss:

<u>DOF</u>	<u>Grid/Dir</u>
27.	2710-3

Mass Simulators:

<u>DOF</u>	<u>Grid/Dir</u>	<u>DOF</u>	<u>Grid/Dir</u>
14.	11-2	31.	21-2
26.	31-2		

Tripod Legs:

<u>DOF</u>	<u>Grid/Dir</u>	<u>DOF</u>	<u>Grid/Dir</u>
19.	30104-2	22.	30203-1
20.	30103-1	34.	30303-1
21.	30204-2	35.	30304-2

Apex Plate:

<u>DOF</u>	<u>Grid/Dir</u>
46.	30003-1

Suspension:

<u>DOF</u>	<u>Grid/Dir</u>	<u>DOF</u>	<u>Grid/Dir</u>
13.	2970-3	30.	2980-3
25.	2990-3		

Table 3 (Cont.)

Distribution of DOFs in Final Model (Cont.)

Actuator Pairs:

<u>DOF</u>	<u>Grid/Dir</u>	<u>DOF</u>	<u>Grid/Dir</u>
11.	2021-3	28.	27111-3
12.	20211-3	29.	271111-3
15.	2231-3	32.	2501-3
16.	22311-3	33.	25011-3
17.	2311-3	47.	300111-3
18.	23111-3	49.	300113-3
23.	2791-3	48.	300112-2
24.	27911-3	50.	300114-2

Final Model Tuning

The 50 degree of freedom model was tuned by hand to more closely resemble the FRFs measured during the second modal test. The mass and stiffness matrices were placed in modal form and orthonormalized to produce unit modal masses and modal stiffnesses equal to the squares of the natural frequencies (in rad/sec).

The model was modified starting with the drive point FRF shown in figure 21. The modal masses and stiffnesses were adjusted to move resonant peaks to coincide more closely with the measured FRF. Modal masses were raised or lowered to alter the height of each peak and the modal stiffnesses were adjusted to maintain the appropriate natural frequency. An attempt was also made to match the phase information in the measured FRF. Resonant peaks which were not dominant in the drive point FRF were adjusted using FRFs from various other

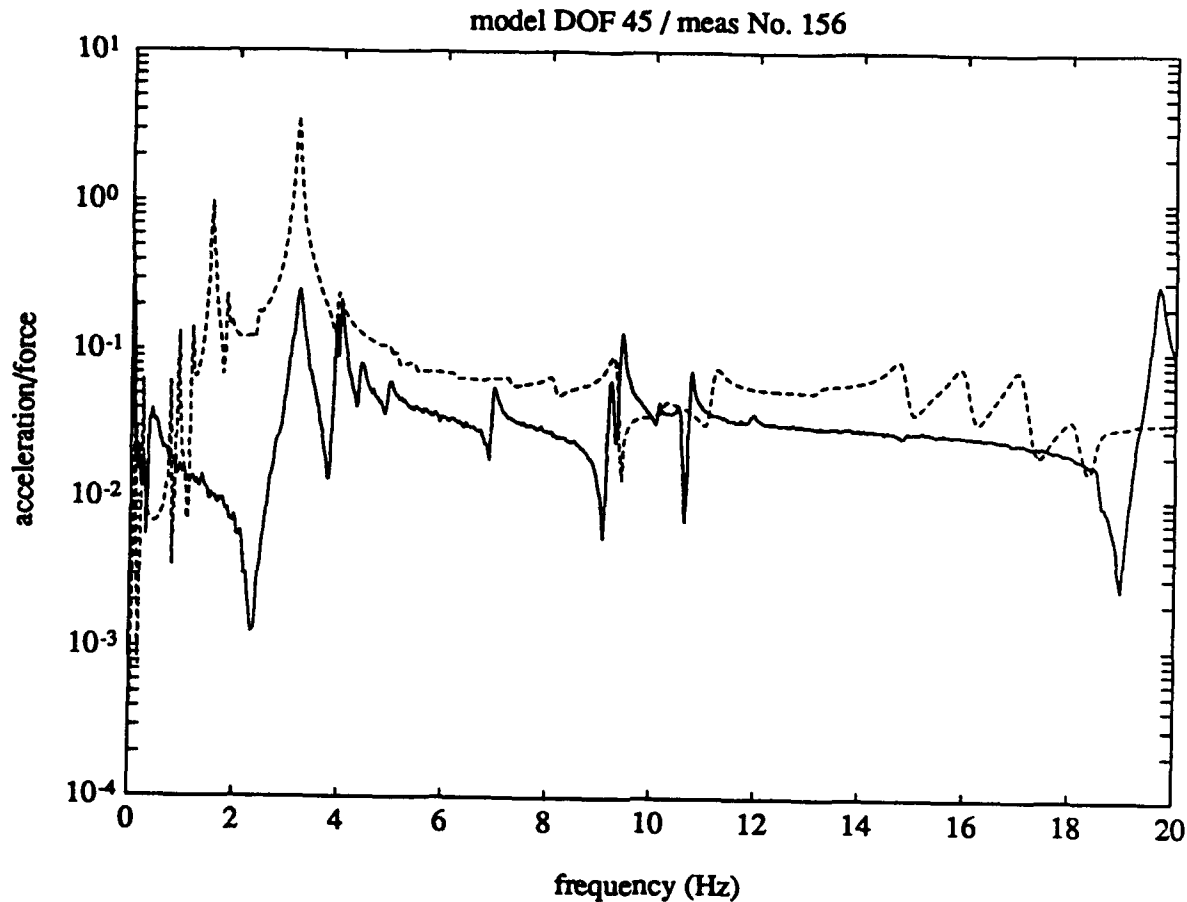


Figure 21. Drive Point FRF Before Model Tuning

points on the structure. The final drive point FRF magnitude and phase plots are shown in figures 22 and 23.

With the drive point FRF tuned to an acceptable level of fidelity, the remaining FRFs were tuned by adjusting the eigenvector components affecting a given FRF. The full set of FRFs after tuning is included in Appendix D.

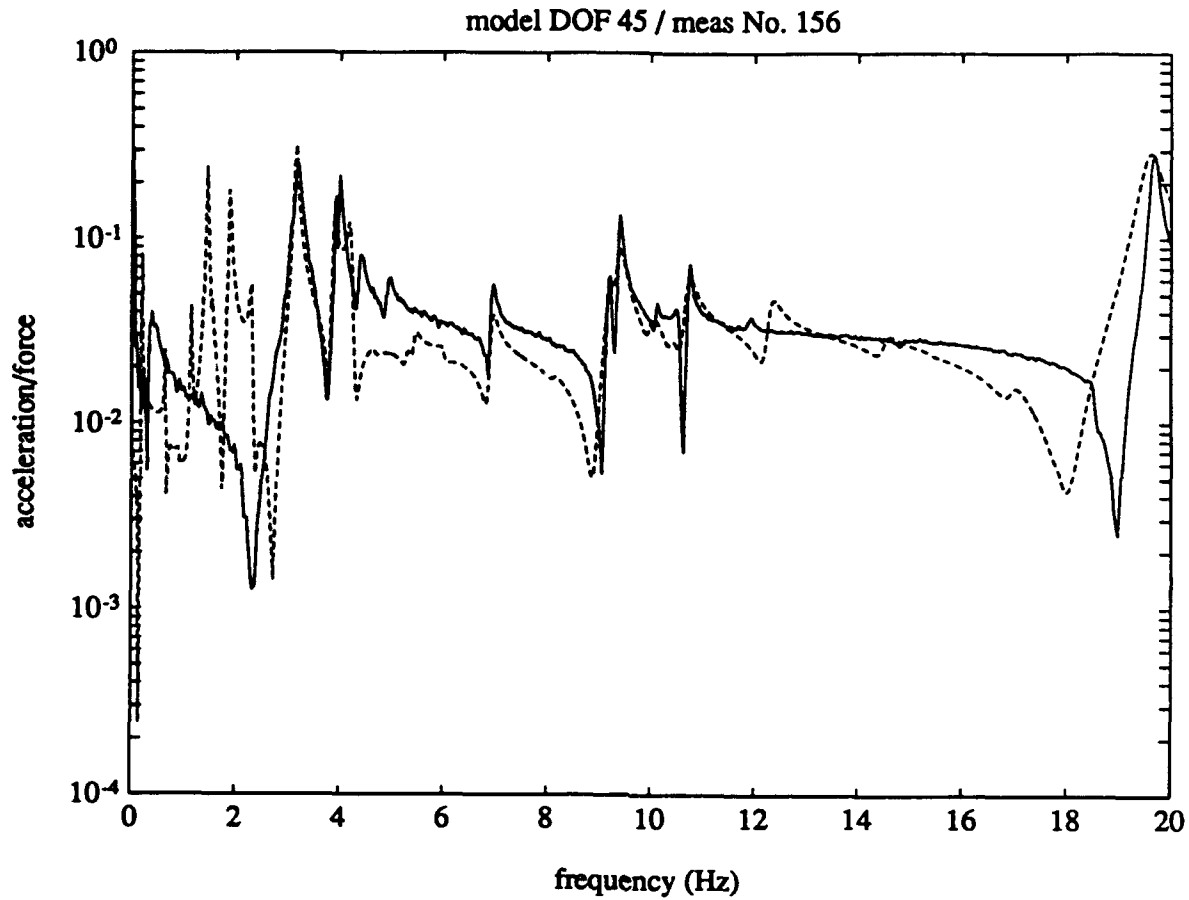


Figure 22. Drive Point FRF After Tuning (Magnitude)

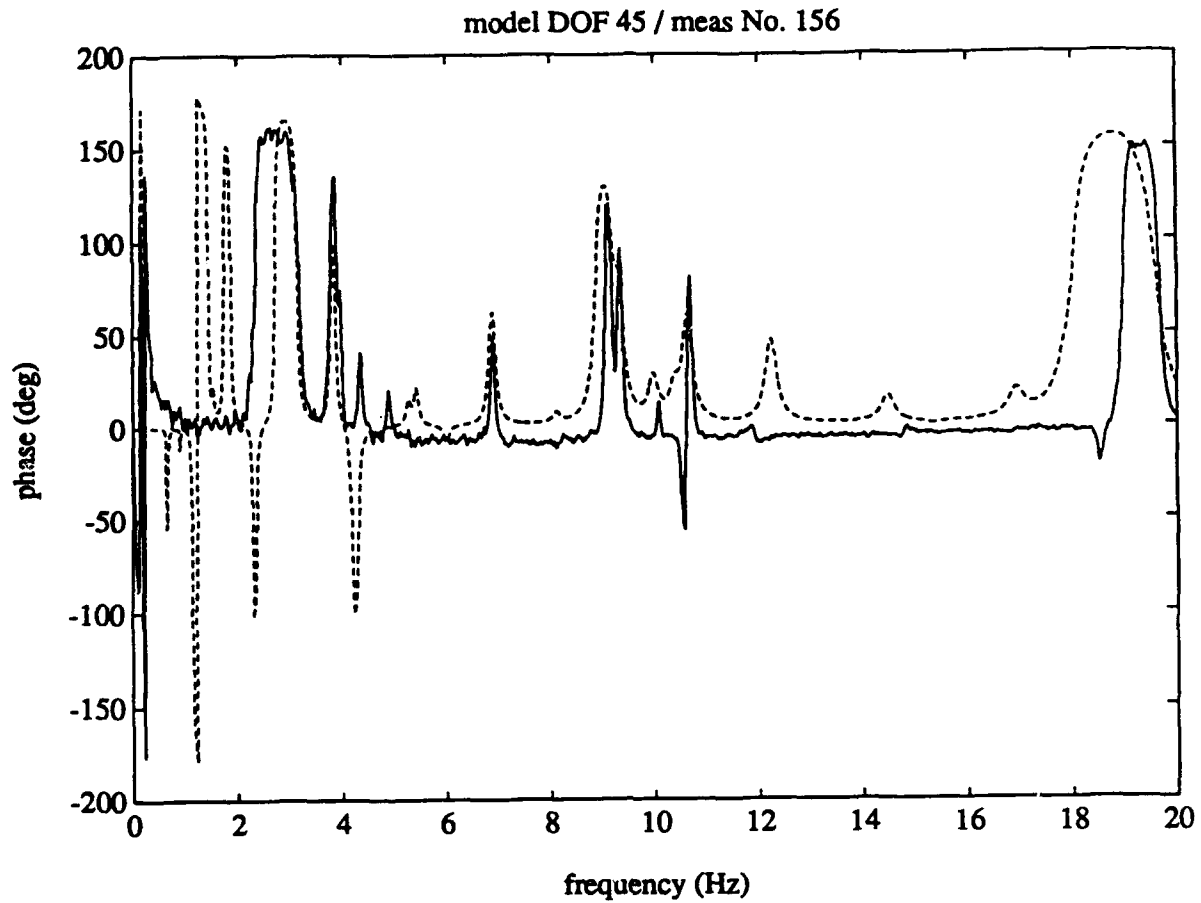


Figure 23. Drive Point FRF After Tuning (Phase)

VI. CONCLUSIONS AND RECOMMENDATIONS

The goals of the research performed in this thesis were to create a lightly damped version of the PACOSS DTA while retaining the characteristics of low frequency, high density modal behavior. Clearly, this objective has been achieved. The FRFs measured during the modal testing indicate that this objective has been achieved. The FRFs measured during the modal testing indicate roughly 30 flexible modes below 20 Hz.

It can also be concluded that results of the modal testing were good. With the exception of the measurements taken from horizontal excitation of the solar array, data quality was in general very good. It should be reiterated that random excitation was used for all measurements in the modal tests. Swept sine excitation was attempted by the Martin Marietta team during preliminary modal testing with very good results, but the higher data quality was judged not worth the additional time required to collect measurements (Gehling, 1990). Although data quality was consistently very good for random excitation, swept sine excitation is recommended to improve data quality for some of the noisier measurements. A swept sine input at the horizontal solar array excitation point using even lower force levels could generate better quality measurements for the horizontal solar array blanket modes. In addition, using an excitation point toward the root

of the solar array (such as +46Y and +46Z) may provide cleaner measurements due to the higher stiffness at these points.

The modal analysis of the experimental FRF data was difficult and provided inconclusive results. Inconsistent results using single and multiple degree of freedom polynomial curvefitting techniques made it impossible to create a purely experimental system model as originally planned. Indication is given that better modal identification techniques are needed for structures with closely spaced vibration modes. This conclusion was shared by the Martin Marietta researchers (Gehling, 1990). It is recommended that further thesis work be directed toward the application of more advanced modal identification algorithms to data acquired from the lightly damped PACOSS structure. It is also recommended that theoretical work be applied to the development of more stable modal analysis techniques for structures with high modal density.

The model tuning effort has been successful enough to provide a system model suitable for use in the design of a purely active vibration control system. The method used to tune the model involved manipulating the terms in the modal formulation of the reduced model until the frequency responses more closely matched the measured responses. While this method was successfully used in this application to create an adequate system model, it proved labor intensive and might be

impractical if used for a full scale deployable space system. It is recommended that effort be given to developing an optimization algorithm to automatically modify a reduced model to to match a reduced set of FRF data where experimental mode shapes are unreliable or difficult to produce.

Bibliography

- Cook, Robert D., et al. Concepts and Applications of Finite Element Analysis. John Wiley and Sons, Inc., 1989.
- Ewins, D. J. Modal Testing: Theory and Practice. Letchworth, Hertfordshire, England: Research Studies Press, Ltd., 1985.
- Freed, Andrew M. and Christopher C. Flanigan. "A Comparison of Test-Analysis Model Reduction Methods", Sound and Vibration: 30-35 (March 1991).
- Gehling, Russell N. Passive and Active Control of Space Structures, Volume 2: Dynamic Test Article Modal Survey, Test and Analysis Results, Final Report, September 1987 - November 1988. CDRL 14, Contract F33615-82-C-3222. Denver, CO: Martin Marietta Astronautics Group, 30 September 1990.
- and Daniel R. Morgenthaler. Passive and Active Control of Space Structures, Volume 3: DTA Finite Element Model, Final Report, September 1987 - November 1988. CDRL 14, Contract F33615-82-C-3222. Denver, CO: Martin Marietta Astronautics Group, 30 September 1990.
- and Daniel R. Morgenthaler. Representative System Report, Contract F33615-82-C-3222. Denver, CO: Martin Marietta Astronautics Group, November 1985.
- MacNeal, Richard H. MSC/NASTRAN Handbook for Dynamic Analysis. The MacNeal-Schwendler Corporation, Los Angeles, CA, 1986.
- . MSC/NASTRAN Handbook for Linear Analysis. The MacNeal-Schwendler Corporation, Los Angeles, CA, 1985.
- . "A Simple Quadrilateral Shell Element", Computers and Structures:8,175-183, 1978.
- . The NASTRAN Theoretical Manual. The MacNeal-Schwendler Corporation, Los Angeles, CA, 1972.
- Meirovitch, Leonard. Analytical Methods in Vibrations. New York: Macmillan Publishing Company, 1967.
- . Elements of Vibration Analysis. New York: McGraw-Hill Book Company, 1986.

Morgenthaler, Daniel R., et al. Passive and Active Control of Space Structures: Design and Fabrication of the PACOSS Dynamic Test Article, CDRL 10, Contract F33615-82-C-3222. Denver, CO: Martin-Marietta Astronautics Group, 30 September 1990.

----- . Passive and Active Control of Space Structures, Volume 1: Damping Design Methodology, Final Report, September 1987 - November 1988, Contract F33615-82-C-3222. Denver, CO: Martin-Marietta Astronautical Group, September 1990.

Rajoram, S. and J. L. Junkins. "Identification of Vibrating Flexible Systems", Journal of Guidance, 8: 463-470 (July - August 1985).

Reymond, Michael A. MSC/NASTRAN User's Manual. The MacNeal-Schwendler Corporation, Los Angeles, CA, 1991.

Richardson, Mark H. and David L. Formenti. "Parameter Estimation from Frequency Response Measurements Using Rational Fraction Polynomials", Proceedings of the International Modal Analysis Conference, Orlando, FL, Nov 1982.

Structural Measurement Systems. The STAR System: Theory and Applications, Issue A. Milpitas, CA, 25 January 1990.

Appendix A. MEASUREMENT TABLES

This appendix contains a log of the serial numbers of the accelerometers installed at each location. The measurement point and direction are included for reference.

The following pages show the accelerometer locations and directions for all measurements taken on the undamped structure. The corresponding degrees of freedom in the MSC/NASTRAN finite element model are also given.

Also included are detailed drawings depicting the measurement points and measurement numbers.

Accelerometer Installation Logs

The following pages show the instruments used to collect the accelerations at each of the measured degrees of freedom. These logs were used as checklists when taking full data sets of FRFs.

All output measurements were taken using Kistler Model 8632A5 piezoelectric accelerometers with a calibration value of 1 Volt/g.

Input measurements were taken using Kistler Model 9712A5 Force Accelerometer (serial number C49401) with a calibration value of 0.811 Volt/Lbf.

ACCELEROMETER INSTALLATION LOG

<u>Meas. Number</u>	<u>Point & Dir.</u>	<u>Serial Number</u>	<u>Location</u>
1	+1X	C87831	Box Truss Mass Simulators
2	-1Y	C87832	
3	-1Z	C87833	
4	+2X	C87834	
5	+2Y	C87836	
6	-2Z	C87815	
7	+3X	C86812	
8	+3Y	C87816	
9	-3Z	C86813	
10 - 38			Not Used
39	+34Y	C85896	Solar Array 1
40	+34Z	C87838	
41	+35Y	C87929	
42	-35Z	C87928	
43	-36Y	C87924	
44	-36Z	C87921	
45	+37Y	C87926	
46	+37Z	C87925	
47	+38Y	C87923	
48	+38Z	C87910	
49	+39Y	C87911	
50	+39Z	C87912	

ACCELEROMETER INSTALLATION LOG (Cont.)

<u>Meas. Number</u>	<u>Point & Dir.</u>	<u>Serial Number</u>	<u>Location</u>
51	+40Y	C87913	Solar Array 1 (Cont.)
52	+40Z	C87914	
53	+41Y	C87903	
54	+41Z	C87917	
55	+42Y	C87919	
56	+42Z	C87920	
57	+43Y	C87902	
58	+43Z	C87900	
59	+44Y	C87904	
60	+44Z	C87796	
61	+45Y	C87907	
62	-45Z	C87909	
63	+46Y	C87888	
64	+46Z	C87889	
65 - 68			Not Used
69	+51Y	C87879	Solar Array 2
70	+51Z	C87878	
71	+52Y	C87870	
72	-52Z	C87864	
73	+53Y	C87843	
74	+53Z	C87844	
75	-54Y	C87869	

ACCELEROMETER INSTALLATION LOG (Cont.)

<u>Meas. Number</u>	<u>Point & Dir.</u>	<u>Serial Number</u>	<u>Location</u>
76	+54Z	C87842	Solar Array 2 (Cont.)
77	+55Y	C87862	
78	+55Z	C87860	
79	+56Y	C87793	
80	+56Z	C85897	
81	+57Y	C85895	
82	+57Z	C87845	
83	+58Y	C85883	
84	+58Z	C87848	
85	+59Y	C87867	
86	+59Z	C87851	
87	+60Y	C87857	
88	+60Z	C87856	
89	+61Y	C87849	
90	+61Z	C85881	
91	+62Y	C87852	
92	+62Z	C87855	
93	+63Y	C87854	
94	+63Z	C87850	
95 - 98			Not Used
99	+68X	C87794	Ring Truss and Tripod
100	+68Y	C87795	

ACCELEROMETER INSTALLATION LOG (Cont.)

<u>Meas. Number</u>	<u>Point & Dir.</u>	<u>Serial Number</u>	<u>Location</u>
101	+68Z	C86801	Ring Truss and Tripod (Cont.)
102	+69Z	C86797	
103	+70X	C86784	
104	-70Y	C86796	
105	+70Z	C87863	
106	+71Z	C87800	
107	+72X	C87801	
108	+72Z	C86811	
109	+73Z	C87825	
110	-74X	C87827	
111	-74Y	C87765	
112	+74Z	C86805	
113	+75Z	C87806	
114	+76X	C87805	
115	+76Y	C87807	
116	+76Z	C87784	
117	-77X	C87785	
118	+77Y	C87786	
119	+77Z	C86816	
120	+78Z	C86810	
121	+79Z	C87813	
122	-80X	C87812	

ACCELEROMETER INSTALLATION LOG (Cont.)

<u>Meas. Number</u>	<u>Point & Dir.</u>	<u>Serial Number</u>	<u>Location</u>
123	+80Z	C87812	Ring Truss and Tripod (Cont.)
124	+81Z	C86817	
125	+82Z	C86807	
126	+83X	C87828	
127	+83Y	C87829	
128	+83Z	C87830	
129	+84X	C87797	
130	-84Y	C87798	
131	+84Z	C87799	
132	+85X	C87811	
133	+85Z	C87810	
134-135			
136	-88X	C87802	
137	-88Y	C87792	
138	+88Z	C87804	
139	+89X	C87787	
140	+89Y	C87788	
141	+89Z	C87789	
142	-90X	C87791	
143	+90Z	C87790	
144	+91X	C87837	
145	+91Y	C87905	

ACCELEROMETER INSTALLATION LOG (Cont.)

<u>Meas. Number</u>	<u>Point & Dir.</u>	<u>Serial Number</u>	<u>Location</u>
146	+91Z	C87897	Ring Truss and Tripod (Cont.)
147	+92X	C87808	
148	+92Y	C87809	
149	+92Z	C87814	
150	+93Z	C86795	
151	+94Z	C86794	
152	+95Z	C86793	
153	+96X	C87766	Apex Plate
154	+96Y	C87767	
155	-96Z	C87768	
156	+97X	C87769	
157	+97Y	C87770	
158	-97Z	C87771	
159	+98X	C87772	
160	+98Y	C86808	
161	-98Z	C87901	
162	+99X	C86792	Ground
163	+99Y	C86791	
164	+99Z	C86789	
165	+100X	C86786	
166	-100Y	C86788	
167	+100Z	C86800	

ACCELEROMETER INSTALLATION LOG (Cont.)

<u>Meas. Number</u>	<u>Point & Dir.</u>	<u>Serial Number</u>	<u>Location</u>
168	-101X	C86785	Ground (Cont.)
169	+101Y	C86799	
170	+101Z	C86798	
171	+102X	C87775	Tripod Leg 1
172	+102Y	C87776	
173	+103X	C87782	
174	+103Y	C87780	
175	+104X	C87777	Tripod Leg 2
176	+104Y	C87774	
177	+105X	C86818	
178	+105Y	C86819	
179	+106X	C87778	Tripod Leg 3
180	-106Y	C87773	
181	+107X	C87783	
182	-107Y	C87781	

The following pages show the coordinates of the measurement points on the modified structure. All coordinates are given in the global Cartesian coordinate system. The origin is in the center of the ring truss, the +Z axis is vertical through the secondary plate, the +X axis extends in the direction of solar array 1. Corresponding MSC/NASTRAN grid numbers and degrees of freedom are also included.

Mass Simulators

Meas. Number	NASTRAN Grid	Point & Dir	X (in.)	Y (in.)	Z (in.)
1	11-2	1X	38.25	38.25	-15.4
2	11-3	1Y			
3	11-1	1Z			
4	21-2	2X	-38.25	38.25	-15.4
5	21-3	2Y			
6	21-1	2Z			
7	31-2	3X	0.0	-51.0	-16.9
8	31-3	3Y			
9	31-1	3Z			
10 - 38	Unused				

Solar Array 1

Meas. Number	NASTRAN Grid	Point & Dir	X (in.)	Y (in.)	Z (in.)
39	70001-3	34Y	65.27	0.0	3.80
40	70001-1	34Z			
41	70003-3	35Y	111.03	0.0	2.55
42	70002-1	35Z			
43	70004-3	36Y	162.53	0.0	2.55
44	70004-1	36Z			
45	70005-3	37Y	65.27	1.8	13.25
46	70005-1	37Z			
47	70006-3	38Y	93.93	2.2	12.75
48	70006-1	38Z			
49	70008-3	39Y	122.93	2.2	12.75
50	70008-1	39Z			
51	70009-3	40Y	142.33	2.2	12.75
52	70009-1	40Z			
53	70010-3	41Y	162.13	1.8	13.25
54	70010-1	41Z			
55	70016-3	42Y	162.13	1.8	-8.15
56	70016-1	42Z			
57	70015-3	43Y	142.33	2.2	-7.65
58	70015-1	43Z			
59	70014-3	44Y	122.93	2.2	-7.65
60	70014-1	44Z			
61	70012-3	45Y	93.93	2.2	-7.65
62	70012-1	45Z			
63	70011-3	46Y	65.27	1.8	-8.15
64	70011-1	46Z			
65 - 68	Unused				

Solar Array 2

Meas. Number	NASTRAN Grid	Point & Dir	X (in.)	Y (in.)	Z (in.)
69	90001-3	51Y	-65.27	0.0	3.80
70	90001-1	51Z			
71	90003-3	52Y	-111.03	0.0	2.55
72	90002-1	52Z			
73	90004-3	53Y	-162.53	0.0	2.55
74	90004-1	53Z			
75	90005-3	54Y	-65.27	1.8	13.25
76	90005-1	54Z			
77	90006-3	55Y	-93.93	2.2	12.75
78	90006-1	55Z			
79	90008-3	56Y	-122.93	2.2	12.75
80	90008-1	56Z			
81	90009-3	57Y	-142.33	2.2	12.75
82	90009-1	57Z			
83	90010-3	58Y	-162.13	1.8	13.25
84	90010-1	58Z			
85	90016-3	59Y	-162.13	1.8	-8.15
86	90016-1	59Z			
87	90015-3	60Y	-142.33	2.2	-7.65
88	90015-1	60Z			
89	90014-3	61Y	-122.93	2.2	-7.65
90	90014-1	61Z			
91	90012-3	62Y	-93.93	2.2	-7.65
92	90012-1	62Z			
93	90011-3	63Y	-65.27	1.8	-8.15
94	90011-1	63Z			
95 - 98	Unused				

Ring Truss and Tripod Interface

Meas. Number	NASTRAN Grid	Point & Dir	X (in.)	Y (in.)	Z (in.)
99	7005-1	68X	59.1	0.0	5.1
100	7005-2	68Y			
101	7005-3	68Z			
102	2070-3	69Z	55.25	14.80	5.1
103	2145-1	70X	38.25	38.25	5.1
104	2145-2	70Y			
105	2145-3	70Z			
106	2230-3	71Z	14.80	55.25	5.1
107	2265-1	72X	0.0	54.10	5.1
108	2265-3	72Y			
109	2310-3	73Z	-14.80	55.25	5.1
110	2385-1	74X	-38.25	38.25	5.1
111	2385-2	74Y			
112	2385-3	74Z			
113	2470-3	75Z	-55.25	14.80	5.1
114	9005-1	76X	-59.1	0.0	5.1
115	9005-2	76Y			
116	9005-3	76Z			
117	2585-1	77X	-46.85	-27.05	5.1
118	2585-2	77Y			
119	2585-3	77Z			
120	2670-1	78Z	-28.6	-49.54	5.1
121	2710-3	79Z	-14.80	-55.25	5.1

Ring Truss and Tripod Interface (Cont.)

Meas. Number	NASTRAN Grid	Point & Dir	X (in.)	Y (in.)	Z (in.)
122	2745-1	80X	0.0	-54.1	5.1
123	2745-3	80Z			
124	2790-3	81Z	14.80	-55.25	5.1
125	2830-1	82Z	28.60	-49.54	5.1
126	2905-1	83X	46.85	-27.05	5.1
127	2905-2	83Y			
128	2905-3	83Z			
129	2119-1	84X	39.24	37.24	-1.85
130	2119-2	84Y			
131	2119-3	84Z			
132	2279-1	85X	1.34	50.98	9.25
133	2279-3	85Z			
134-135	Unused				
136	2359-1	88X	-39.24	37.24	-1.85
137	2359-2	88Y			
138	2359-3	88Z			
139	2599-1	89X	-44.82	-24.34	5.65
140	2599-2	89Y			
141	2599-3	89Z			
142	27151-1	90X	1.34	-51.28	9.25
143	27151-3	90Z			
144	4002-1	91X	0.0	-59.1	5.65
145	4002-2	91Y			
146	4002-3	91Z			
147	2919-1	92X	44.82	-24.34	9.25
148	2919-2	92Y			
149	2919-3	92Z			

Ring Truss and Tripod Interface (Cont.)

Meas. Number	NASTRAN Grid	Point & Dir	X (in.)	Y (in.)	Z (in.)
150	2970-3	93Z	38.25	38.25	128.0
151	2980-3	94Z	-38.25	38.25	128.0
152	2990-3	95Z	0.0	-54.10	128.0
153	30002-1	96X	5.75	0.0	113.0
154	30002-2	96Y			
155	30002-3	96Z			
156	30003-1	97X	-5.75	0.0	113.0
157	30003-2	97Y			
158	30003-3	97Z			
159	30001-1	98X	0.0	-5.75	113.0
160	30001-2	98Y			
161	30001-3	98Z			
162	Ground	99X	38.25	38.25	173.0
163		99Y			
164		99Z			
165	Ground	100X	-38.25	38.25	173.0
166		100Y			
167		100Z			
168	Ground	101X	0.0	-54.10	173.0
169		101Y			
170		101Z			

Tripod Leg 1

Meas. Number	NASTRAN Grid	Point & Dir	X (in.)	Y (in.)	Z (in.)
171	30103-1	102X	0.0	23.69	70.4
172	30104-2	102Y			
173	31002-1	103X	0.0	5.72	110.3
174	31006-2	103Y			

Tripod Leg 2

Meas. Number	NASTRAN Grid	Point & Dir	X (in.)	Y (in.)	Z (in.)
175	30303-1	104X	-20.52	-11.85	70.4
176	30304-2	104Y			
177	33002-1	105X	-4.95	-2.86	110.3
178	33006-2	105Y			

Tripod Leg 3

Meas. Number	NASTRAN Grid	Point & Dir	X (in.)	Y (in.)	Z (in.)
179	30203-1	106X	20.52	-11.85	70.4
180	30204-2	106Y			
181	32002-1	107X	4.95	-2.86	110.3
182	32006-2	107Y			

The drawings on the following pages show details of the positions of the measurement points and measurement numbers on the modified structure.

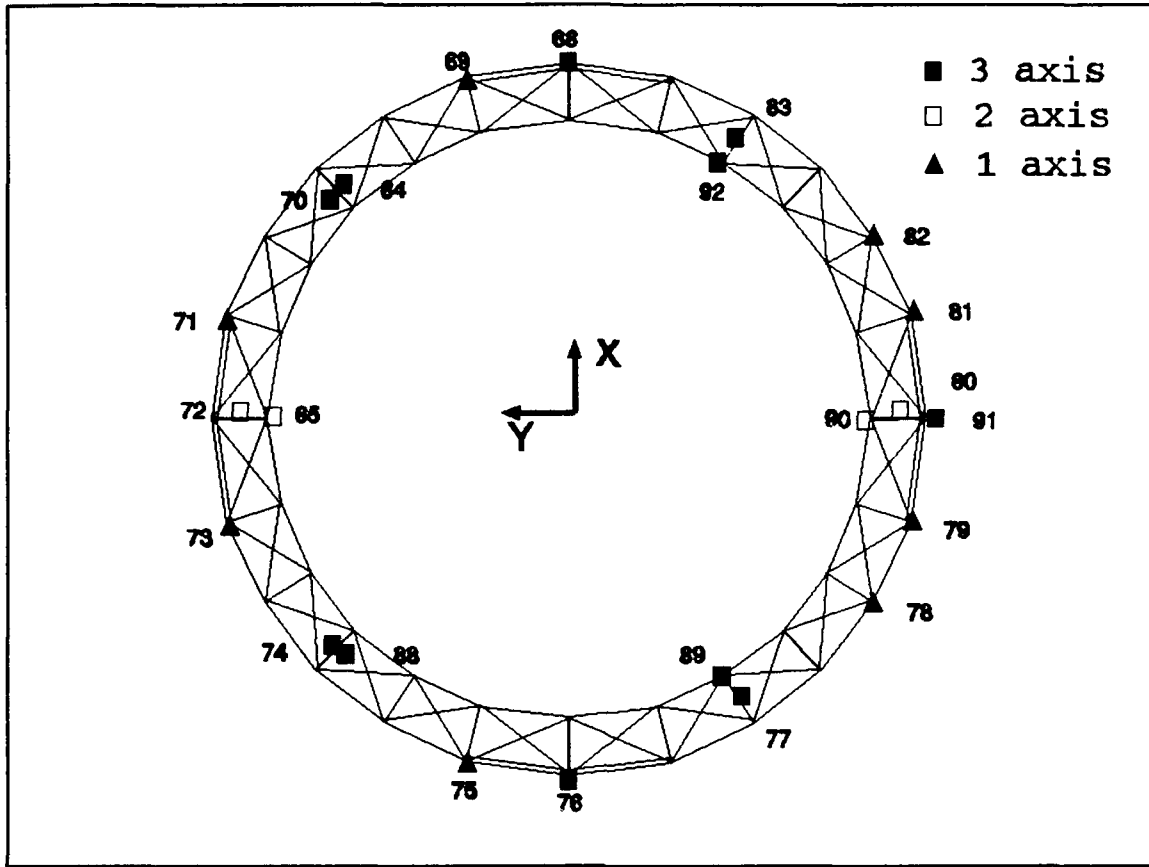


Figure 24. Ring Truss Measurement Points

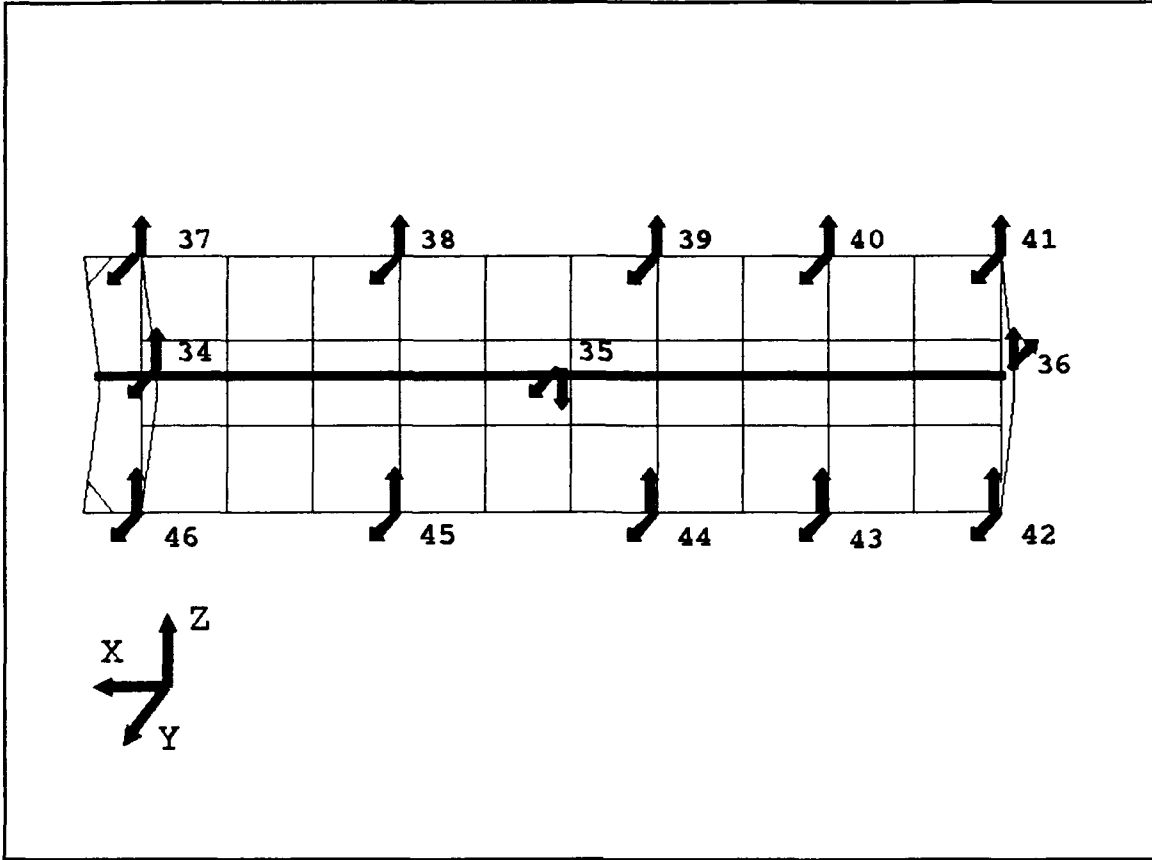


Figure 25. Solar Array 1 Measurement Points

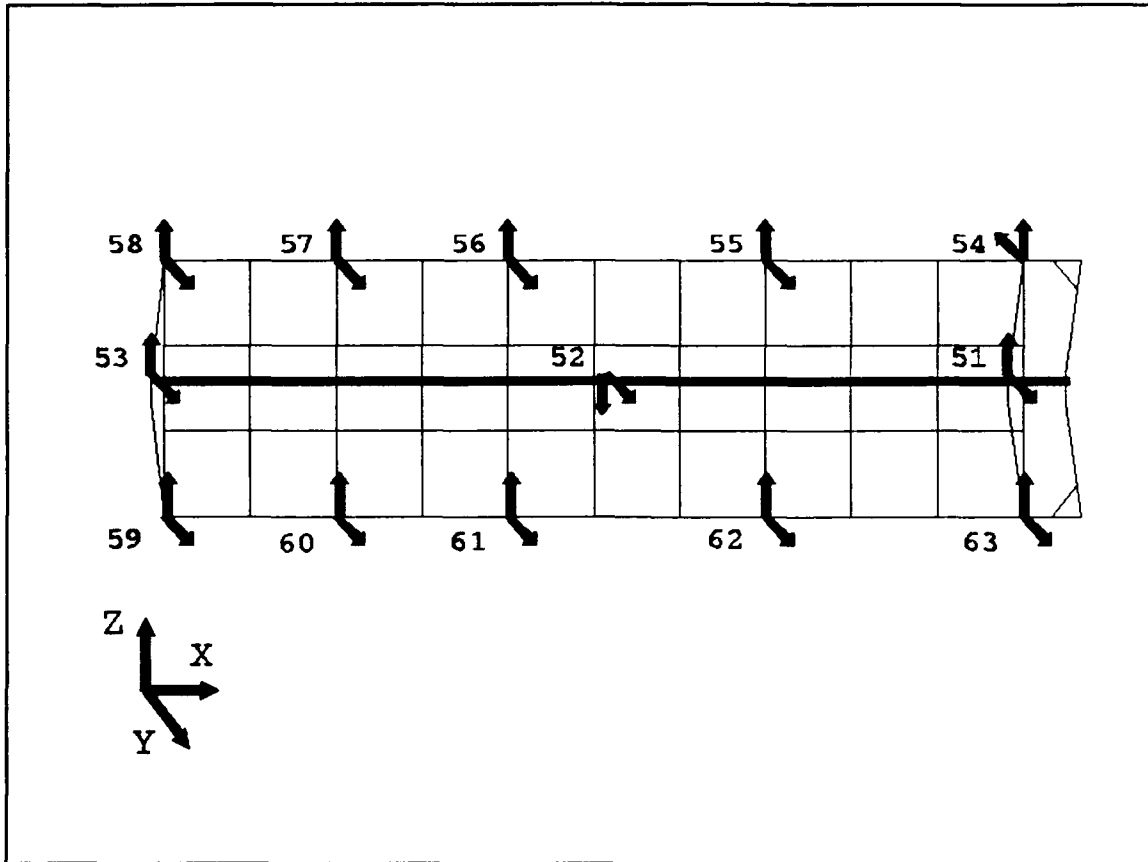


Figure 26. Solar Array 2 Measurement Points

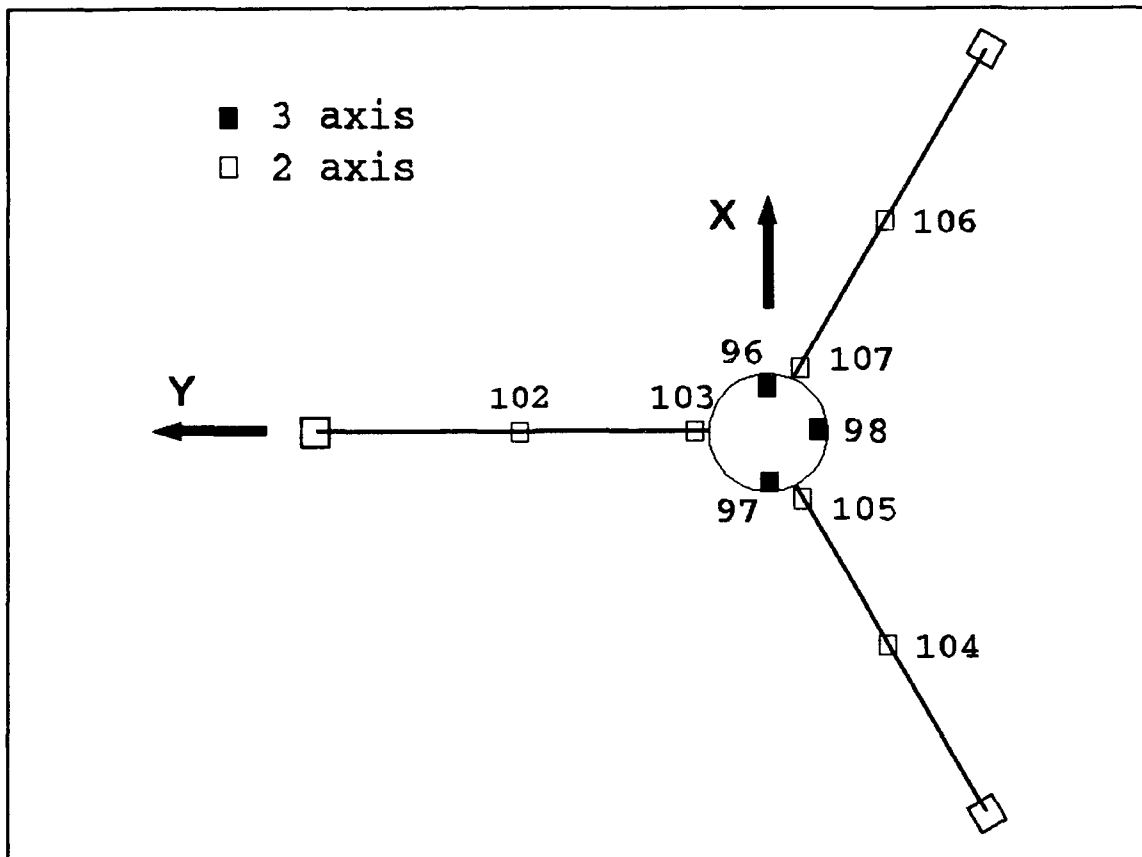


Figure 27. Tripod Measurement Points

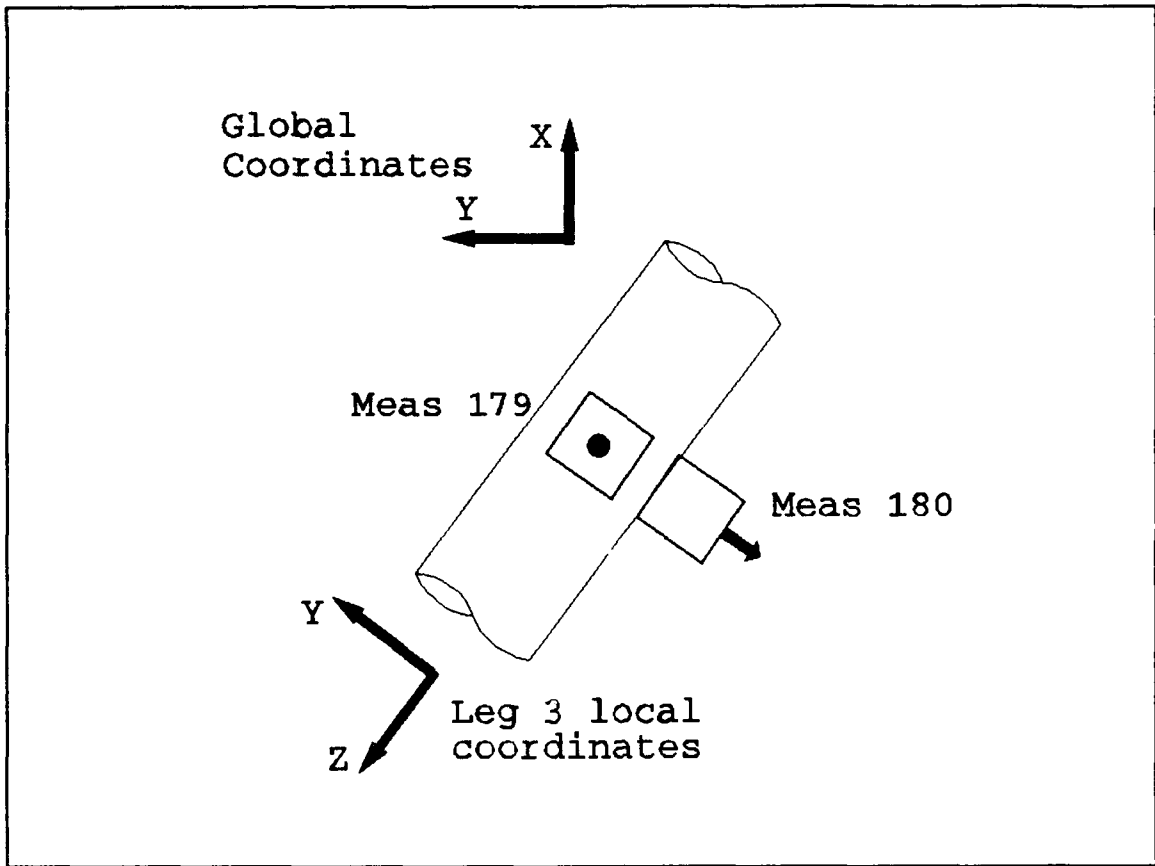


Figure 28. Detail of Typical Tripod Leg Measurements

Appendix B. Guyan-Reduced Model Information

This appendix includes reference information pertaining to the Guyan-reduction of the finite element model to 182 DOF. Included are a listing of the 182 retained DOF and the resulting 48 mode shapes below 20 Hz.

DOF in the Guyan-Reduced 182 DOF Model

182 DOF <u>Row</u>	NASTRAN <u>Grid-Dir</u>	182 DOF <u>Row</u>	NASTRAN <u>Grid-Dir</u>
1	70003-1	41	70005-1
2	70003-3	42	70005-3
3	70002-1	43	70001-1
4	70002-3	44	70001-3
5	70004-1	45	2070-3
6	70004-3	46	2021-3
7	7173-1	47	20211-3
8	7173-2	48	2970-3
9	7173-3	49	2145-1
10	7173-4	50	2145-2
11	7173-5	51	2145-3
12	7173-6	52	2119-1
13	70010-1	53	2119-2
14	70010-3	54	2119-3
15	70016-1	55	11-1
16	70016-3	56	11-2
17	7172-1	57	11-3
18	7172-2	58	2230-3
19	7172-3	59	5402-3
20	7172-4	60	5401-3
21	7172-5	61	2231-3
22	7172-6	62	22311-3
23	70015-1	63	2265-1
24	70015-3	64	2265-3
25	70009-1	65	2279-1
26	70009-3	66	2279-3
27	70014-1	67	2310-3
28	70014-3	68	2311-3
29	70008-1	69	23111-3
30	70008-3	70	30104-2
31	70013-1	71	30103-1
32	70013-3	72	31002-1
33	70007-1	73	31006-2
34	70007-3	74	2905-1
35	70012-1	75	2905-2
36	70012-3	76	2905-3
37	70006-1	77	2919-1
38	70006-3	78	2919-2
39	70011-1	79	2919-3
40	70011-3	80	2830-1

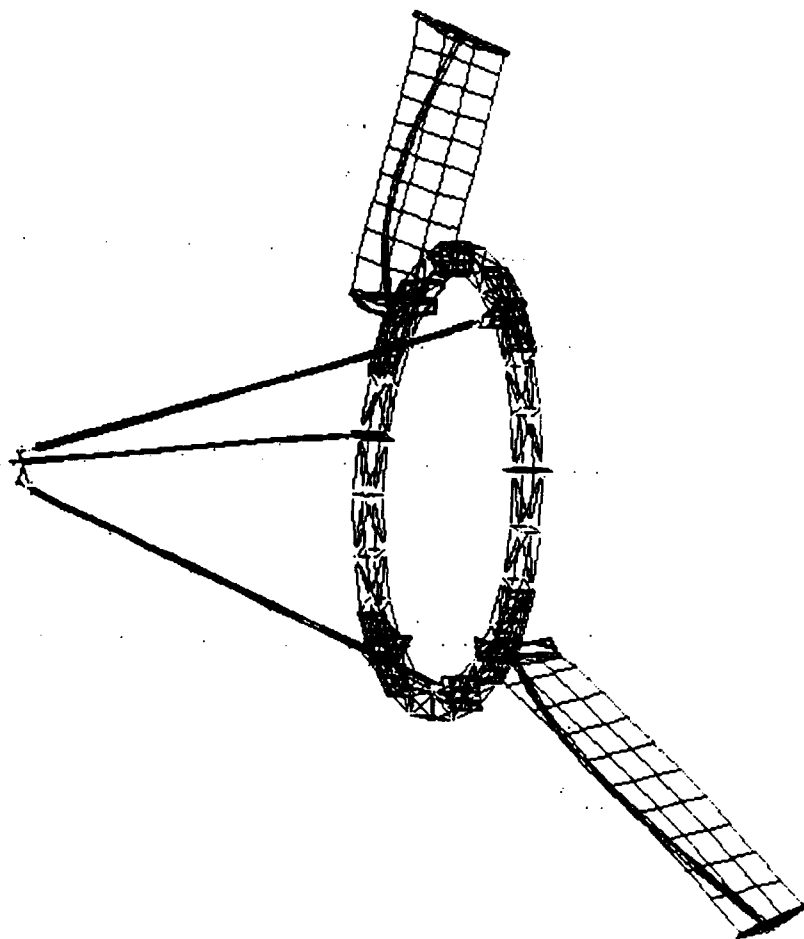
DOF in the Guyan-Reduced 182 DOF Model (Cont.)

182 DOF <u>Row</u>	NASTRAN <u>Grid-Dir</u>	182 DOF <u>Row</u>	NASTRAN <u>Grid-Dir</u>
81	30204-2	121	30303-1
82	30203-1	122	30304-2
83	32002-1	123	33002-1
84	32006-2	124	33006-2
85	2790-3	125	2470-3
86	4002-1	126	90005-1
87	4002-2	127	90005-3
88	4002-3	128	90011-1
89	2791-3	129	90011-3
90	27911-3	130	90001-1
91	2745-1	131	90001-3
92	2745-3	132	90003-1
93	2990-3	133	90003-3
94	27151-1	134	90002-1
95	27151-3	135	90002-3
96	31-1	136	90006-1
97	31-2	137	90006-3
98	31-3	138	90012-1
99	2710-3	139	90012-3
100	27111-3	140	90007-1
101	271111-3	141	90007-3
102	2670-1	142	90013-1
103	2980-3	143	90013-3
104	2385-1	144	90008-1
105	2385-2	145	90008-3
106	2385-3	146	90014-1
107	2359-1	147	90014-3
108	2359-2	148	90009-1
109	2359-3	149	90009-3
110	21-1	150	90015-1
111	21-2	151	90015-3
112	21-3	152	90010-1
113	2585-1	153	90010-3
114	2585-2	154	9172-1
115	2585-3	155	9172-2
116	2599-1	156	9172-3
117	2599-2	157	9172-4
118	2599-3	158	9172-5
119	2501-3	159	9172-6
120	25011-3	160	90016-1

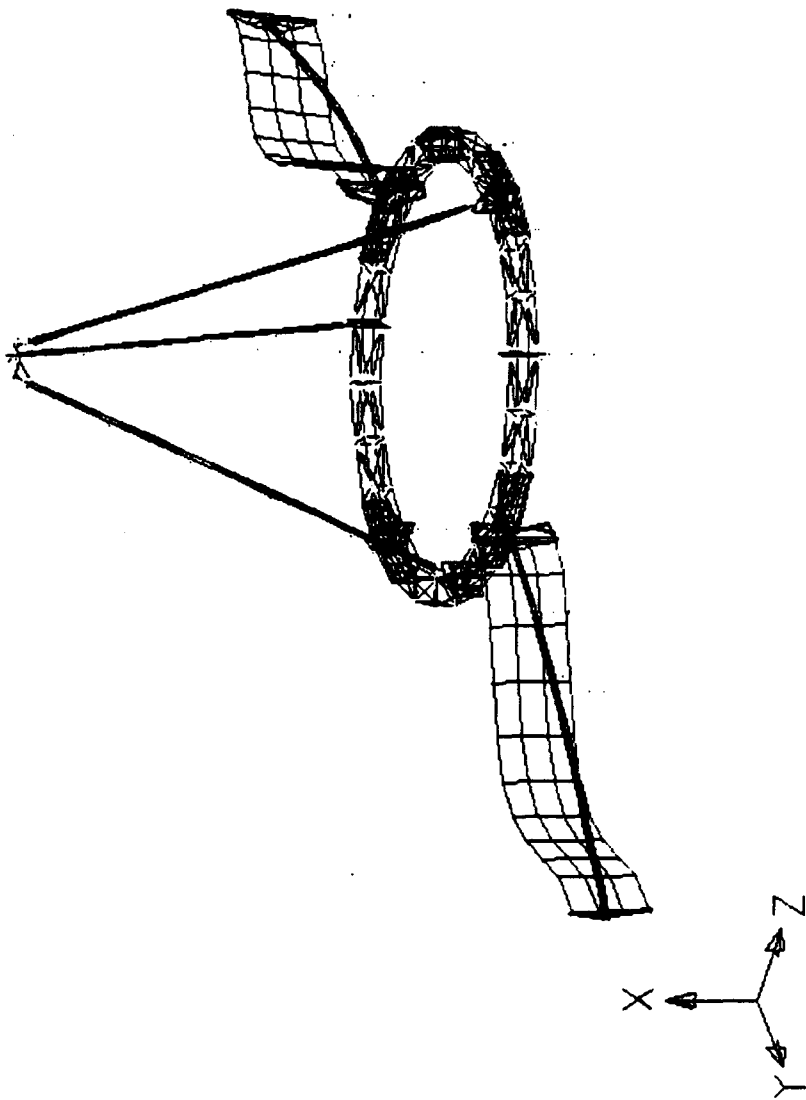
DOF in the Guyan-Reduced 182 DOF Model (Cont.)

182 DOF <u>Row</u>	<u>NASTRAN</u> <u>Grid-Dir</u>
161	90016-3
162	9173-1
163	9173-2
164	9173-3
165	9173-4
166	9173-5
167	9173-6
168	90004-1
169	90004-3
170	30001-1
171	30001-2
172	30001-3
173	30002-1
174	30002-2
175	30002-3
176	30003-1
177	30003-2
178	30003-3
179	300111-3
180	300112-2
181	300113-3
182	300114-2

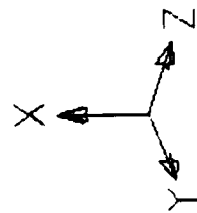
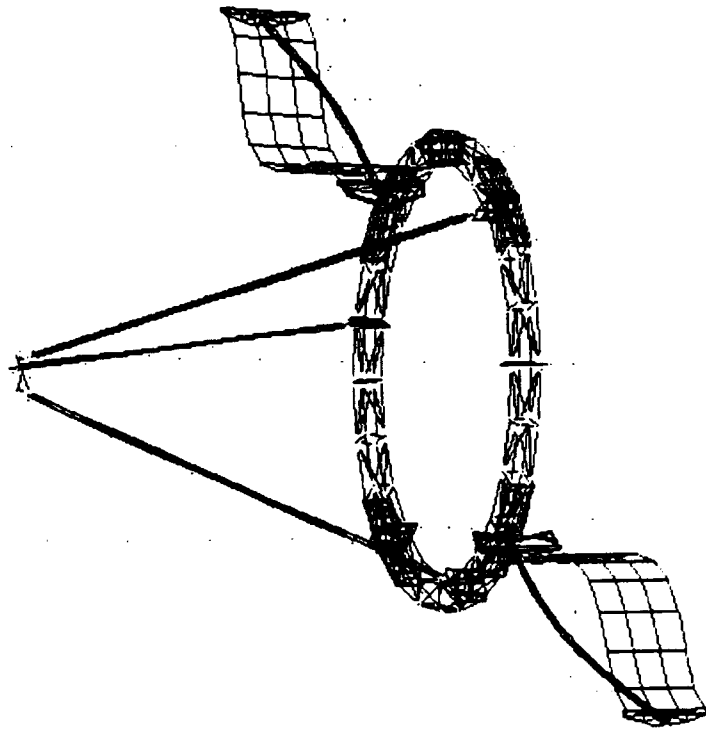
The following pages depict the 34 of the 48 mode shapes below 20 Hz as determined by the Guyan-reduced model. The first six modes are rigid body suspension modes and the 7th through 14th modes are actuator modes. These modes are not included for simplicity. These plots were generated by MSC/XL from the compatible results database produced by MSC/NASTRAN.



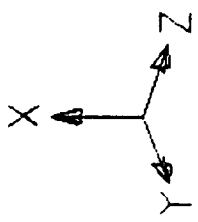
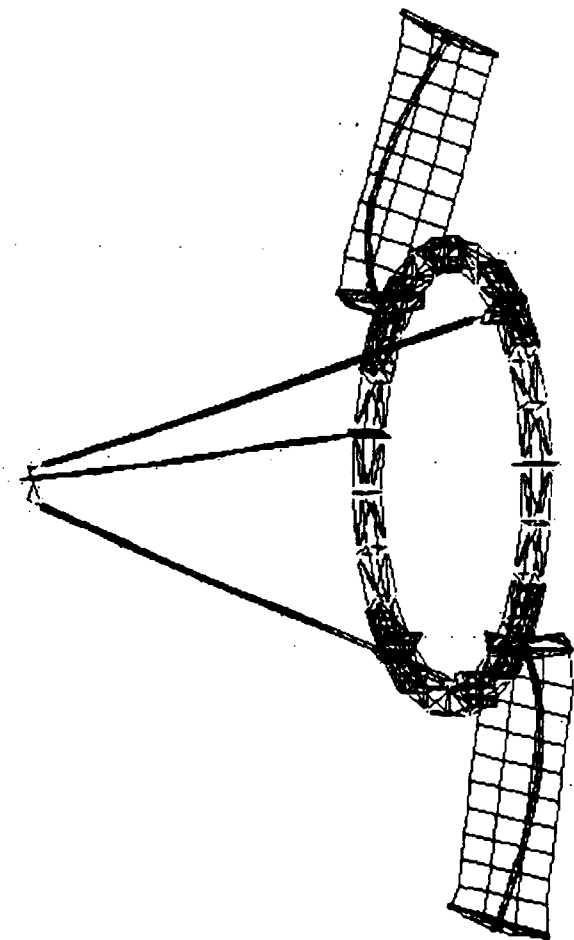
Mode 15. 1.634 Hz



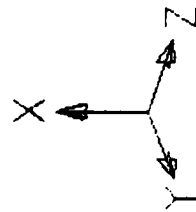
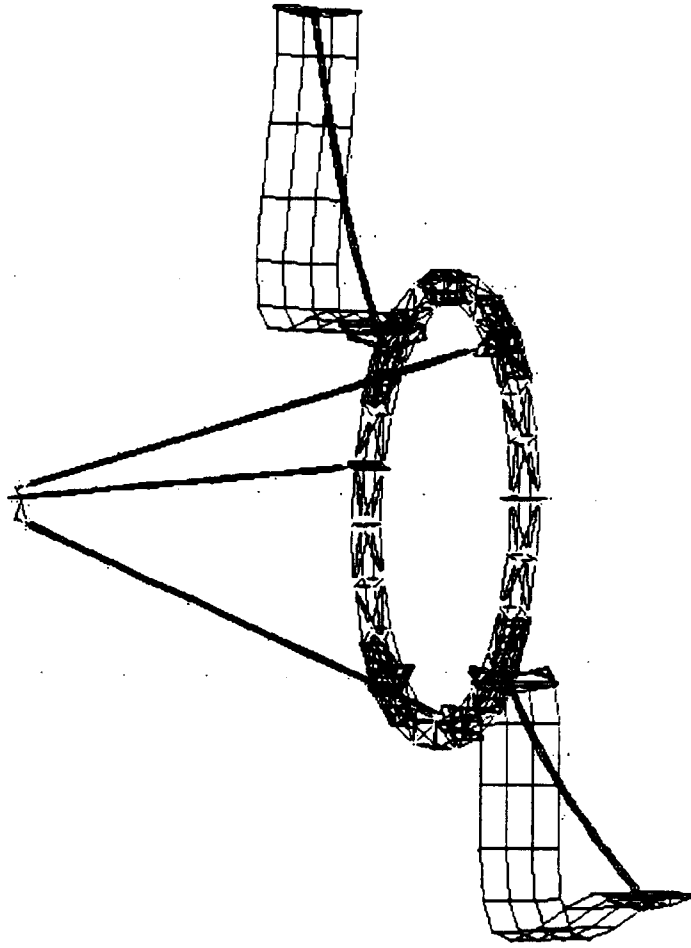
Mode 16. 1.715 Hz



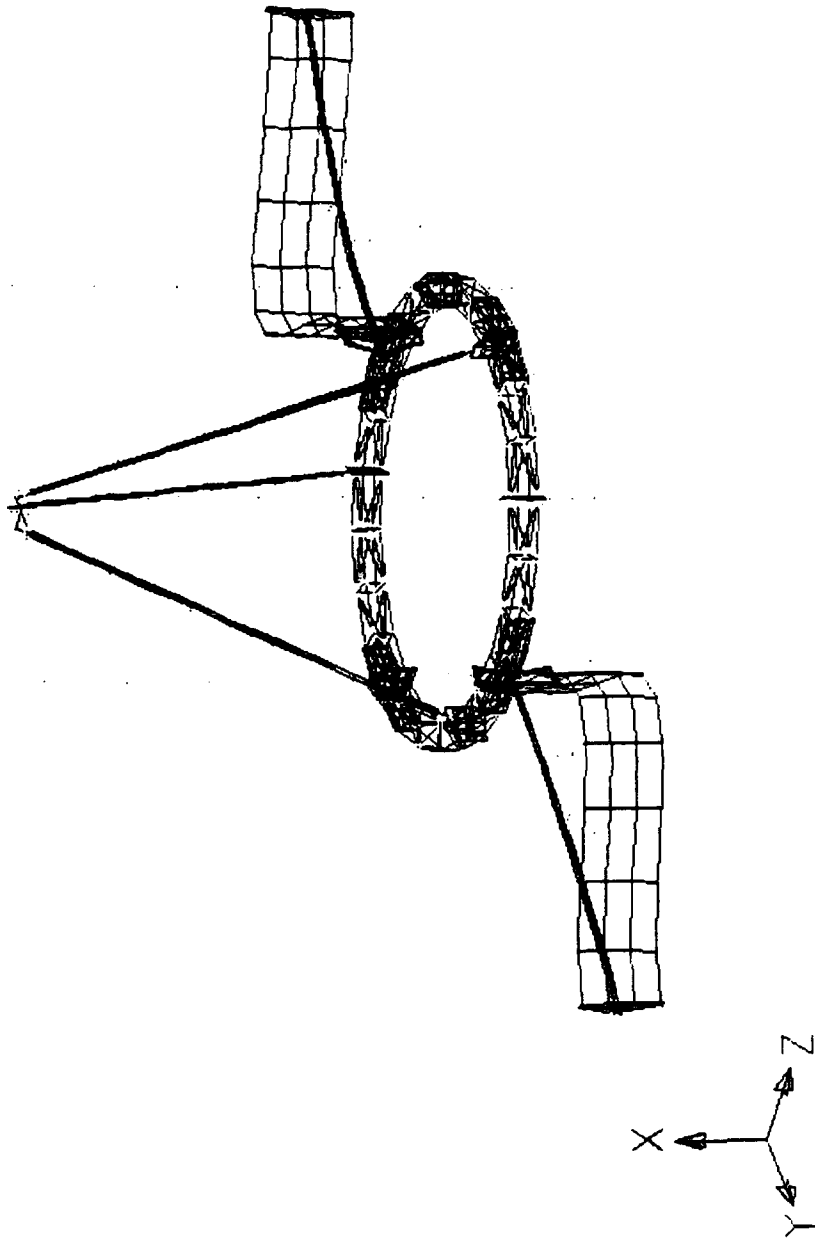
Mode 17. 1.813 Hz



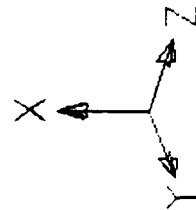
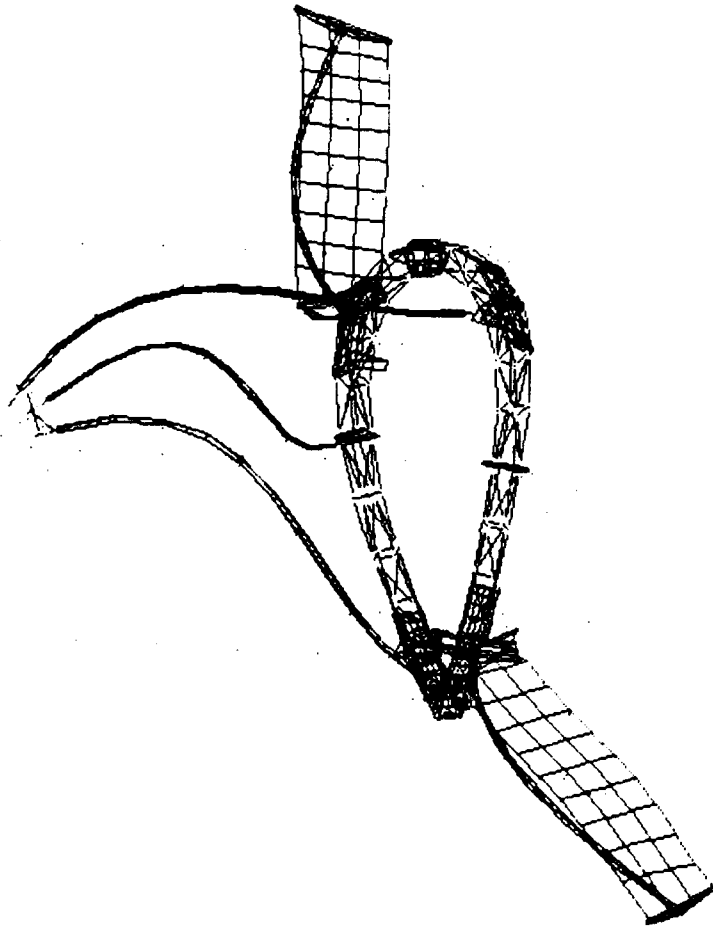
Mode 18. 1.845 Hz



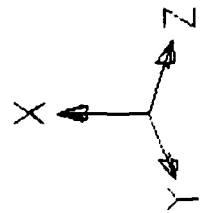
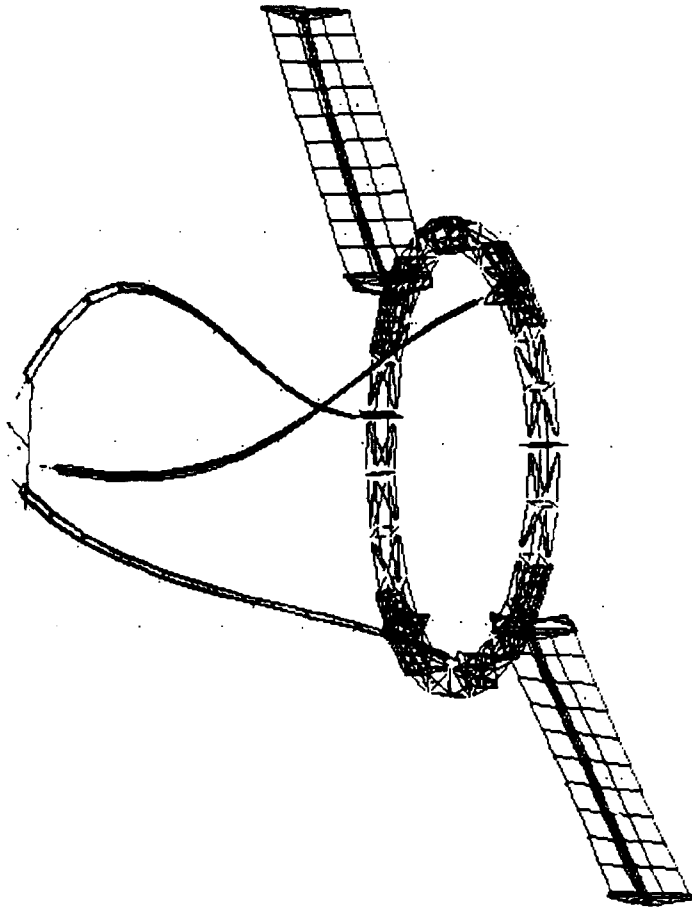
Mode 19. 2.406 Hz



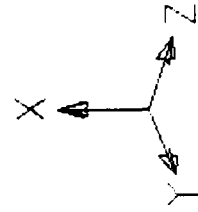
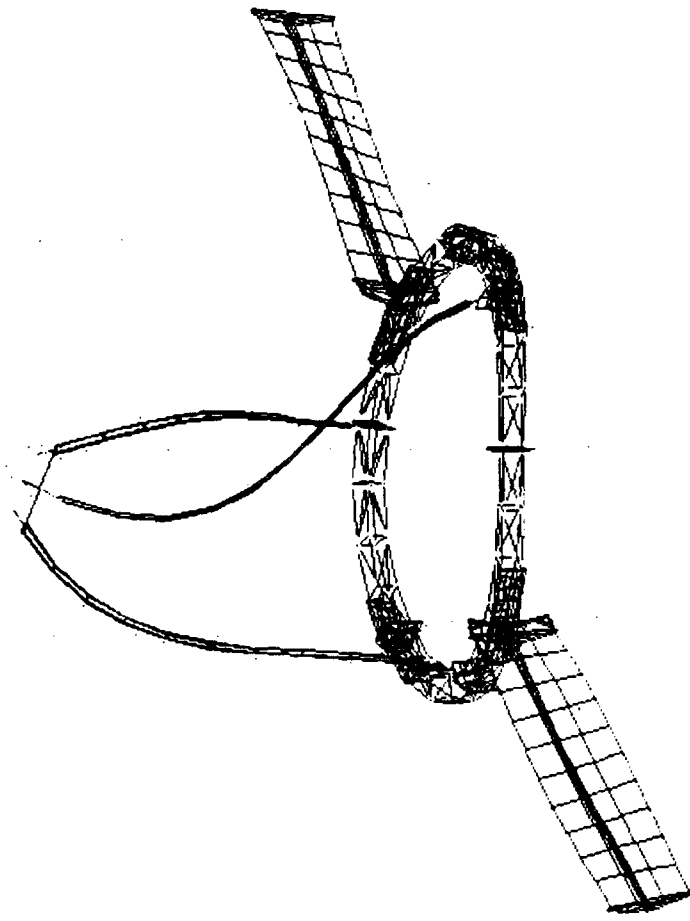
Mode 20. 2.409 Hz



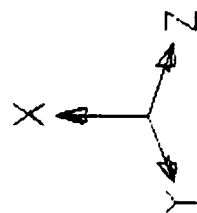
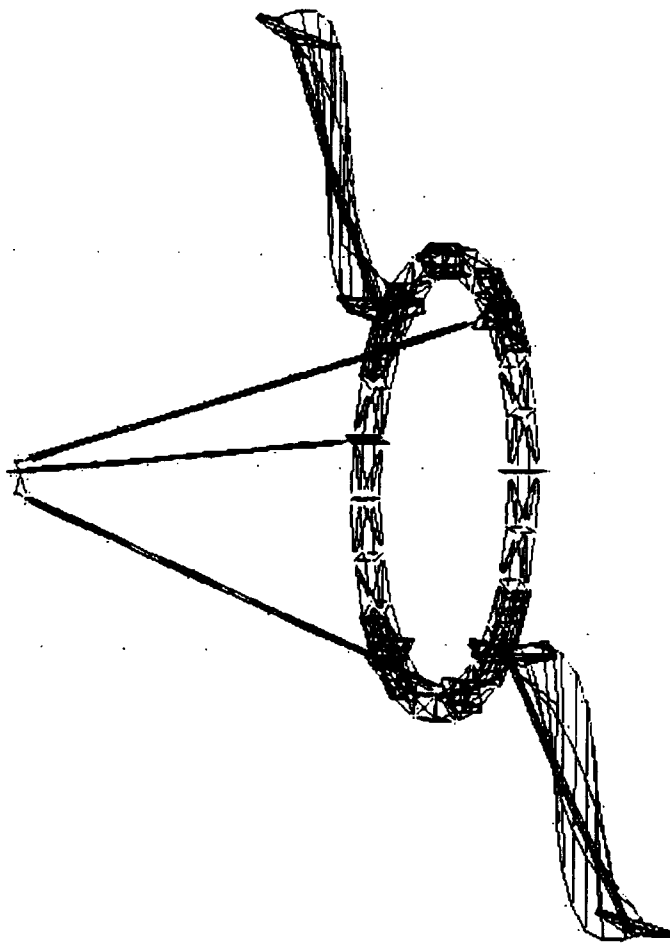
Mode 21. 4.336 Hz



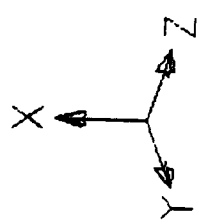
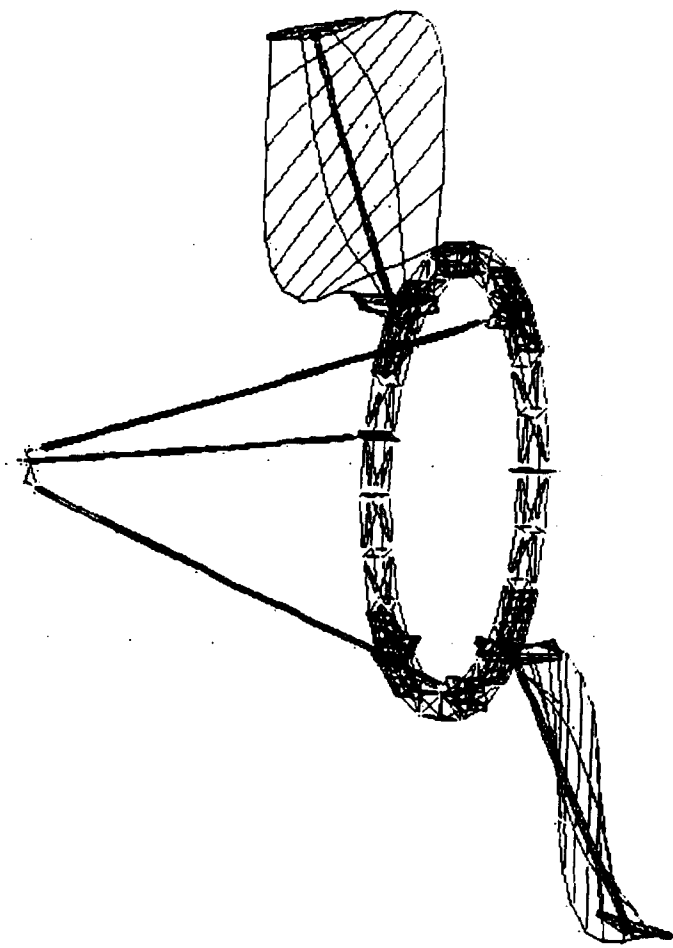
Mode 22. 4.396 Hz



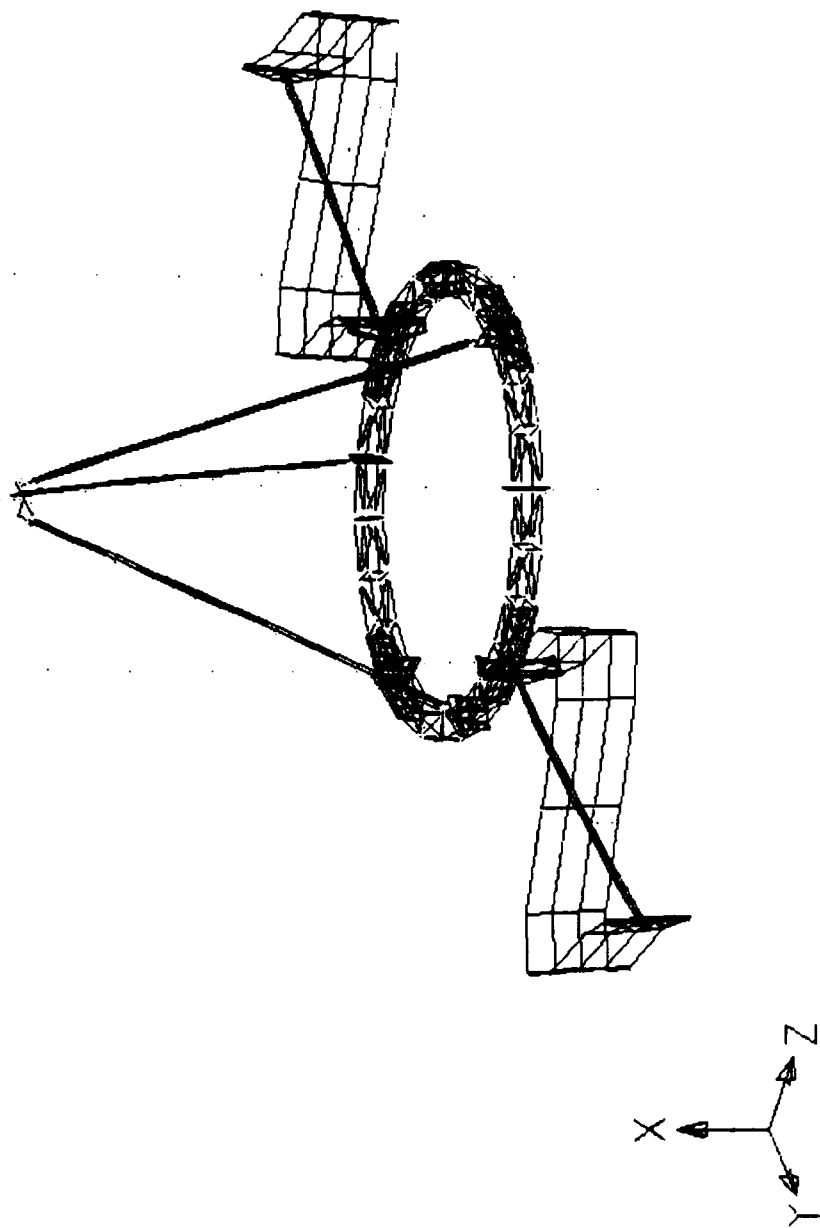
Mode 23. 4.434 Hz



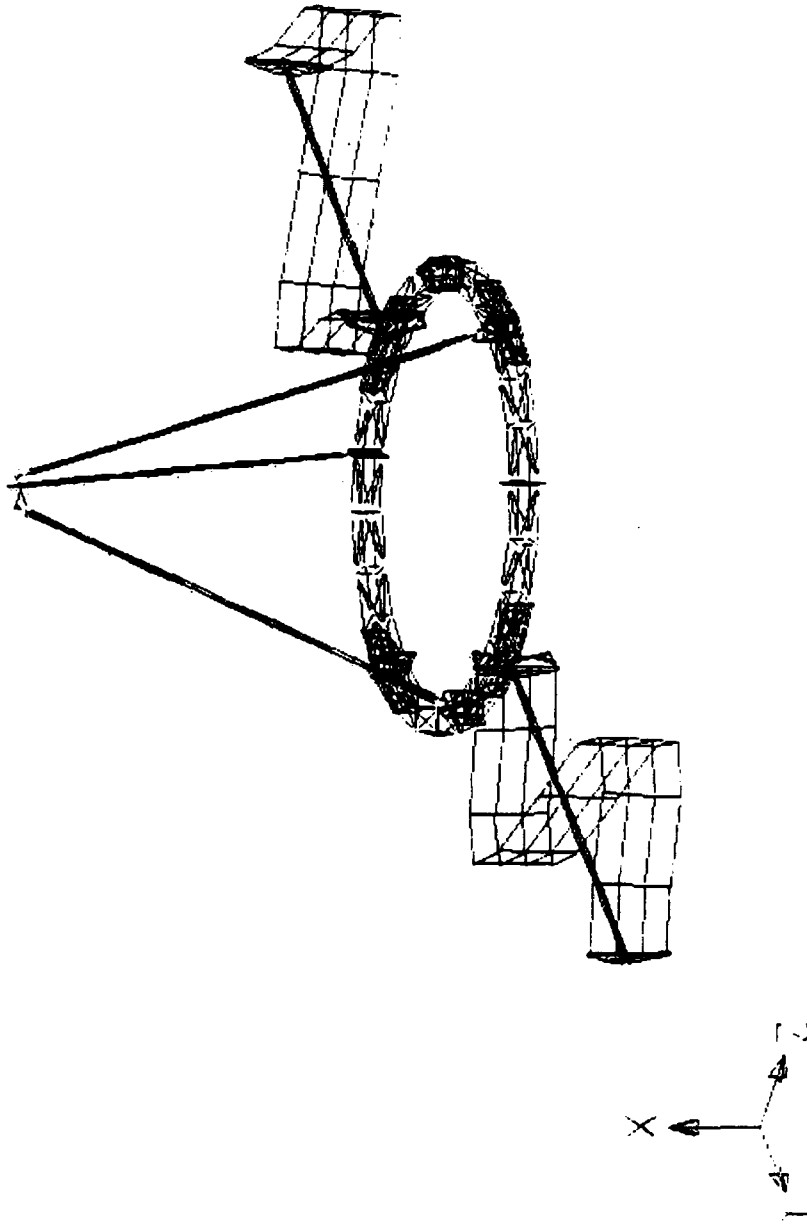
Mode 24. 5.432 Hz



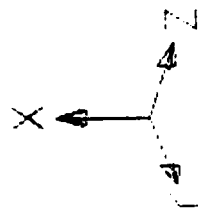
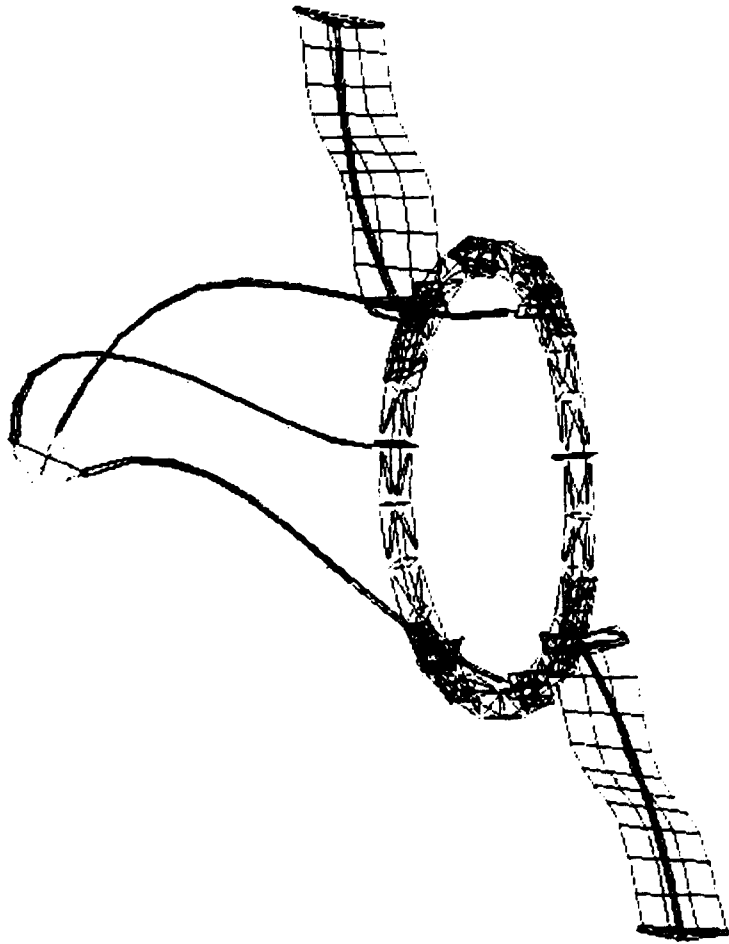
Mode 25. 5.433 Hz



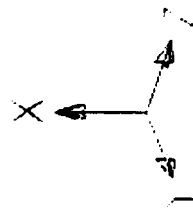
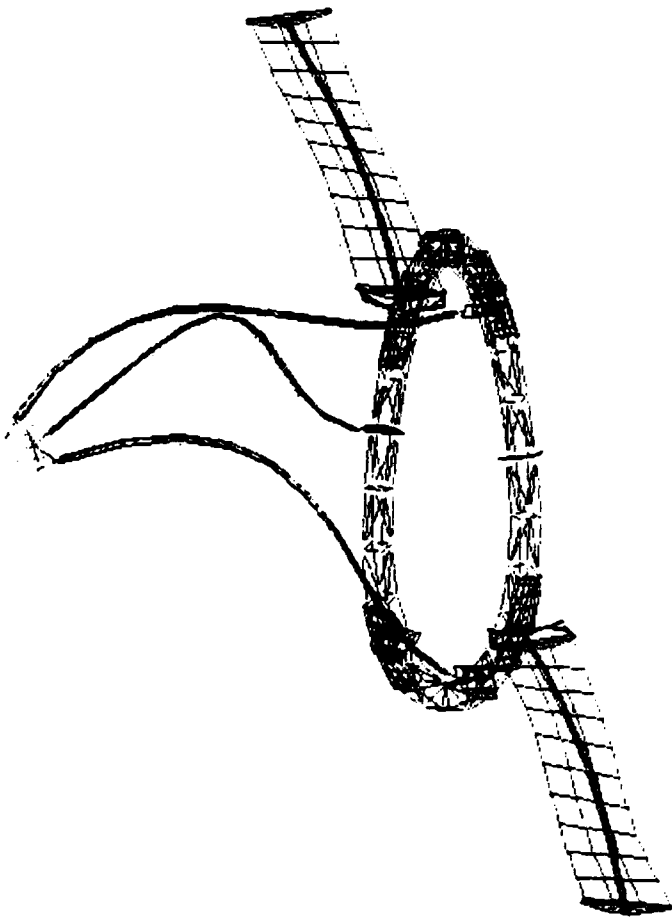
Mode 26. 6.183 Hz



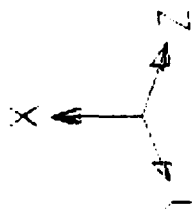
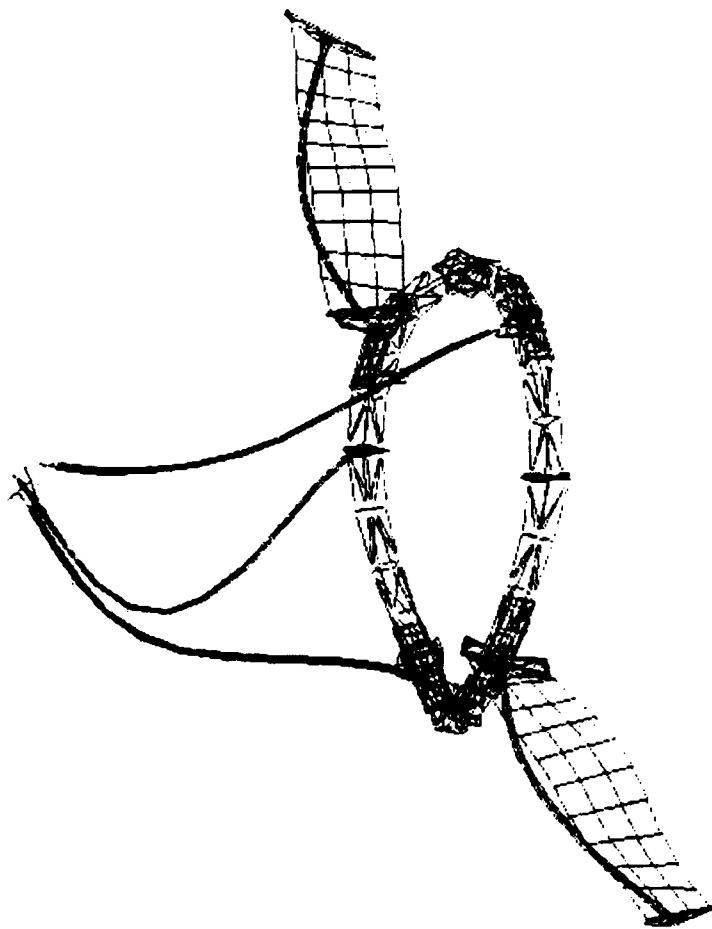
Mode 27. 6.184 Hz



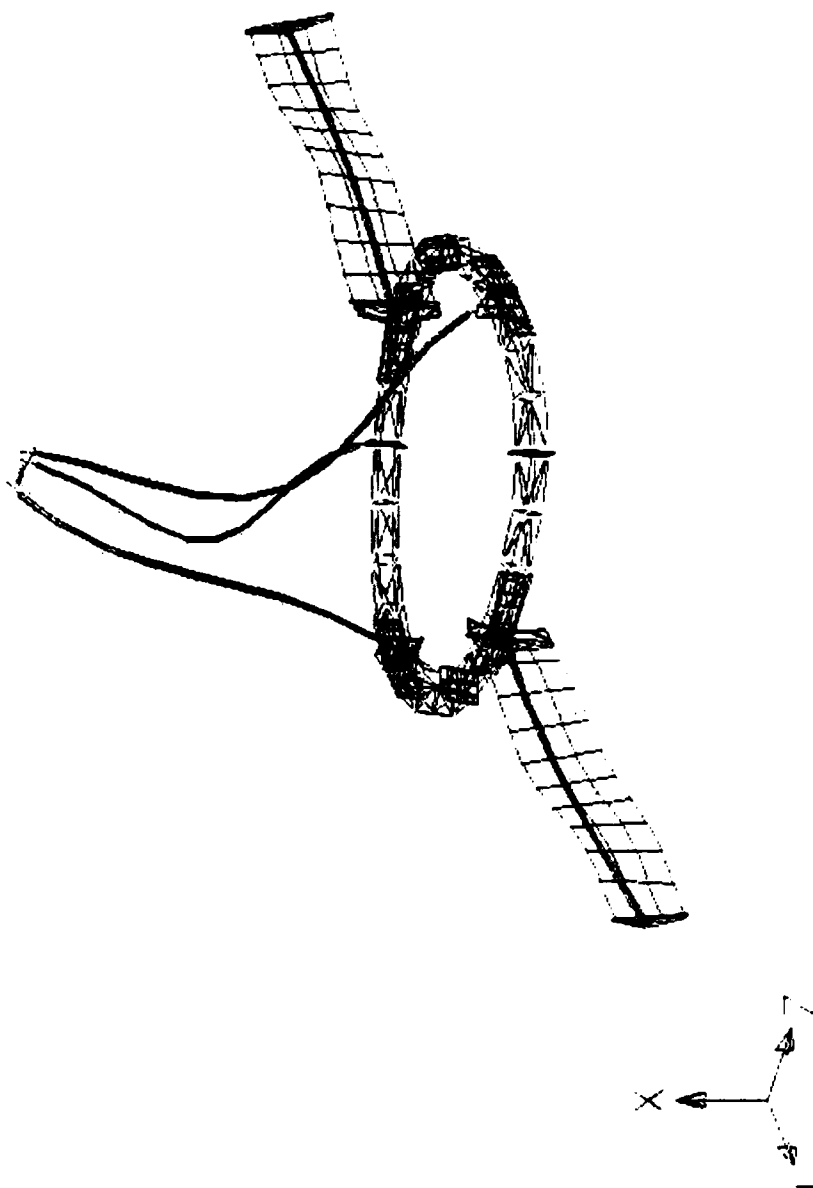
Mode 28. 6.900 Hz



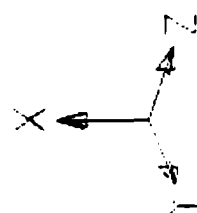
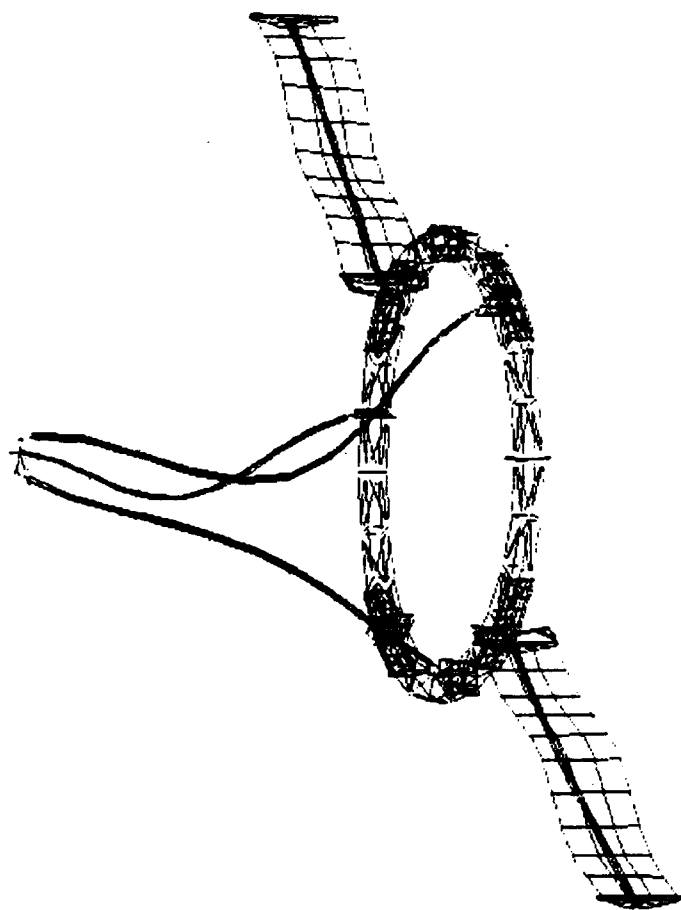
Mode 29. 7.008 Hz



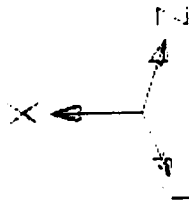
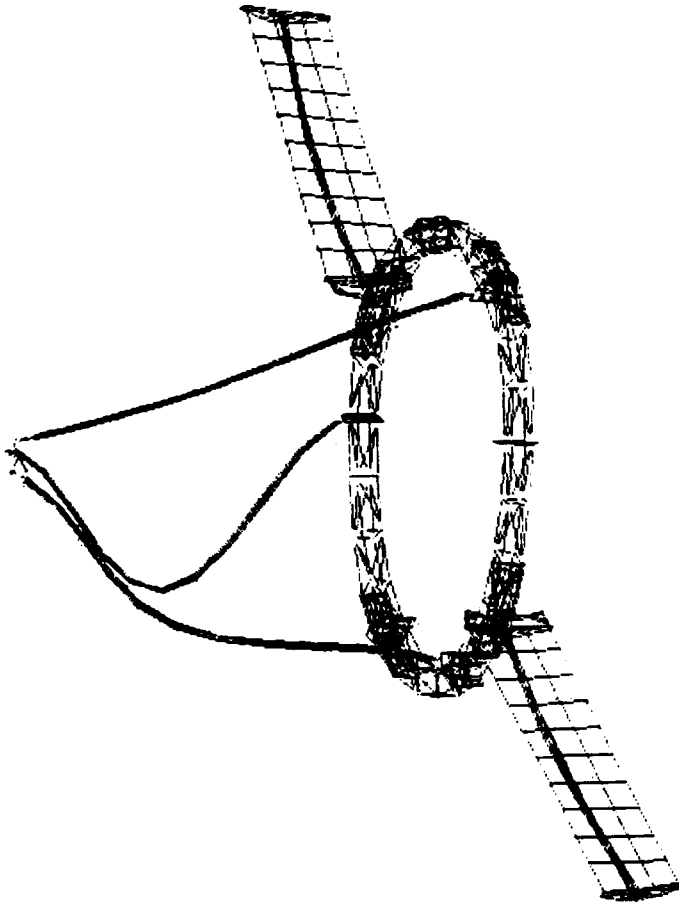
Mode 30. 9.277 Hz



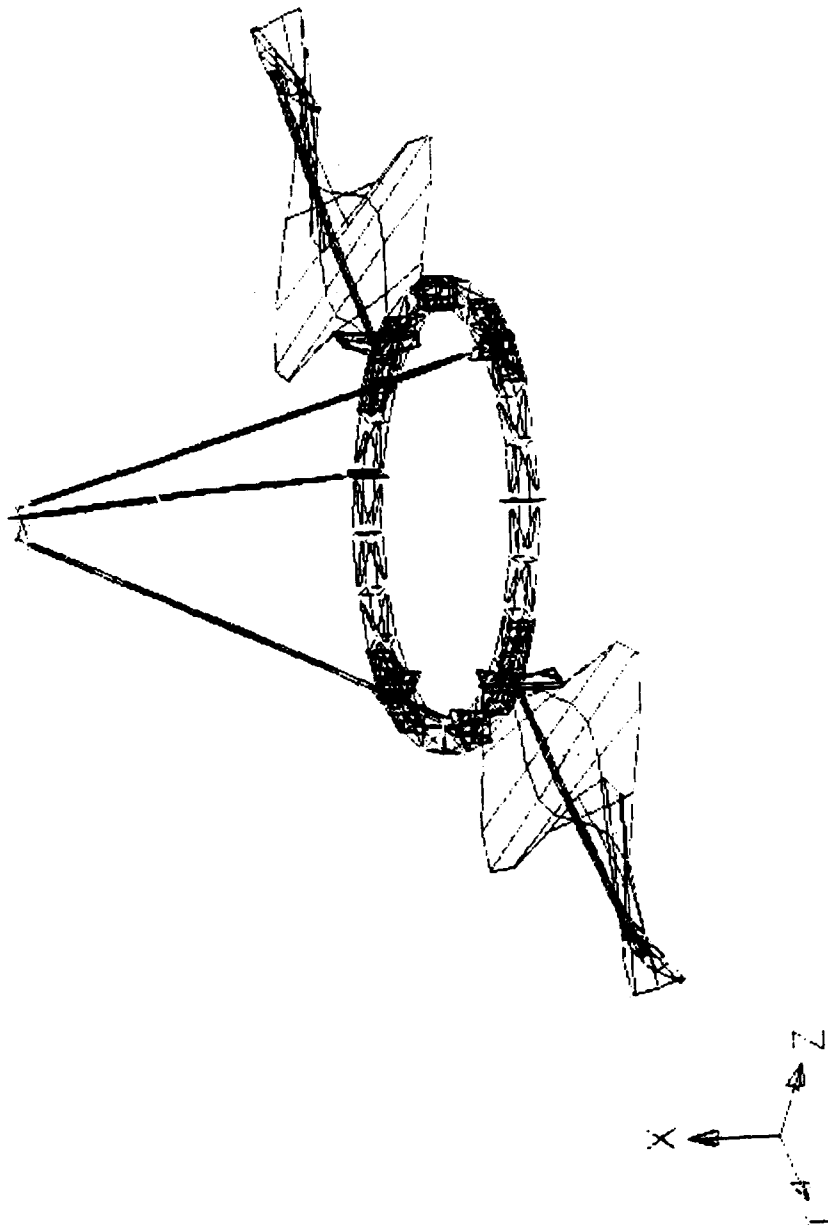
Mode 31. 9.463 Hz



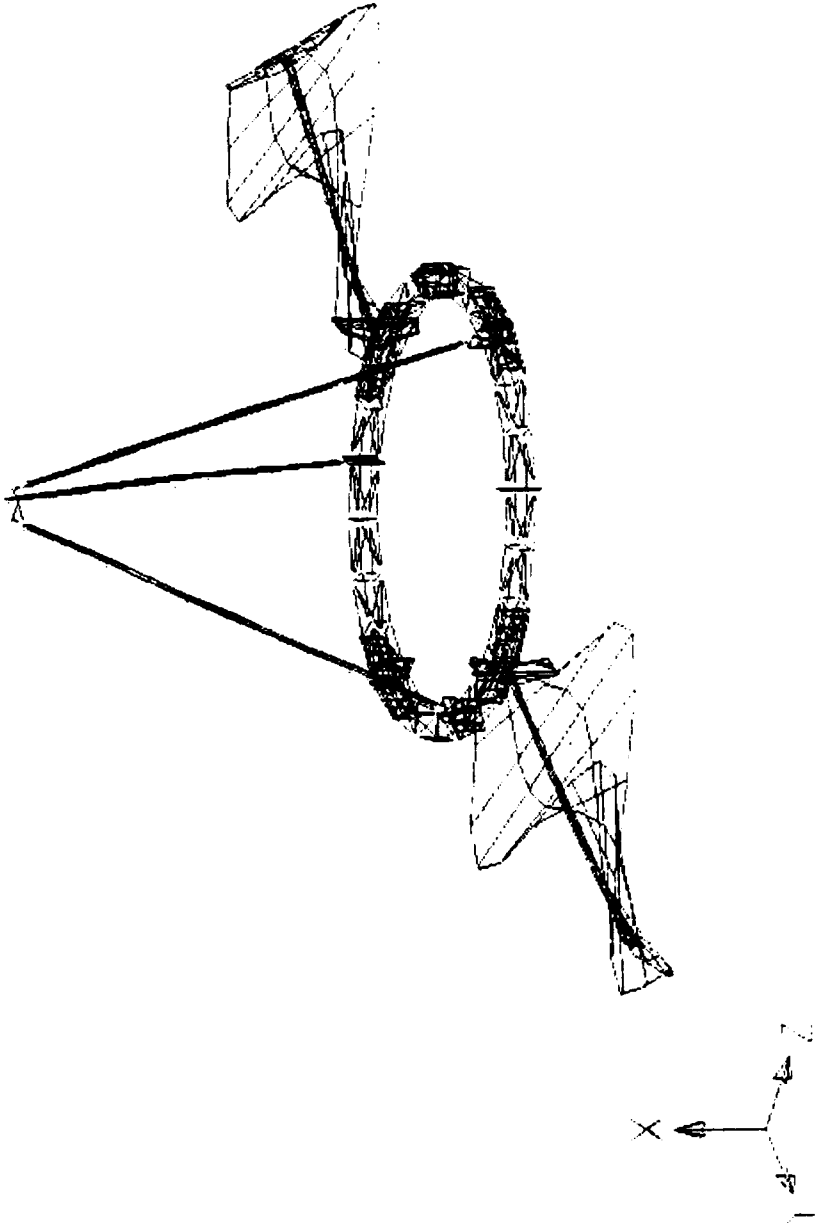
Mode 32. 10.915 Hz



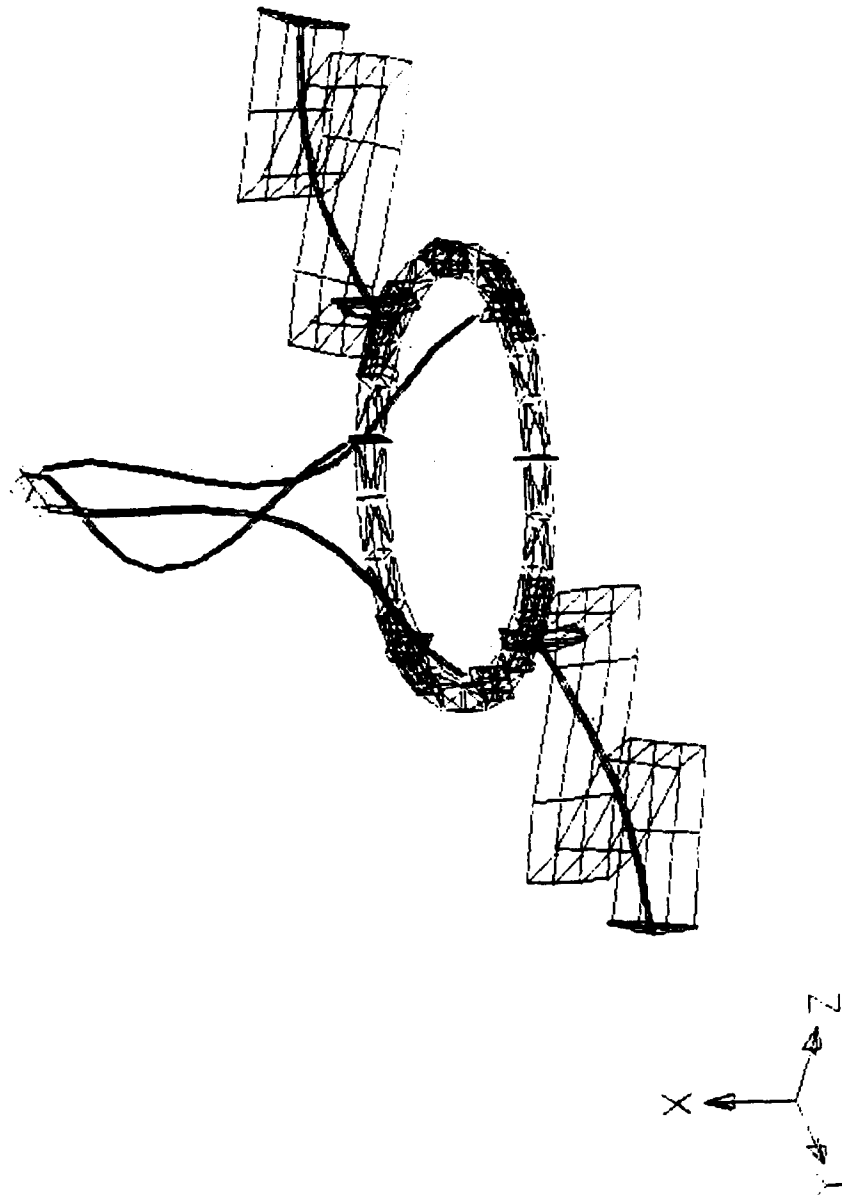
Mode 33. 10.962 Hz



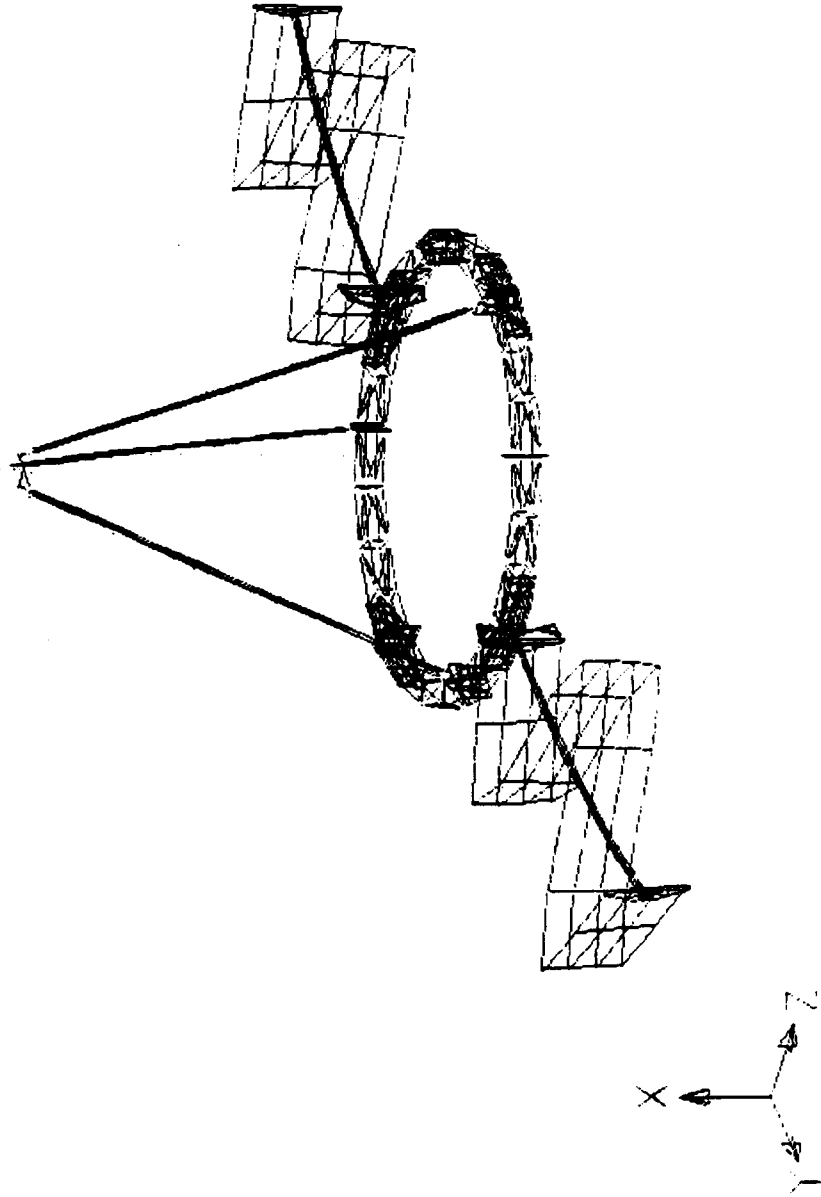
Mode 34. 11.152 Hz



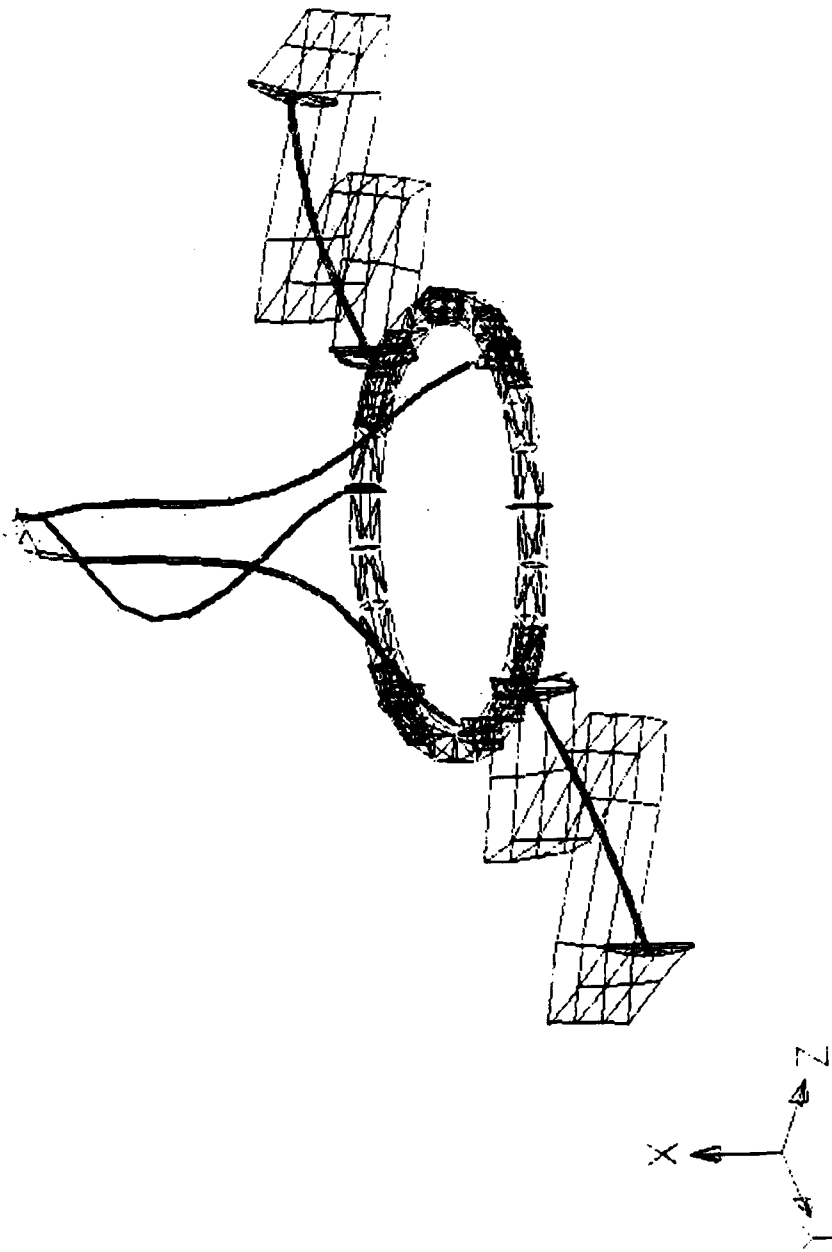
Mode 35. 11.152 Hz



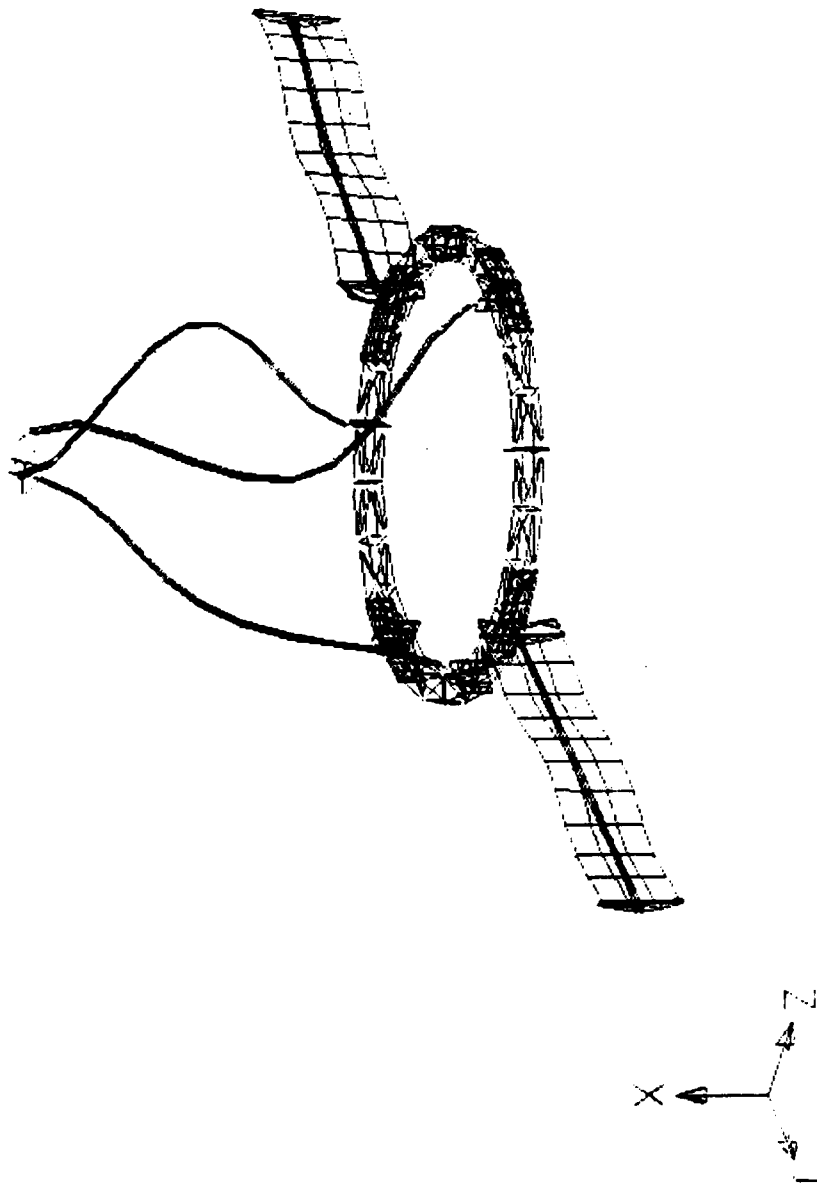
Mode 36. 12.377 Hz



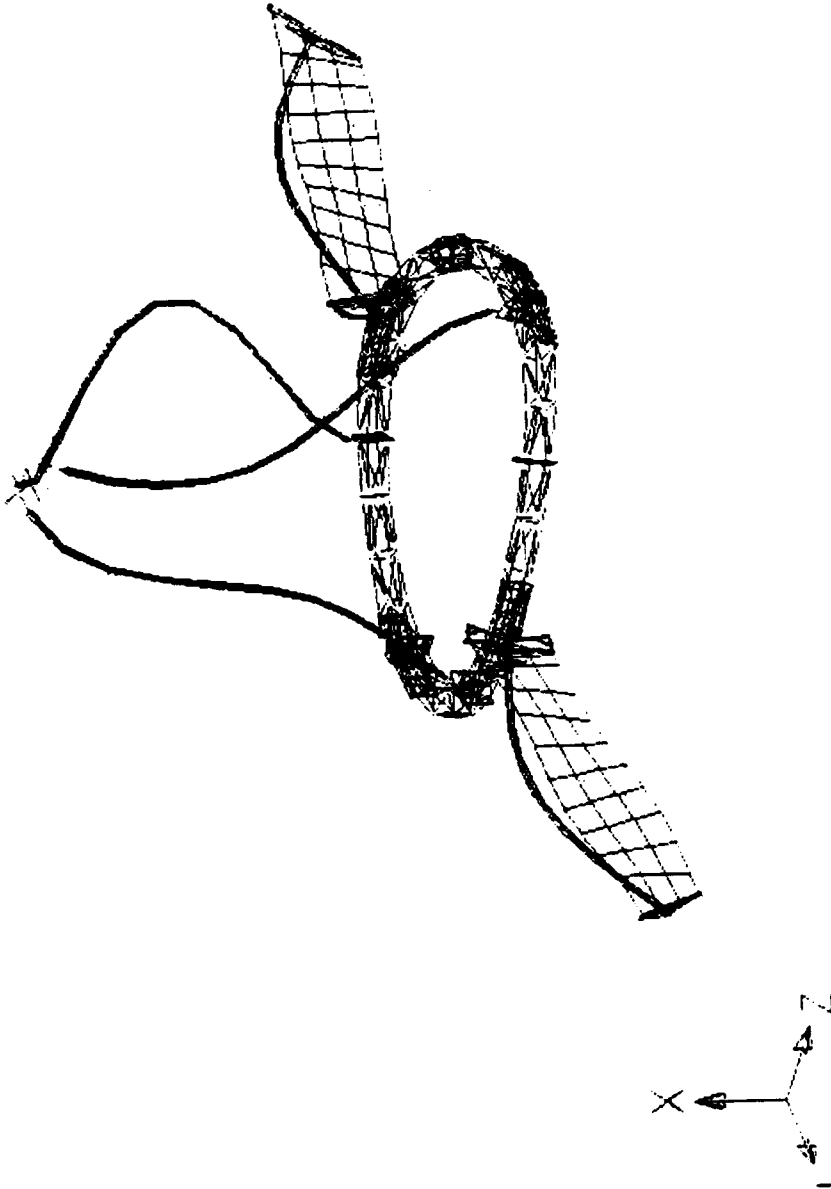
Mode 37. 12.729 Hz



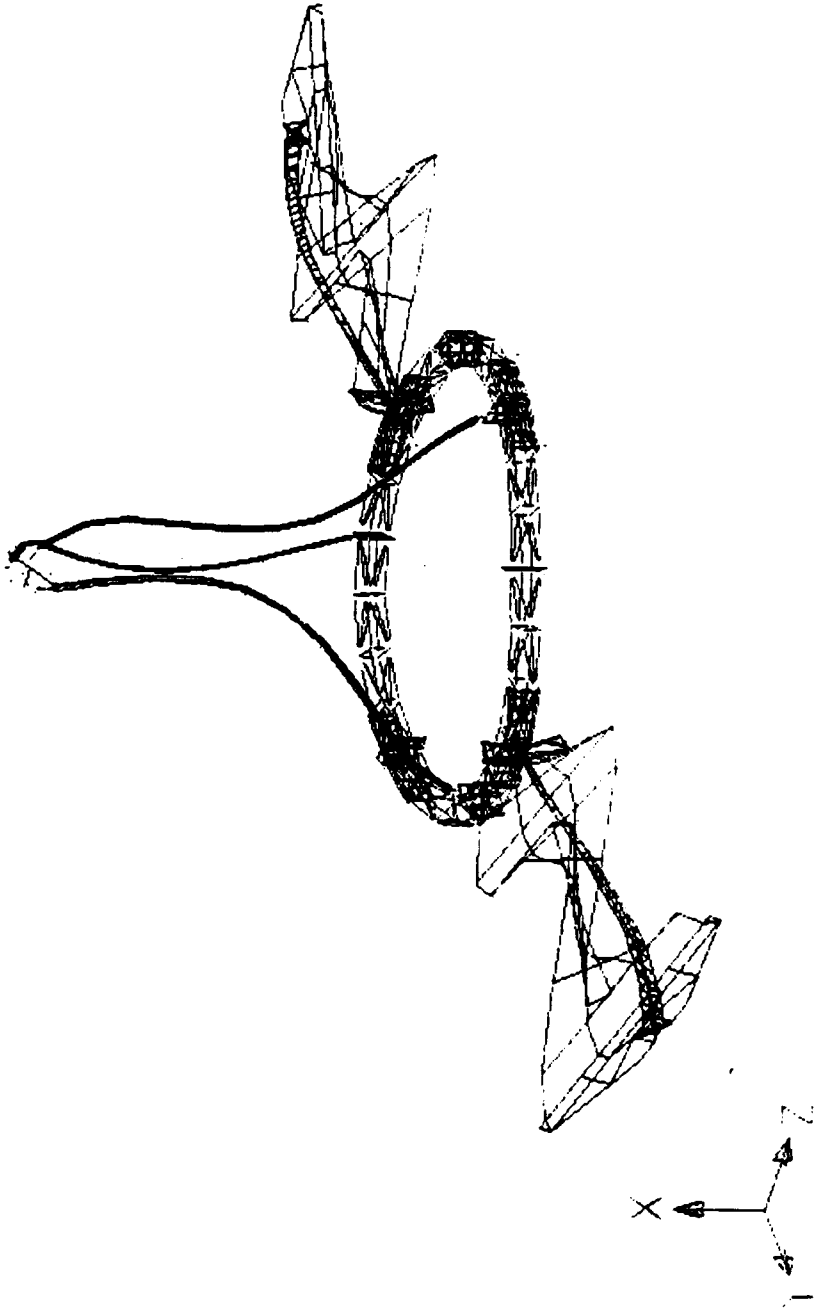
Mode 38. 12.745 Hz



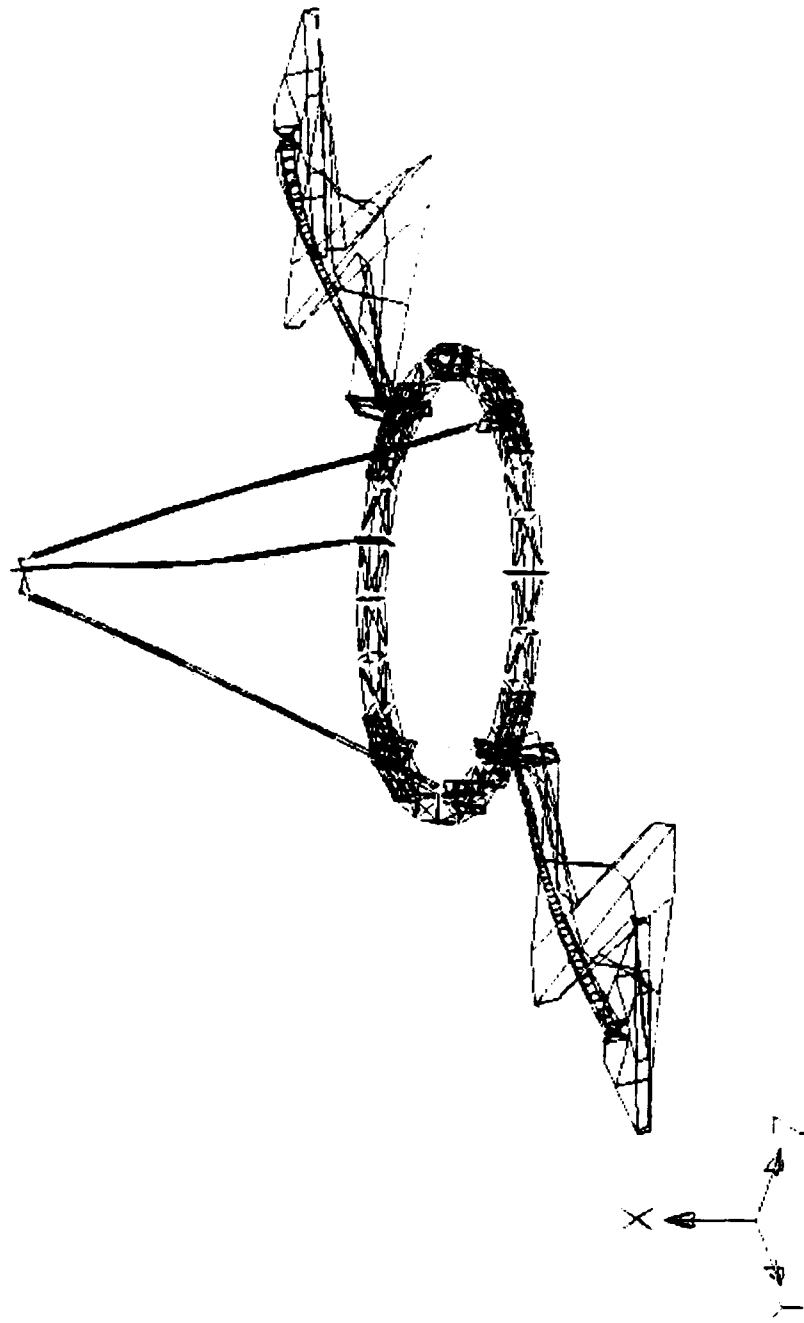
Mode 39. 12.865 Hz



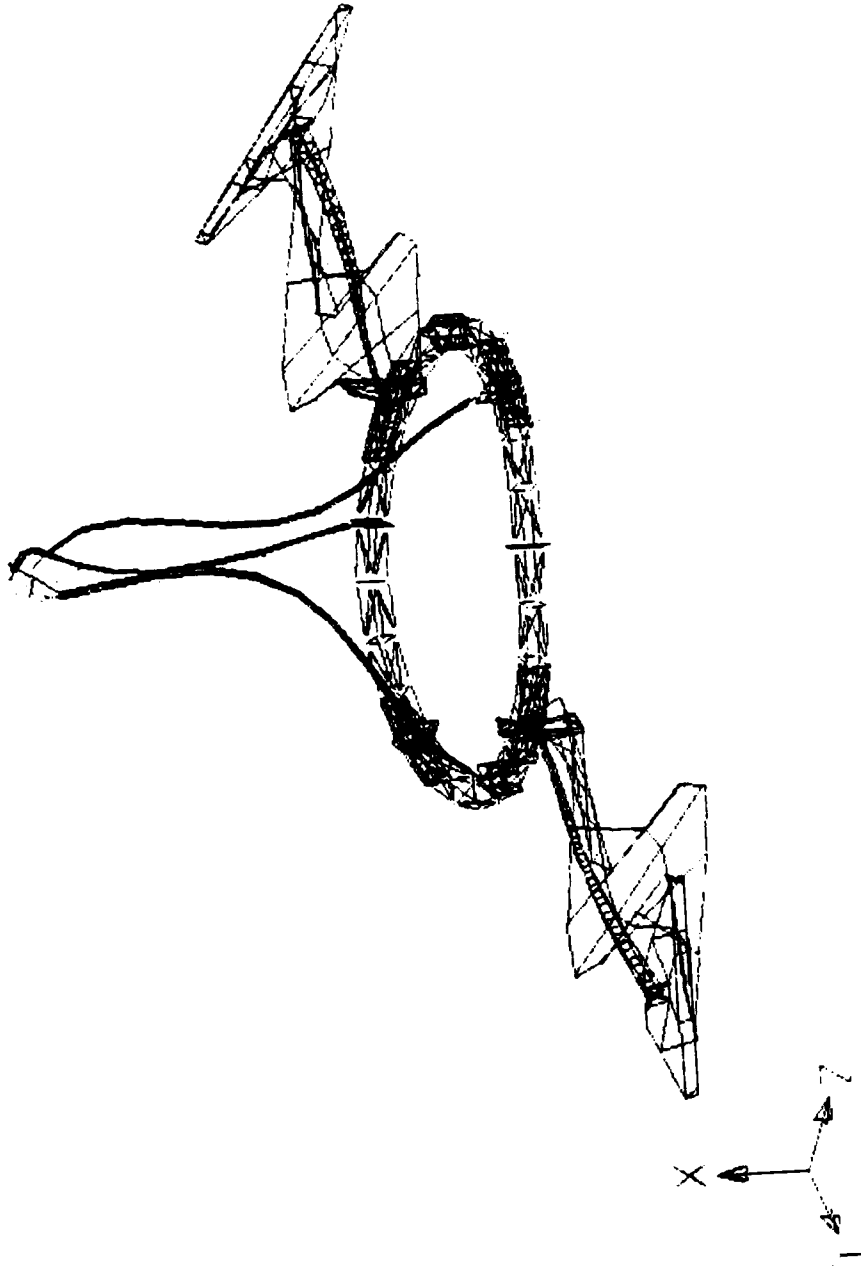
Mode 40. 13.595 Hz



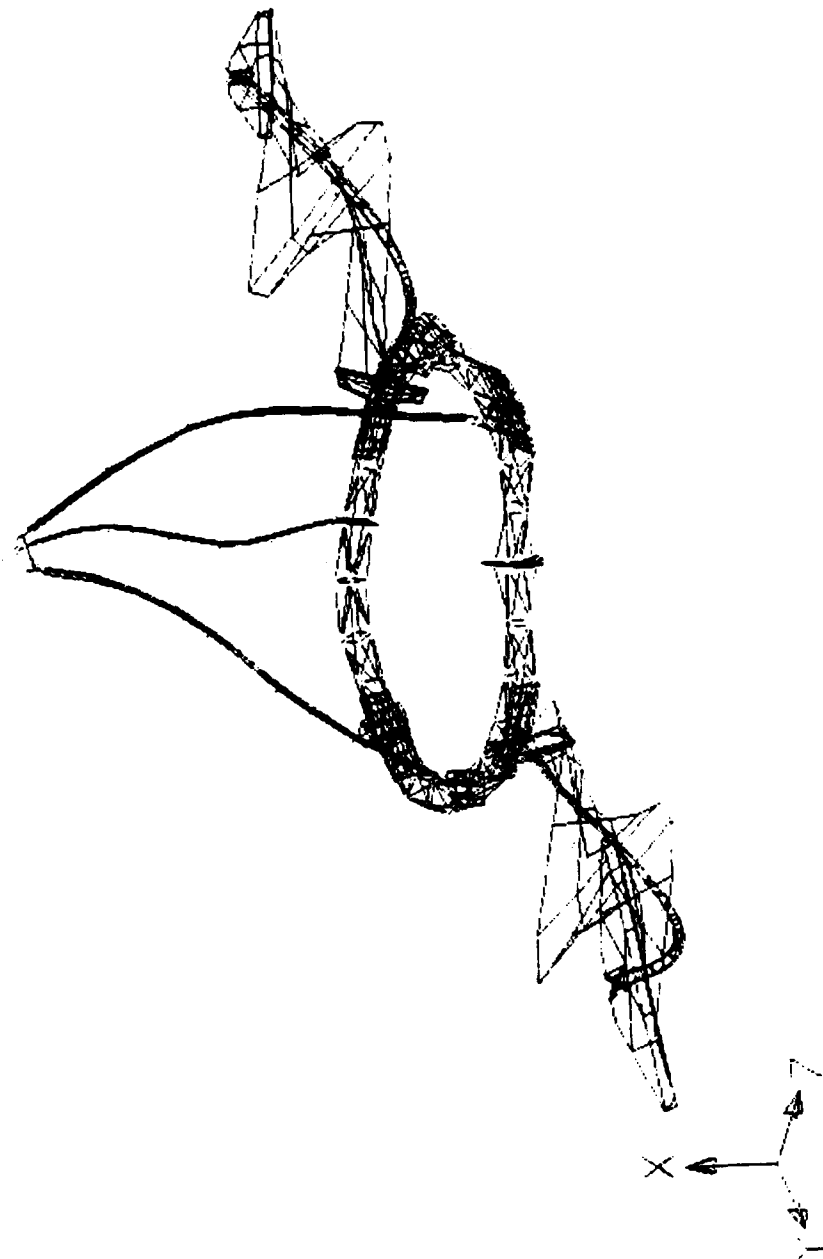
Mode 41. 15.317 Hz



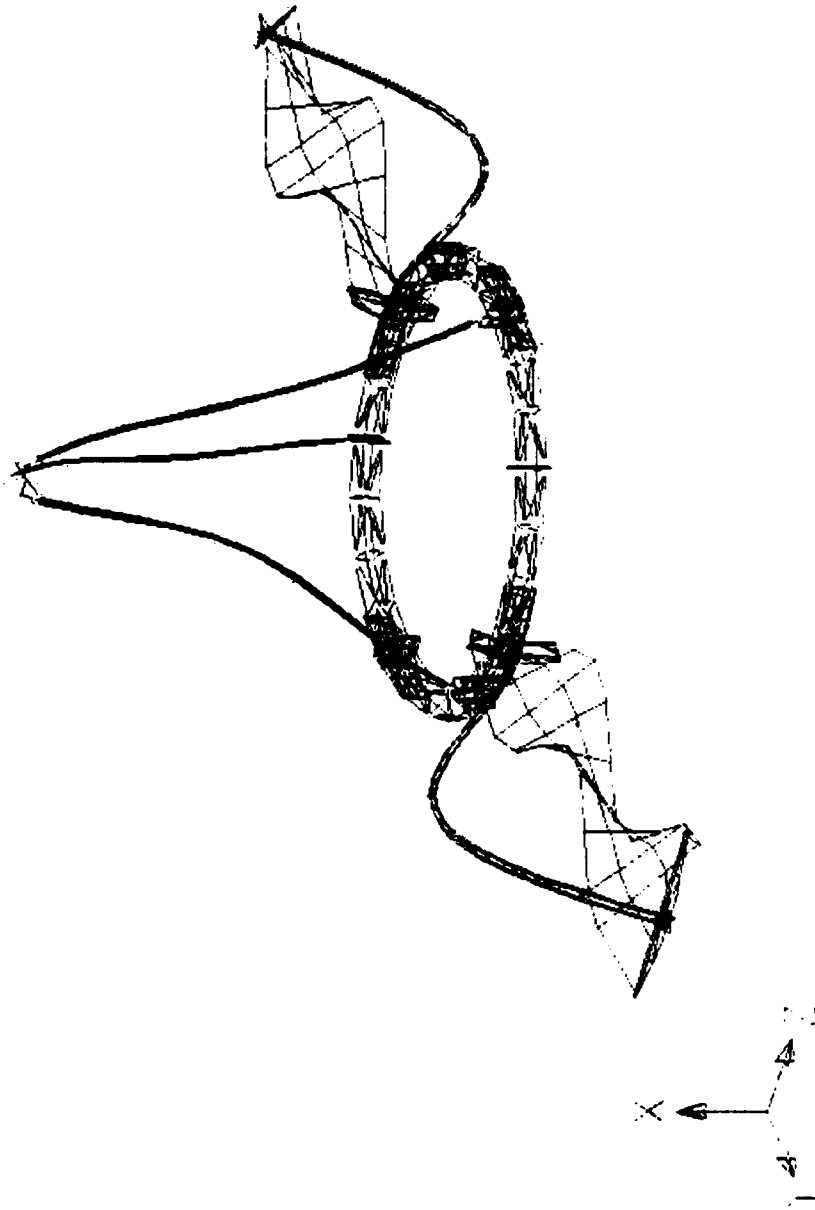
Mode 42. 15.402 Hz



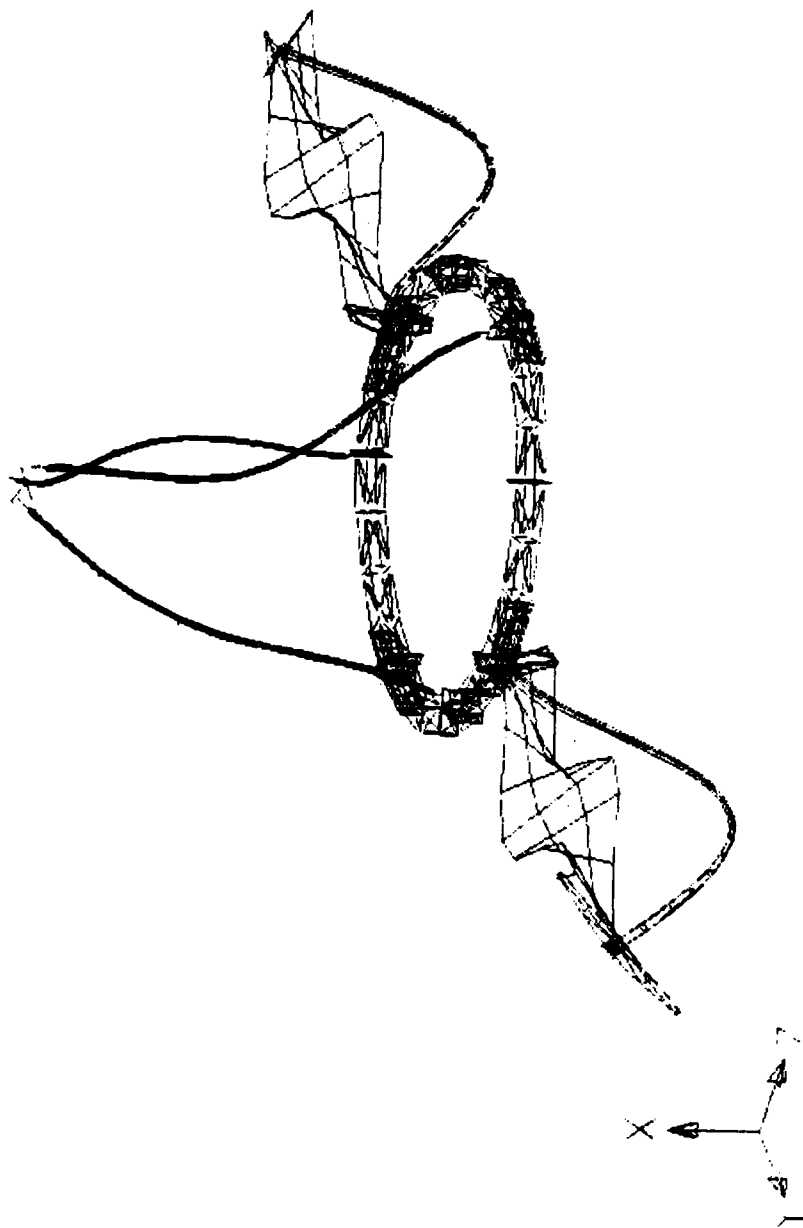
Mode 43. 15.575 Hz



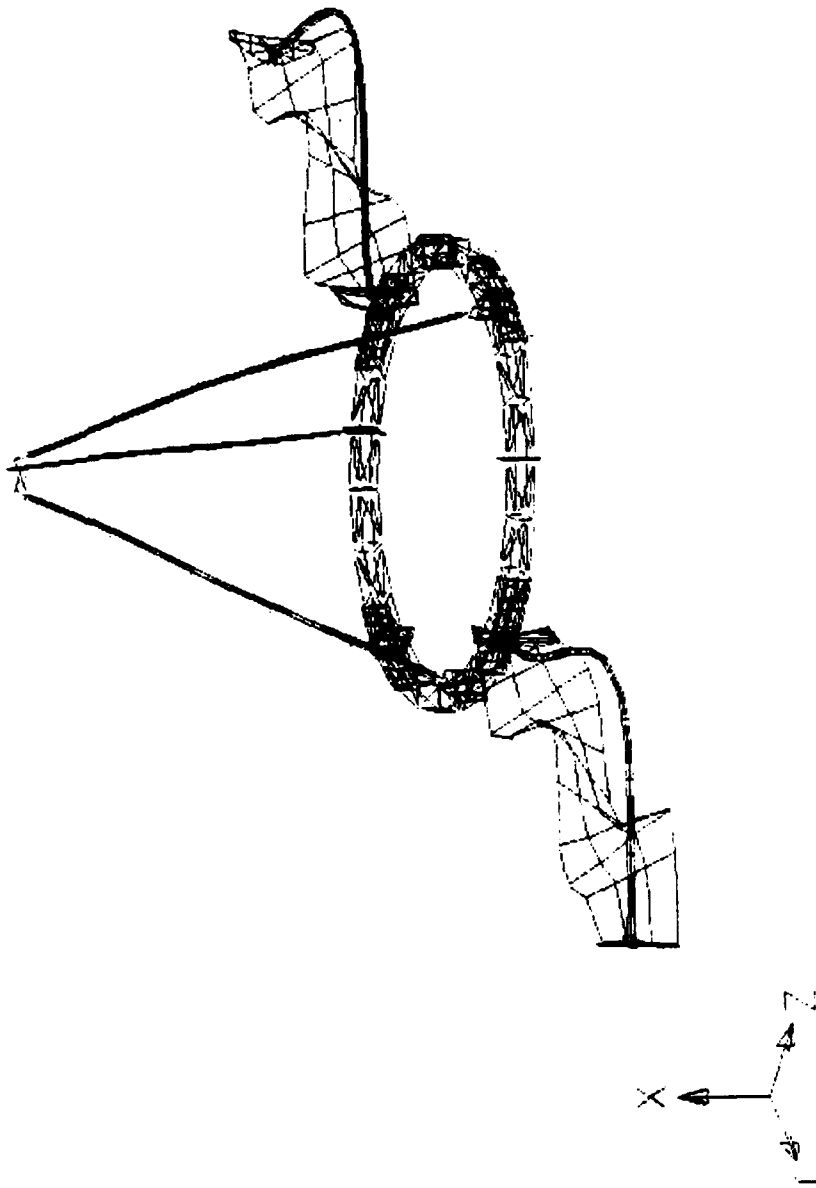
Mode 44. 16.282 Hz



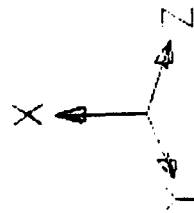
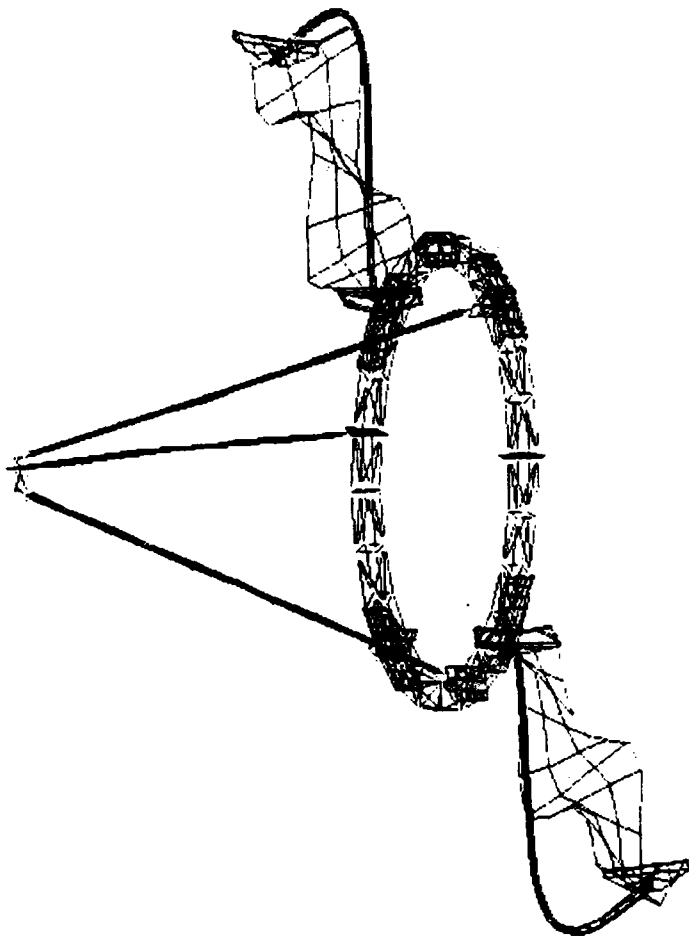
Mode 45. 17.272 Hz



Mode 46. 18.134 Hz



Mode 47. 19.175 Hz



Mode 48. 19.218 Hz

Appendix C. Model Reduction Utilities

This appendix contains a detailed explanation of how the final model reduction was accomplished, including the MSC/NASTRAN executive and case control decks and some bulk data cards used to produce FRFs and to extract reduced mass and stiffness matrices for the 182 DOF model.

Also included are some PRO-MATLAB m-files that were useful in reducing the 182 DOF model to 50 DOF. The function of each m-file is explained with the file listing.

The final 50 DOF are listed in the table at the end of this appendix.

Explanation of the Final Model Reduction

The mass and stiffness matrices from the 182 degree of freedom Guyan reduction process were extracted from the MSC/NASTRAN output file. The executive deck and case control deck used for accomplishing this are included. The DMAP ALTER statements cause the KAA and MAA matrices to be printed by column in the MSC/NASTRAN fortran output (f06) file. The output lists all nonzero elements in each column versus the corresponding grid point number and degree of freedom. The FORTRAN program column.f was used to translate a block text file from the MSC/NASTRAN output file into a column text file. The zero elements were added in the appropriate rows (corresponding to actuator degrees of freedom) by the FORTRAN program addzero.f to produce one text file for each column of the 182 x 182 mass and stiffness matrices.

The columns of the mass and stiffness matrices were loaded into PRO-MATLAB and formed into matrices using the m-files formk.m and formm.m included. The m-file eigsolve.m loads the 182 degree of freedom mass and stiffness matrices and performs an eigensolution to produce a 182 x 182 matrix of eigenvectors and a corresponding diagonal matrix of eigenvalues. The 182 x 50 phil reduced transformation matrix is formed by selecting the eigenvectors corresponding to the first 50 eigenvalues (columns 133 through 182). The matrix phil is used to produce 50 x 50 diagonal mass and stiffness

matrices $mbar1$ and $kbar1$.

Partitioning of $phil$ into a 50×50 matrix $phir$ is performed by the m-file `partphi.m`. The modal matrix $phir$ represents the modal matrix described in a selected set of degrees of freedom. The retained set of degrees of freedom in the final model are defined in the vector $rset$, which is made up of row numbers corresponding to the degrees of freedom chosen for retention. Given the 50×50 matrices $mbar1$, $kbar1$, and $phir$, 50×50 degree of freedom mass and stiffness matrices are created called $newk$ and $newm$.

The 50 degrees of freedom in the final model are listed in the following pages. The degrees of freedom were selected to include each actuator mass and its attachment point on the ring truss, all points likely to be used as excitation points, and sufficient points on the tripod and solar arrays to distinguish similar mode shapes. It is important that care be used in selecting the final retained degrees of freedom. If any two similar mode shapes become indistinguishable, the 50×50 modal matrix becomes singular. The Table 3 in Chapter V shows how the degrees of freedom in the final model are distributed throughout the structure. The Appendix C listing of the 50 DOF is shown in the order they appear in the final model. It also shows the corresponding row numbers in the 182 DOF model matrices used in PRO-MATLAB.

The following MSC/NASTRAN executive and case control decks were used to produce frequency response solutions to a unit magnitude forcing function. Output is requested in magnitude-phase format for the points in the 182 degree of freedom Guyan reduced model.

```

NASTRAN BUFFSIZE=4097,REAL=0
INIT DBALL LOGICAL=(DBALL(15000))
TIME 6000
SOL 111
CEND
TITLE = undamped dta
MAXLINES=1000000
ECHO=NONE
SET 1=70003,70002,70004,7173,70010,70016,7172,70015,70009,
70014,70008,700013,70007,70012,70006,70011,70005,70001,
2070,2021,20211,2970,2145,2119,11,2230,5402,5401,2231,22311,
2265,2279,2310,2311,23111,30104,30103,31002,31006,2905,2919,
2830,30204,30203,32002,32006,2790,4002,2791,27911,2745,2990,
27151,31,2710,27111,271111,2670,2980,2385,2359,21,2585,2599,
2501,25011,30303,30304,33002,33006,2470,90005,90011,90010,
9172,90016,9173,90004,30001,30002,30003,300111,300112,300113,
300114
ACCELERATION(PHASE)=1
SPC=1
FREQ=1
SDAMP=1
DLOAD=1
METHOD=75
BEGIN BULK

```

The following bulk data cards were used in the frequency response solution to define the frequency dependent load and the 0.5% modal damping for all modes.

```

FREQ1      1      0.0      .01      2000
TABDMP1    1      CRIT
+ABC       0.5      .005      15.5      .005      ENDT
RLOAD1     1      1
DAREA      1      30003     1      1.0
TABLED1    1
           0.5      1.0      9.5      1.0      ENDT

```

The following executive and case control decks were used to write the Guyan-reduced mass and stiffness matrices to the MSC/NASTRAN fortran output file (the f06 file).

```
NASTRAN BUFFSIZE=4097,REAL=0
INIT DBALL LOGICAL=(DBALL(15000))
TIME 6000
SOL 103
COMPILE DMAP=SEMODES, SOUIN=MSCSOU
ALTER 15
MATGPR GPLS,USET,SILS,KAA//'A' $
MATGPR GPLS,USET,SILS,MAA//'A' $
ENDALTER
CEND
TITLE = undamped dta
MAXLINES=1000000
ECHO=NONE
SET 1=70003,70002,70004,7173,70010,70016,7172,70015,70009,
70014,70008,700013,70007,70012,70006,70011,70005,70001,
2070,2021,20211,2970,2145,2119,11,2230,5402,5401,2231,22311,
2265,2279,2310,2311,23111,30104,30103,31002,31006,2905,2919,
2830,30204,30203,32002,32006,2790,4002,2791,27911,2745,2990,
27151,31,2710,27111,271111,2670,2980,2385,2359,21,2585,2599,
2501,25011,30303,30304,33002,33006,2470,90005,90011,90010,
9172,90016,9173,90004,30001,30002,30003,300111,300112,300113,
300114
SPC=1
METHOD=75
BEGIN BULK
```

The following executive and case control decks were used to write the MSC/NASTRAN-generated eigenvectors to the fortran output file (the f06 file) in the basic coordinate system.

```
NASTRAN BUFFSIZE=4097,REAL=0
INIT DBALL LOGICAL=(DBALL(15000))
TIME 6000
SOL 103
COMPILE DMAP=SEDRCVR, SOUIN=MSCSOU
ALTER 107
VECPLOT UGVS,BGPDTS,EQEXINS,CSTMS,CASEDR,LAMA/UGVSB/0/0/1 $
UPARTN USET,UGVSB/UGVSBA,,,'G'/'A'/'O'/1 $
MATGPR GPLS,USET,SILS,UGVSBA/'H'/'A' $
ENDALTER
CEND
TITLE = undamped dta
MAXLINES=1000000
ECHO=NONE
SET 1=70003,70002,70004,7173,70010,70016,7172,70015,70009,
70014,70008,700013,70007,70012,70006,70011,70005,70001,
2070,2021,20211,2970,2145,2119,11,2230,5402,5401,2231,22311,
2265,2279,2310,2311,23111,30104,30103,31002,31006,2905,2919,
2830,30204,30203,32002,32006,2790,4002,2791,27911,2745,2990,
27151,31,2710,27111,271111,2670,2980,2385,2359,21,2585,2599,
2501,25011,30303,30304,33002,33006,2470,90005,90011,90010,
9172,90016,9173,90004,30001,30002,30003,300111,300112,300113,
300114
DISPLACEMENT=1
SPC=1
METHOD=75
BEGIN BULK
```

This fortran program was used to read block text files cut from the NASTRAN f06 file containing the reduced mass and stiffness terms by column and to create column text files for each mass and stiffness matrix column.

```
PROGRAM COLUMN
CHARACTER DUMMY1*17, DUMMY2*12, V(6)*13, FN*5
C
  READ(5,*) FN
  OPEN(UNIT=8, STATUS='OLD',FILE=FN//'.t')
  OPEN(UNIT=7, STATUS='NEW',FILE=FN//'.p')
C
  DO 50 I=1,35
  READ(8,200)DUMMY1,V(1),DUMMY2,V(2),DUMMY2,V(2),DUMMY2
*,V(4),DUMMY2,V(5)
  WRITE(7,100) V(1),V(2),V(3),V(4),V(5)
50  CONTINUE
100  FORMAT( 4(A13 / ), A13)
200  FORMAT( A17, A13, 4(A12,A13))
  END
```

This fortran program reads the column text files created by the fortran program column.f and inserts zeros into the rows corresponding to the actuator DOFs and their associated attachment points. It is not to be used on columns corresponding to the actuator DOFs or their attachment points.

```
      PROGRAM ADDZERO
      CHARACTER DUMMY*13, FN*5
C
      READ(5,*) FN
      OPEN(UNIT=8, STATUS='OLD', FILE=FN//'.p')
      OPEN(UNIT=9, STATUS='NEW', FILE=FN//'.t')
C
      DO 50 I=1,174
        READ(8,100) DUMMY
        IF (I.EQ.47) WRITE(7,200)
        IF (I.EQ.61) WRITE(7,200)
        IF (I.EQ.67) WRITE(7,200)
        IF (I.EQ.87) WRITE(7,200)
        IF (I.EQ.97) WRITE(7,200)
        IF (I.EQ.115) WRITE(7,200)
        WRITE(7,100) DUMMY
50    CONTINUE
      WRITE (7,200)
      WRITE (7,200)
100   FORMAT( A13)
200   FORMAT( 2X, '0.0' )
      END
```

The following files are various PRO-MATLAB m-files that were useful in creating the 50 x 50 final model. They are included for reference.

The formk.m file reads all 182 ASCII text files representing columns in the Guyan-reduced stiffness matrix and forms them into a 182 x 182 matrix called k. A similar m-file was used to read the mass matrix column files.

"formk.m"

```
k=[];
for i=1:182
    y=num2str(i);
    z=['kcol',y];
    eval(['load ',z,'.t']);
    k=[k,eval(z)];
    eval(['clear ',z]);
end
```


The eigsolve.m file performs an eigensolution on the 182 DOF mass and stiffness matrices and uses the first 50 eigenvectors to form 50 x 50 modal matrices. This m-file calls another m-file (partphi.m) which partitions the 50 eigenvectors into the final 50 DOF and returns a 50 x 50 modal matrix corresponding to the final 50 DOF. This matrix is used to find fully populated 50 DOF mass and stiffness matrices.

"eigsolve.m"

```

load k
load m
[phi,lambda]=eig(k.m);
lambda=real(lambda);
%
%   normalize eigenvectors w.r.t. mass matrix
%
initdof=size(m);
initdof=initdof(1);
for n=1:initdof
    phi(:,n)=phi(:,n)/sqrt(phi(:,n)'*m*phi(:,n));
end
phi=real(phi);
%
%   form 182 x 182 modal matrices
%
mbar=phi'*m*phi;
kbar=phi'*k*phi;
%
%   form 50 x 50 modal matrices
%
findof=50;
phil=phi(:,(initdof-findof+1:initdof));
mbar1=phil'*m*phil;
kbar1=phil'*k*phil;
mbar1=diag(diag(mbar1));
kbar1=diag(diag(kbar1));
%
%   partition phil into phir and phio
%
partphi
%
```

```

% renormalize phir eigenvectors to have
% unit magnitude
%
for n=1:findof
    phir(:,n)=phir(:,n)/sqrt(phir(:,n)'*phir(:,n));
end
%
% construct 50 x 50 m and k matrices
%
mhat=inv(phir')*mbar1*inv(phir);
khat=inv(phir')*kbar1*inv(phir);
%
[newphi,newlam]=eig(khat,mhat);
for n=1:findof
    newphi(:,n)=newphi(:,n)/sqrt(newphi(:,n)'*mhat*newphi(:,n));
end
newphi=real(newphi);
newlam=real(newlam);
mbar2=newphi'*mhat*newphi;
kbar2=newphi'*khat*newphi;
clear n
save

```

The partphi.m file partitions the phil matrix into phir (corresponding to the retained DOF) and phio (corresponding to the omitted DOF). phir is the modal matrix for the 50 DOF reduced model.

"partphi.m"

```

% this m-file partitions the modal matrix into retained
% DOFs and omitted DOFs
% rset is a vector containing row numbers of retained DOFs
% oset is a vector containing row numbers of omitted DOFs
%
% user defines the retained set of DOFs
rset=[5 6 15 16 24 26 28 30 36 38 46 47 48 56 61 62 68 69 70];
rset=[rset 71 81 82 89 90 93 97 99 100 101 103 111 119 120];
rset=[rset 121 122 137 139 145 147 149 151 160 161 168 169];
rset=[rset 176 179 180 181 182];
%
% this set of loops puts all other DOFs in omitted set
%
Nr=length(rset);
oset=[];
for p=1:initdof
    not=1;
    for q=1:Nr
        if p==rset(q)
            not=0;
            break;
        else
            end
        end
    if not==1
        oset=[oset,p];
    else
end
%
% these loops partition phil into phir and phio
%
for p=1:Nr
    phir(p,:)=phil(rset(p),:);
end
for q=1:(initdof-Nr)
    phio(q,:)=phil(oset(q),:);
end
clear p q Nr not

```

Frequency response functions for the 50 DOF model were generated in PRO-MATLAB using the following m-file, freqres.m.

"freqres.m"

```

%
%   define input force vector magnitude
%   and frequency bandwidth
%
F=zeros(1,initdof)';
F(176,1)=1;
F=phil'*F;
omega=[0.0:0.025:20.0]'*2*pi;
%
%   determine number of steps in summation
%
step=size(omega);
step=step(1);
%
%   define natural frequencies and modal damping matrix
%
lambdan=diag(newlam);
pctcrit=ones(findof,1)*.01;
pctcrit(1:8)=pctcrit(1:8)*.005/.01;
for n=1:findof
    cbar2(n)=pctcrit(n)*2*sqrt(kbar2(n)*mbar2(n));
end
%
%   determine spatial portion of response
%
accel=[];
disp=[];
i=sqrt(-1);
for p=1:step
%
%   find modal participation coefficients
%
    a=zeros(findof,1);
    for n=1:findof
a(n)=[newphi(:,n)']*F]
a(n)=a(n)/[omega(p)^2*mbar2(n)+i*omega(p)*cbar2(n)+kbar2(n)];
    end
    u=newphi*a;
%
%   disp and accel are findof x step sized matrices
%   where each row is an FRF
    disp=[disp u];

```

```
    accel=[accel -omega(p)^2*u];  
end  
freq=omega/2/pi;  
dispmag=abs(displ);  
accmag=abs(accel);  
dispphase=angle(displ);  
accphase=angle(accel);  
clear a step p n omega displ lambdan accel u  
clear pctcrit  
save
```

This table lists the DOF retained in the final 50 DOF model. The corresponding row numbers in the 182 DOF model and MSC/NASTRAN grid numbers are also shown.

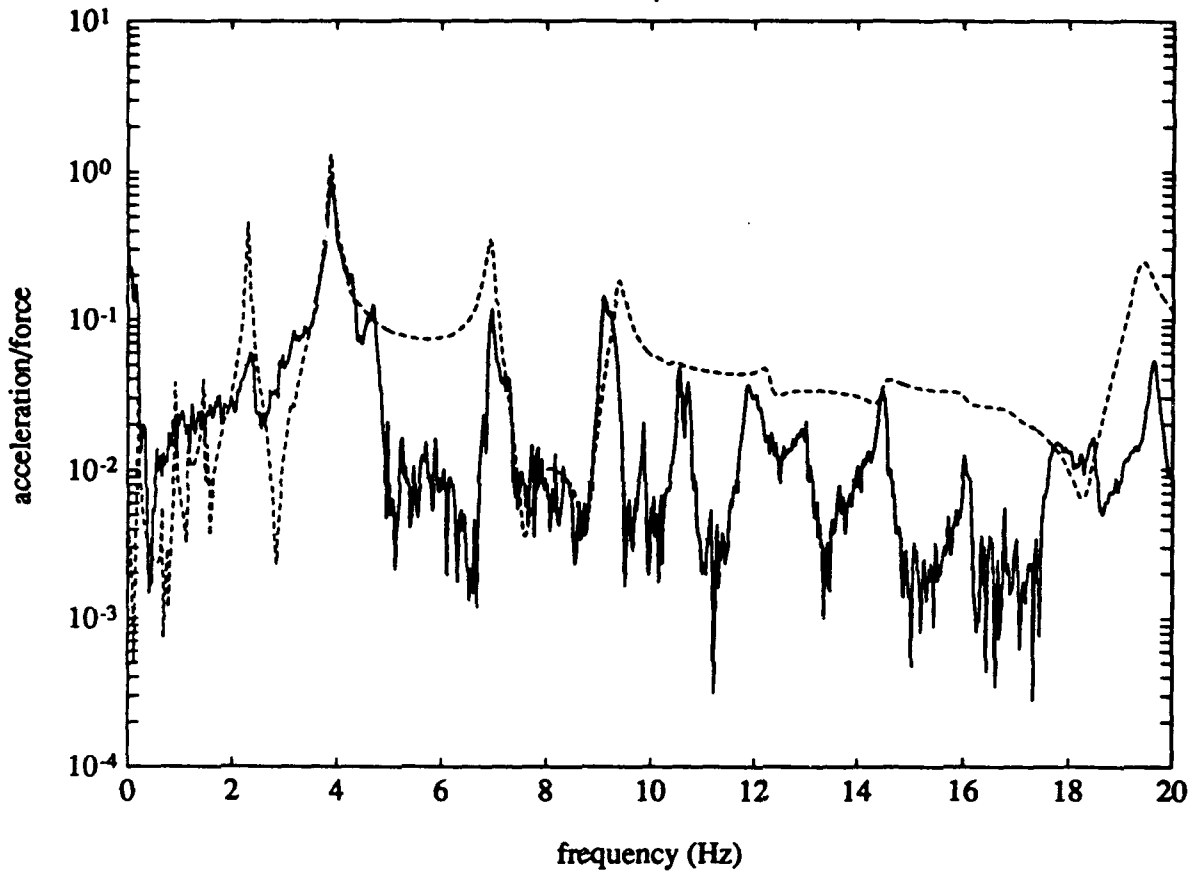
DOF in the Final 50 DOF Model

<u>Final Row</u>	<u>182 DOF Row</u>	<u>NASTRAN Grid-Dir</u>	<u>Final Row</u>	<u>182 DOF Row</u>	<u>NASTRAN Grid-Dir</u>
1	5	70004-1	26	97	31-2
2	6	70004-3	27	99	2710-3
3	15	70016-1	28	100	27111-3
4	16	70016-3	29	101	271111-3
5	24	70015-3	30	103	2980-3
6	26	70009-3	31	111	21-2
7	28	70014-3	32	119	2501-3
8	30	70008-3	33	120	25011-3
9	36	70012-3	34	121	30303-1
10	38	70006-3	35	122	30304-2
11	46	2021-3	36	137	90006-3
12	47	20211-3	37	139	90012-3
13	48	2970-3	38	145	90008-3
14	56	11-2	39	147	90014-3
15	61	2231-3	40	149	90009-3
16	62	22311-3	41	151	90015-3
17	68	2311-3	42	160	90016-1
18	69	23111-3	43	161	90016-3
19	70	30104-2	44	168	90004-1
20	71	30103-1	45	169	90004-3
21	81	30204-2	46	176	30003-1
22	82	30203-1	47	179	300111-3
23	89	2791-3	48	180	300112-2
24	90	27911-3	49	181	300113-3
25	93	2990-3	50	182	300114-2

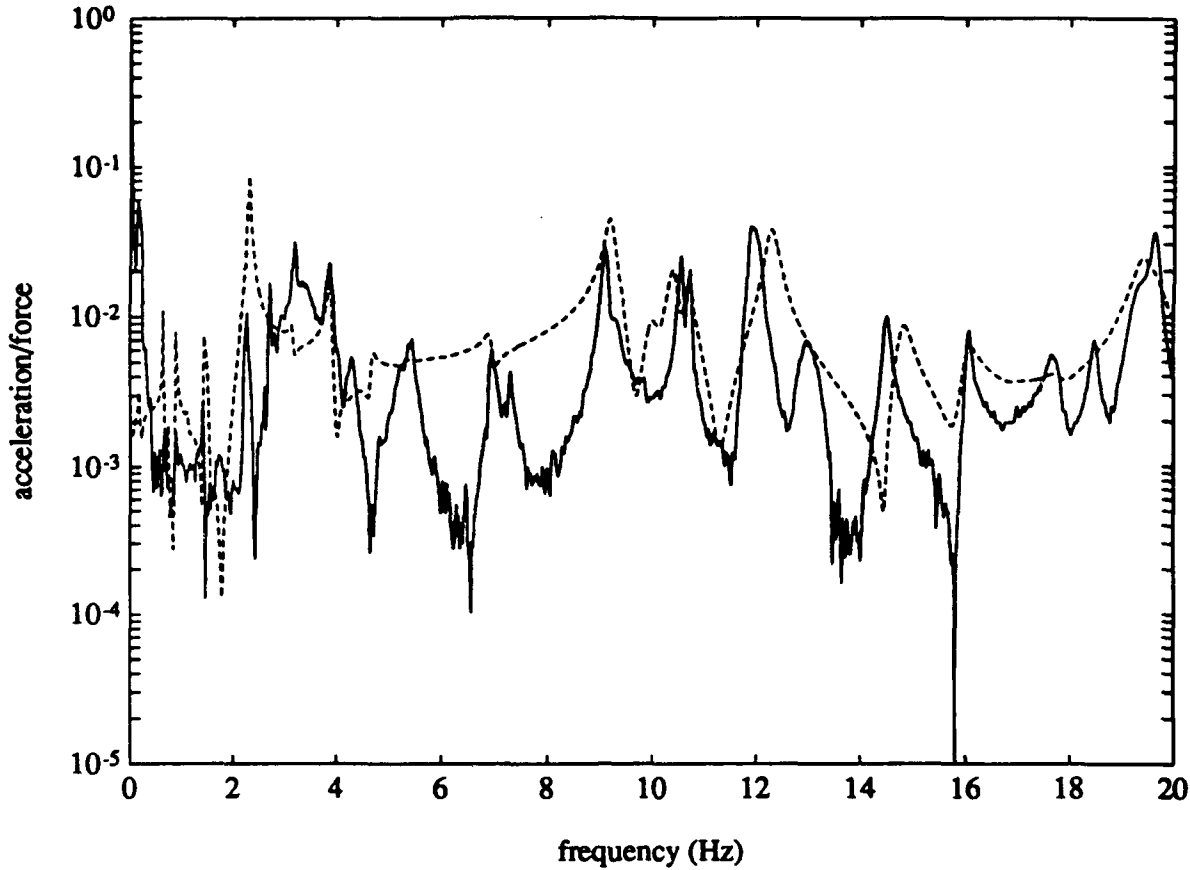
APPENDIX D. FINAL MODEL FREQUENCY RESPONSE FUNCTIONS

The following figures are the frequency response functions produced by the final 50 DOF model after tuning. Only the FRFs with corresponding experimental measurements are shown. The solid line represents the experimental FRFs. The dashed line represents the FRF generated by the final model.

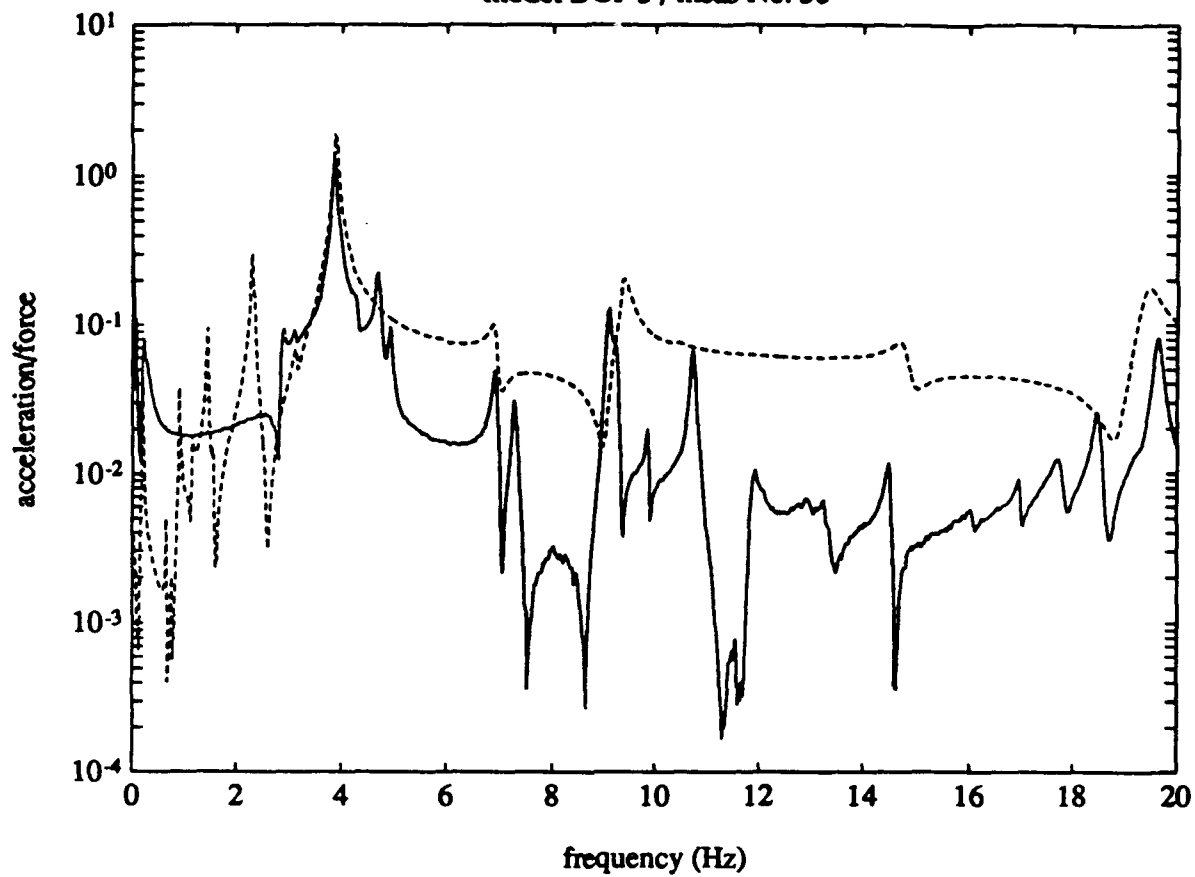
model DOF 1 / meas No. 44



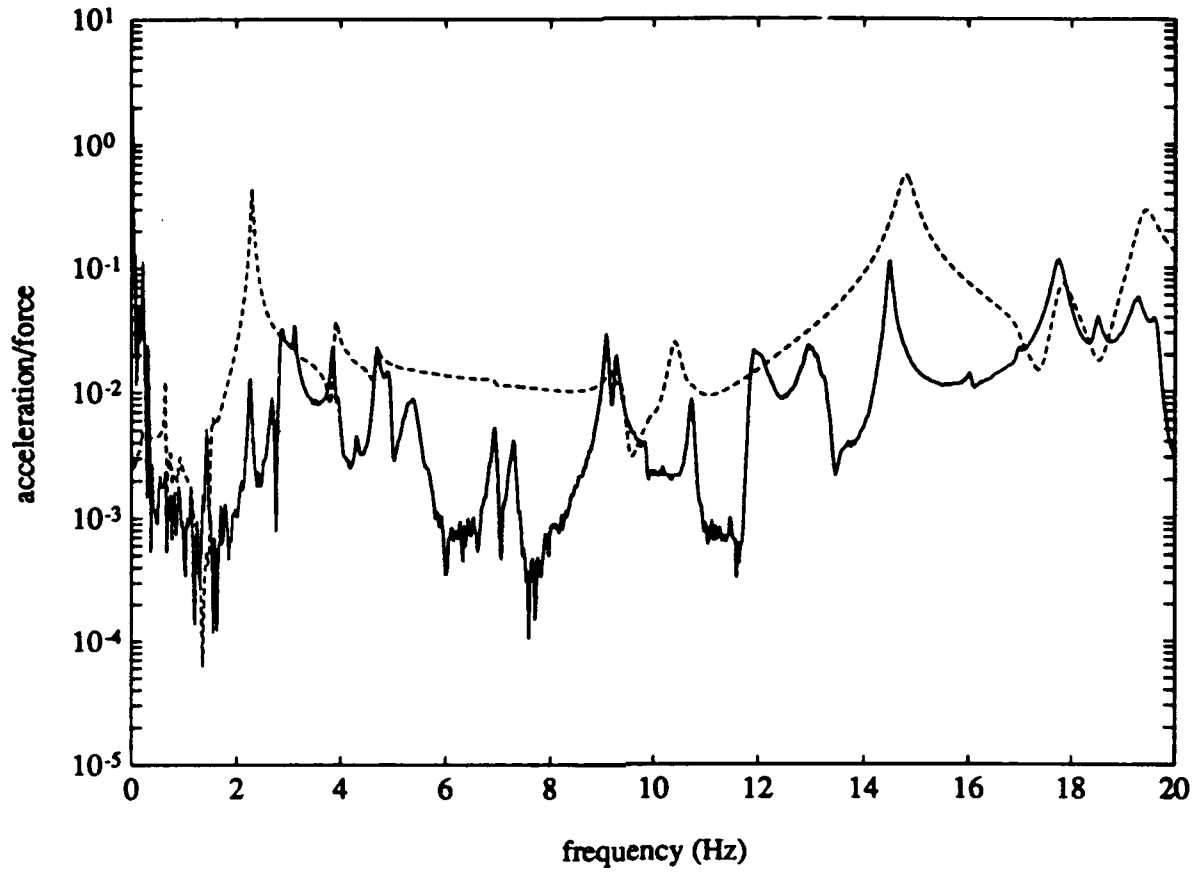
model DOF 2 / meas No. 43



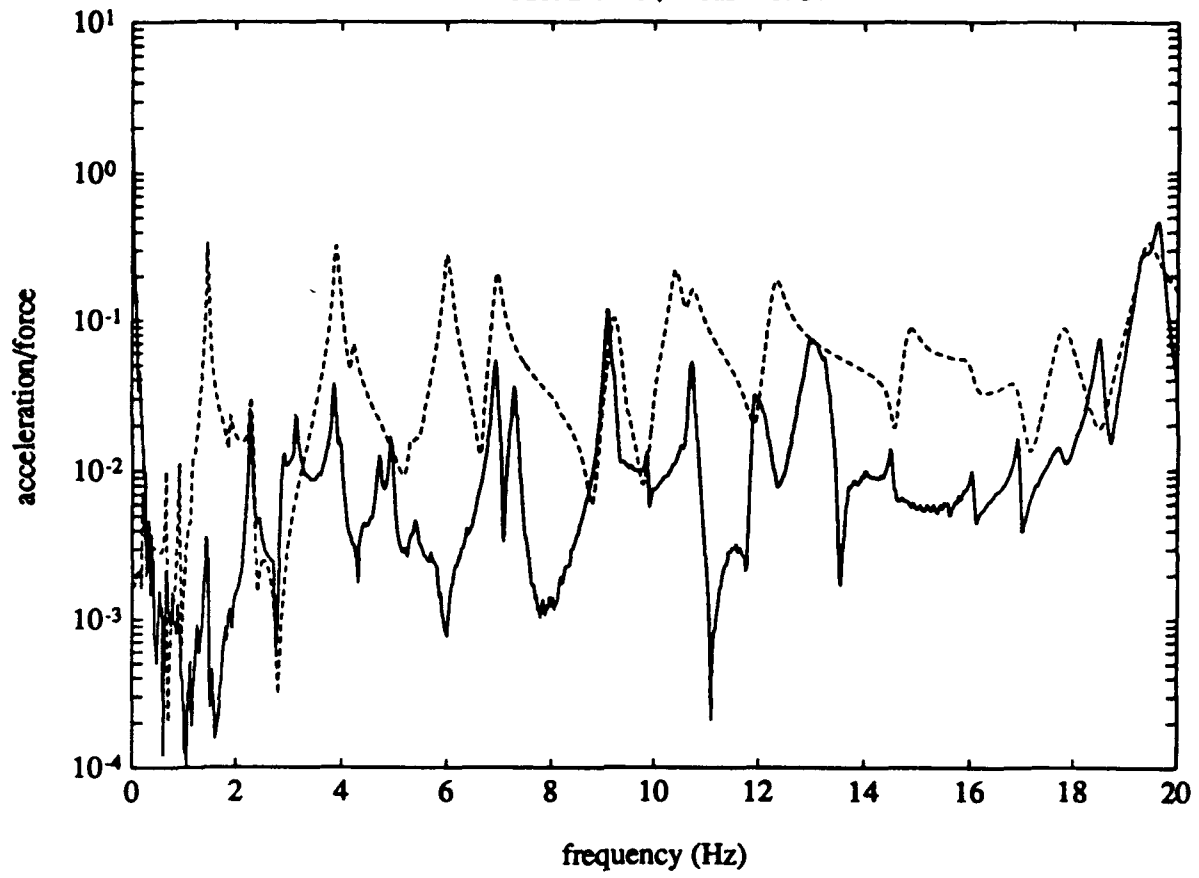
model DOF 3 / meas No. 56

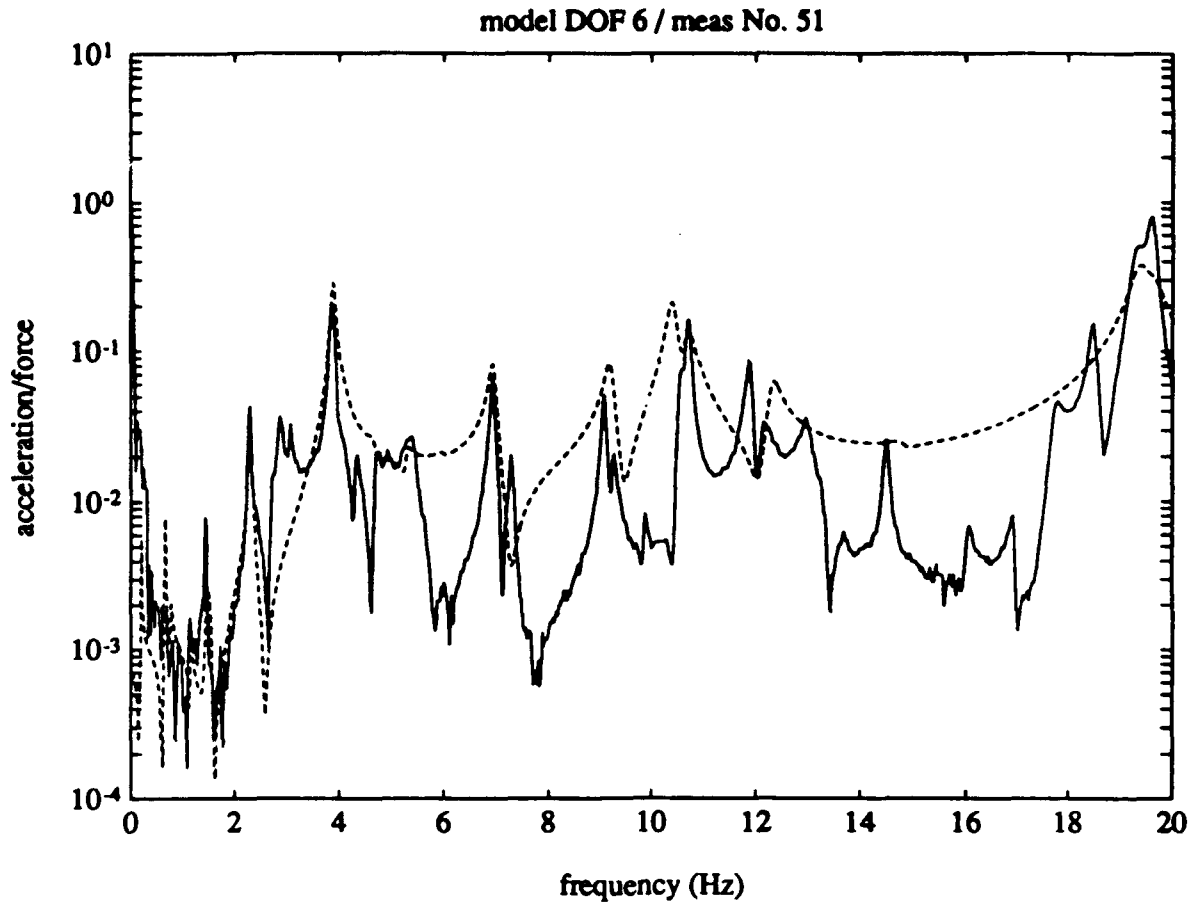


model DOF 4 / meas No. 55

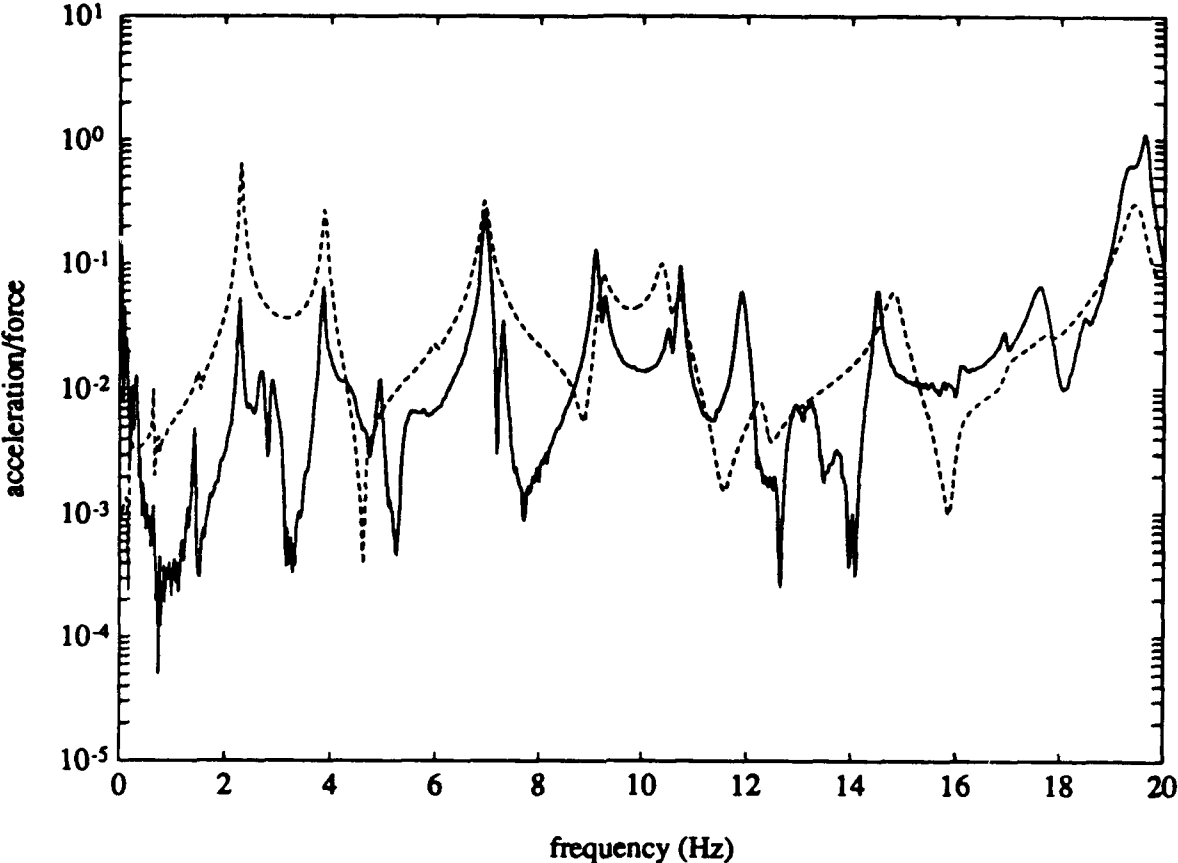


model DOF 5 / meas No. 57

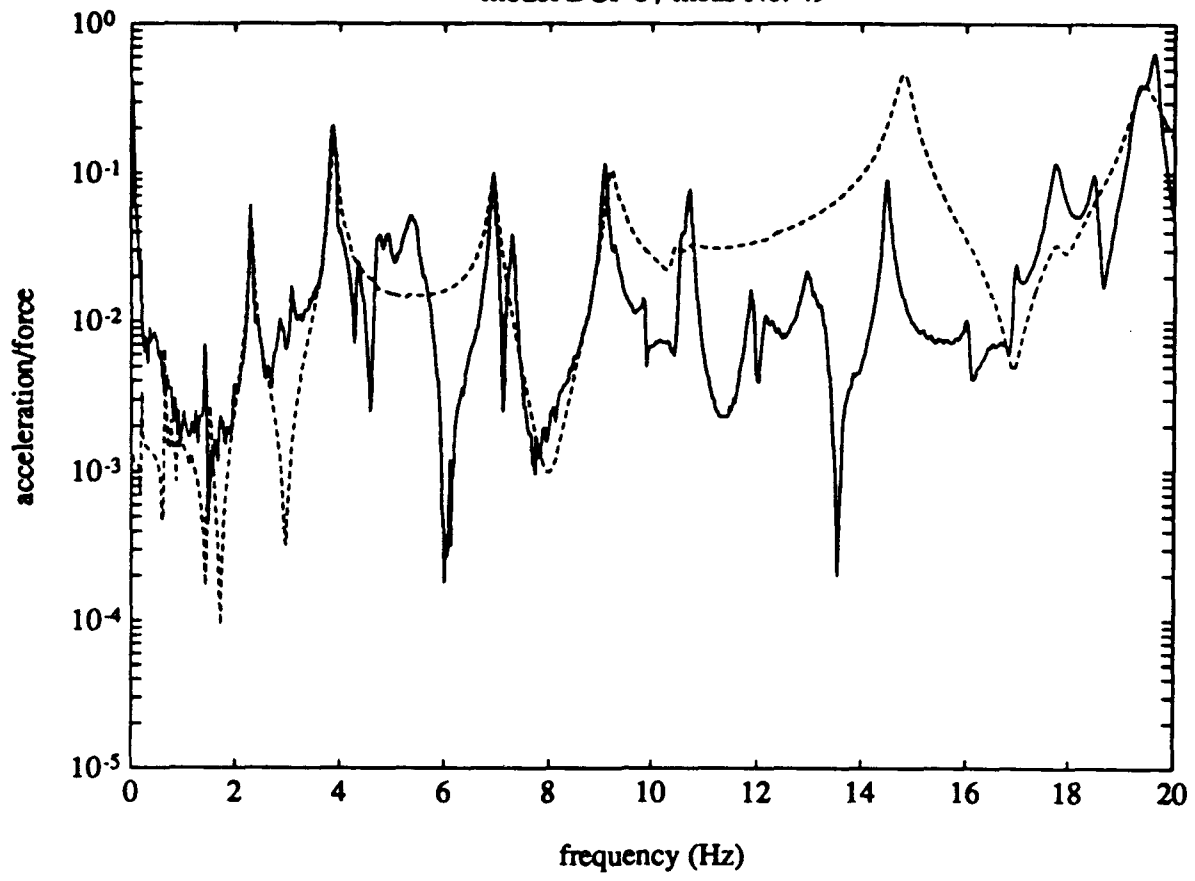




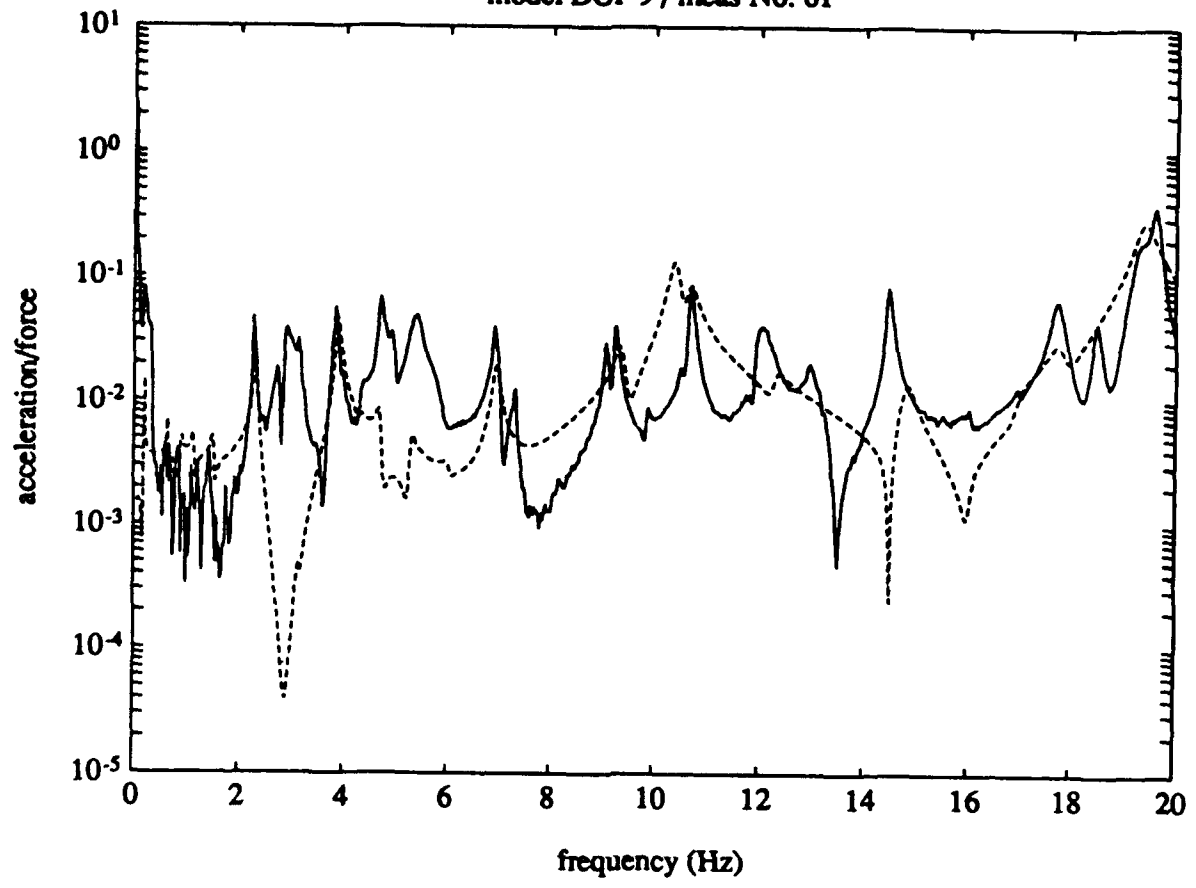
model DOF 7 / meas No. 59

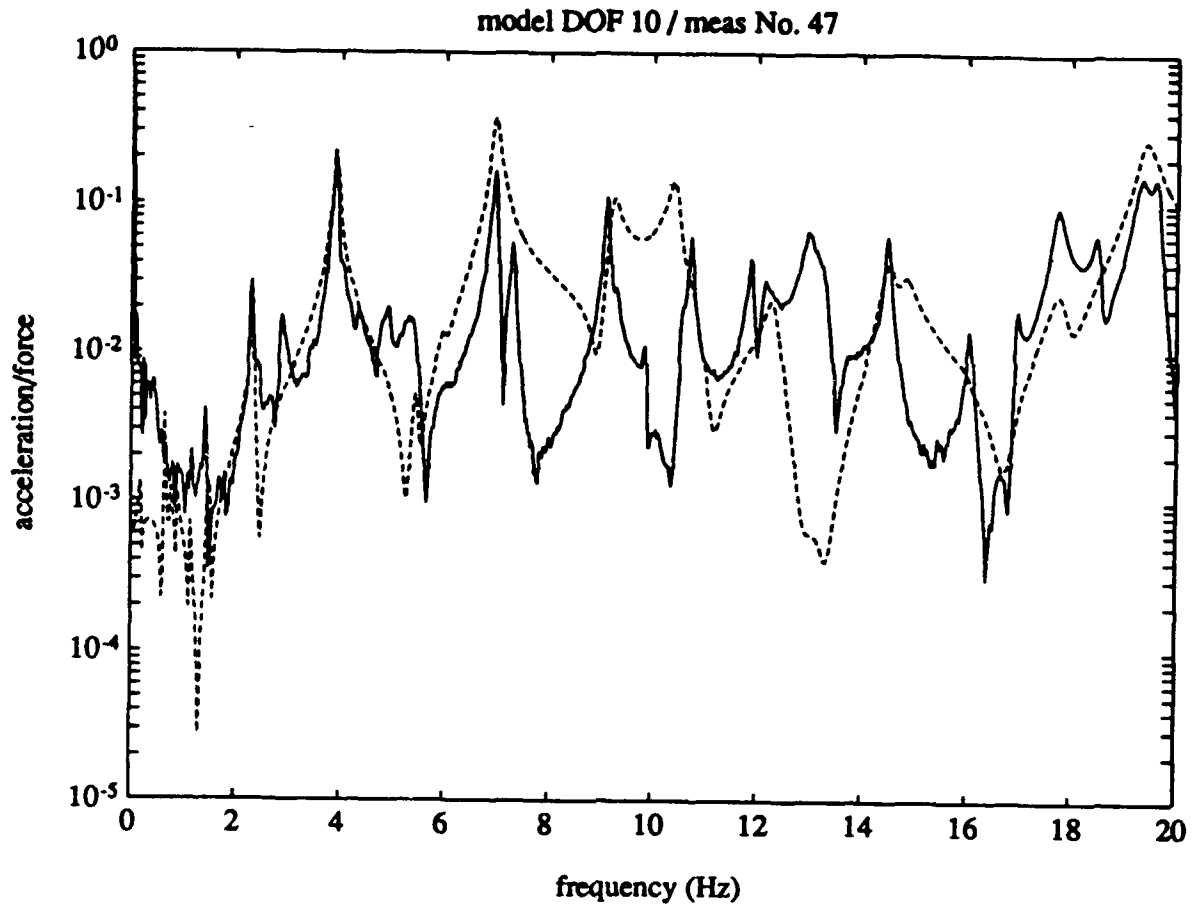


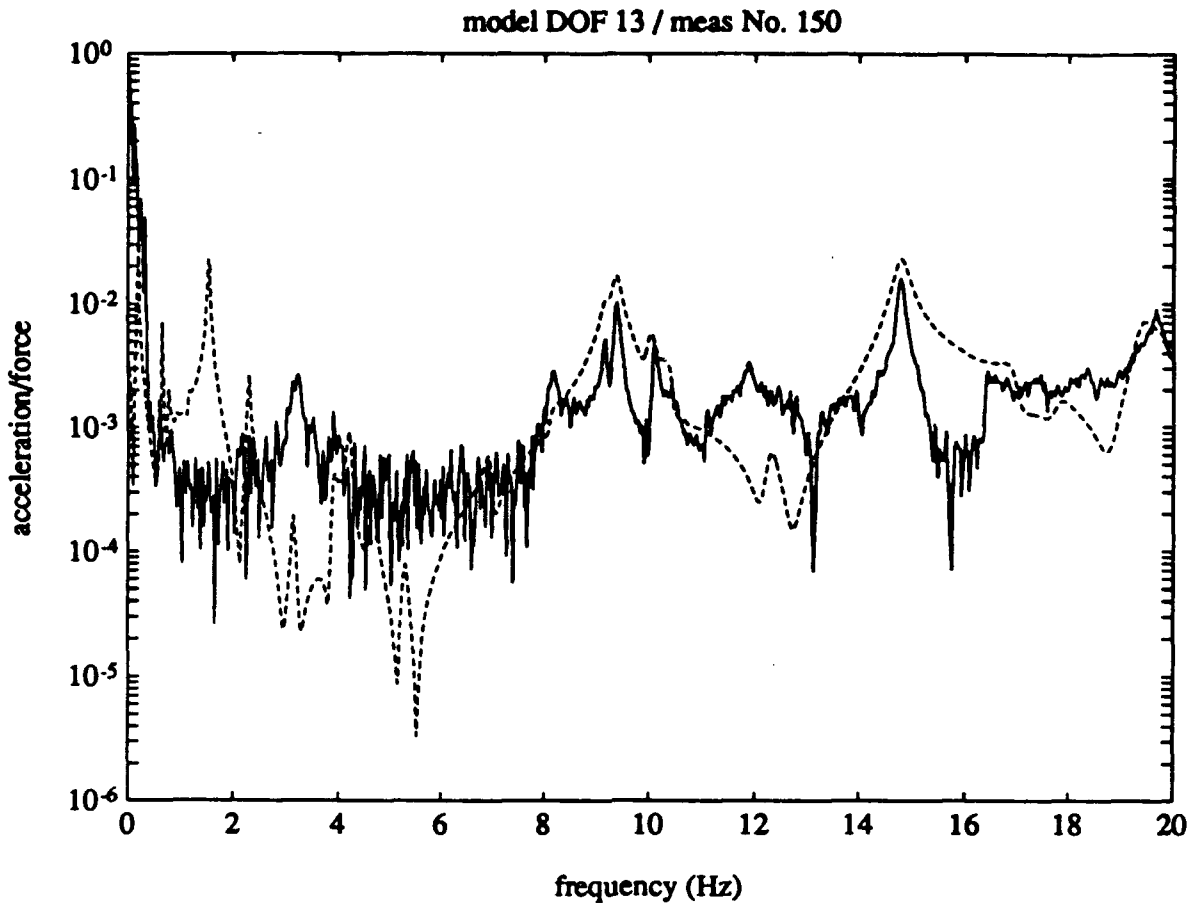
model DOF 8 / meas No. 49



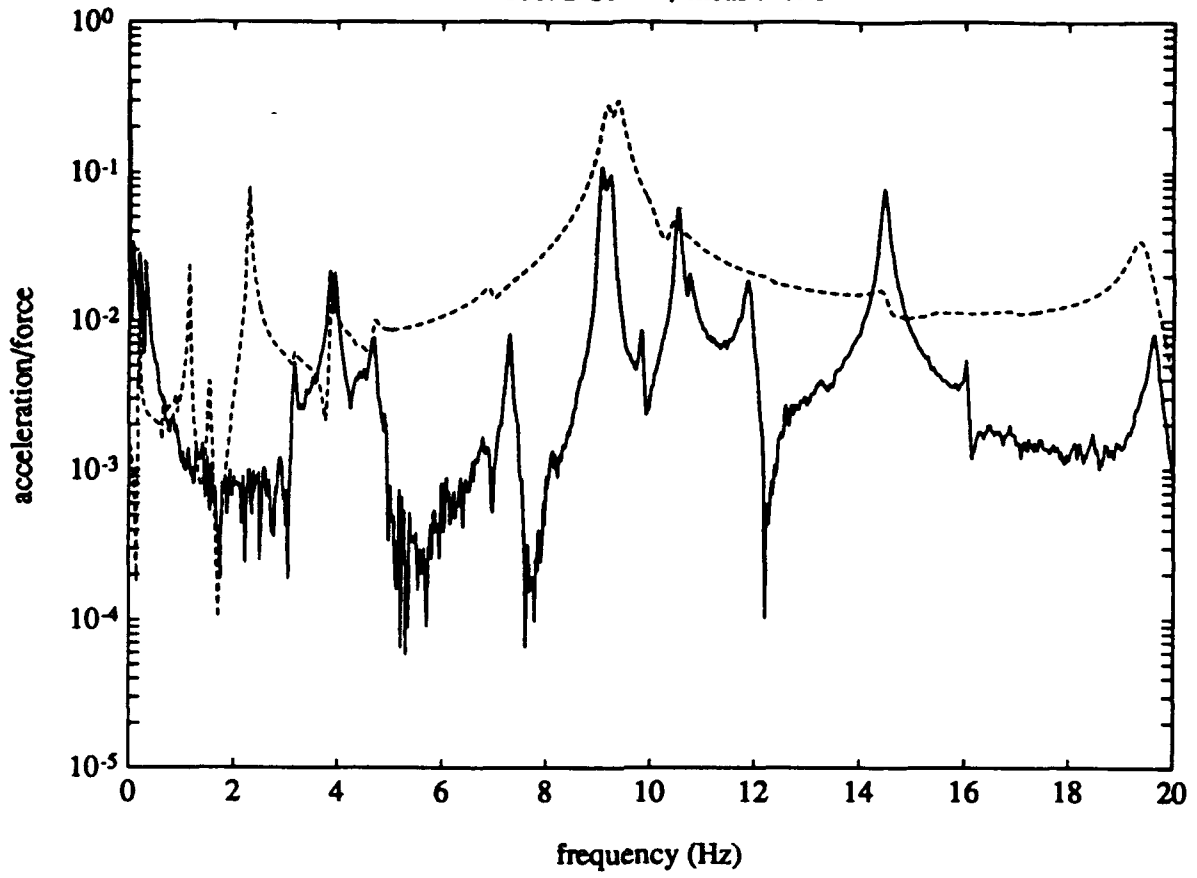
model DOF 9 / meas No. 61



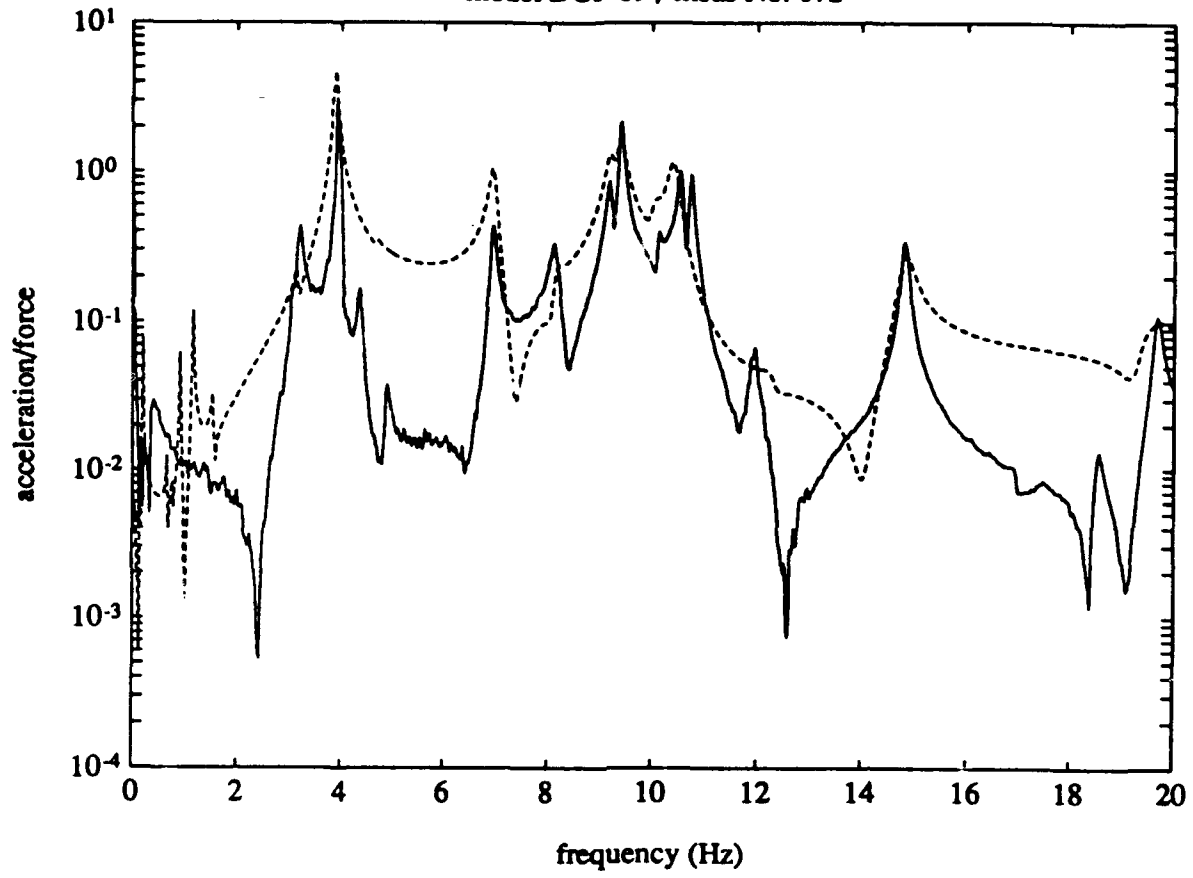




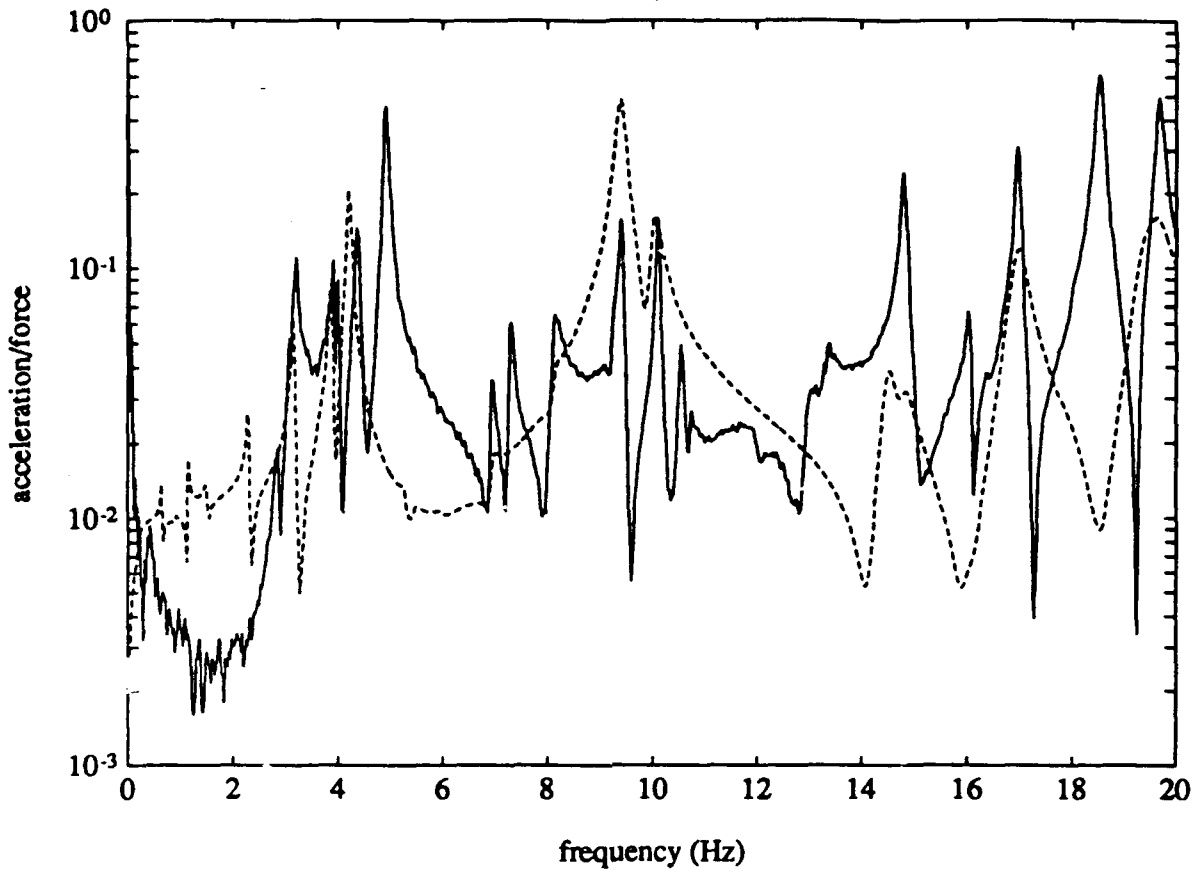
model DOF 14 / meas No. 1



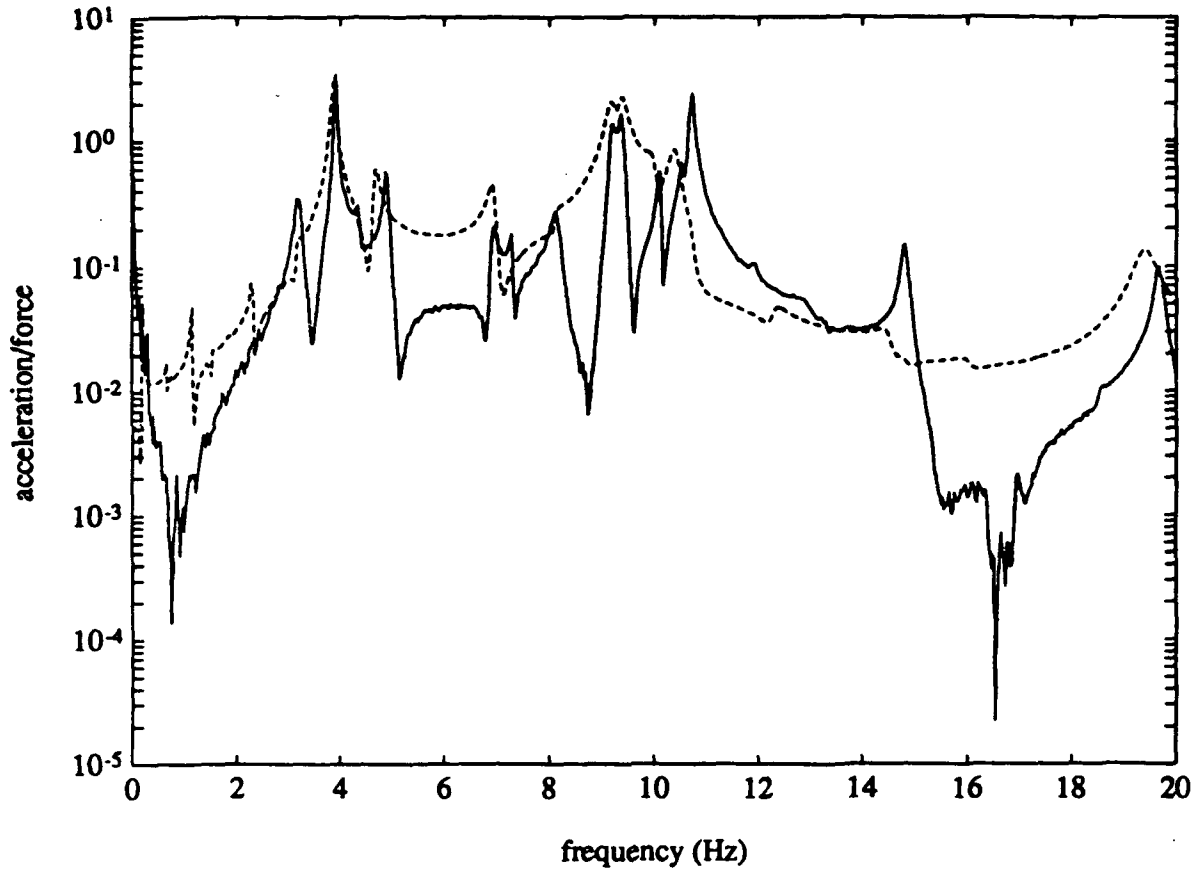
model DOF 19 / meas No. 172

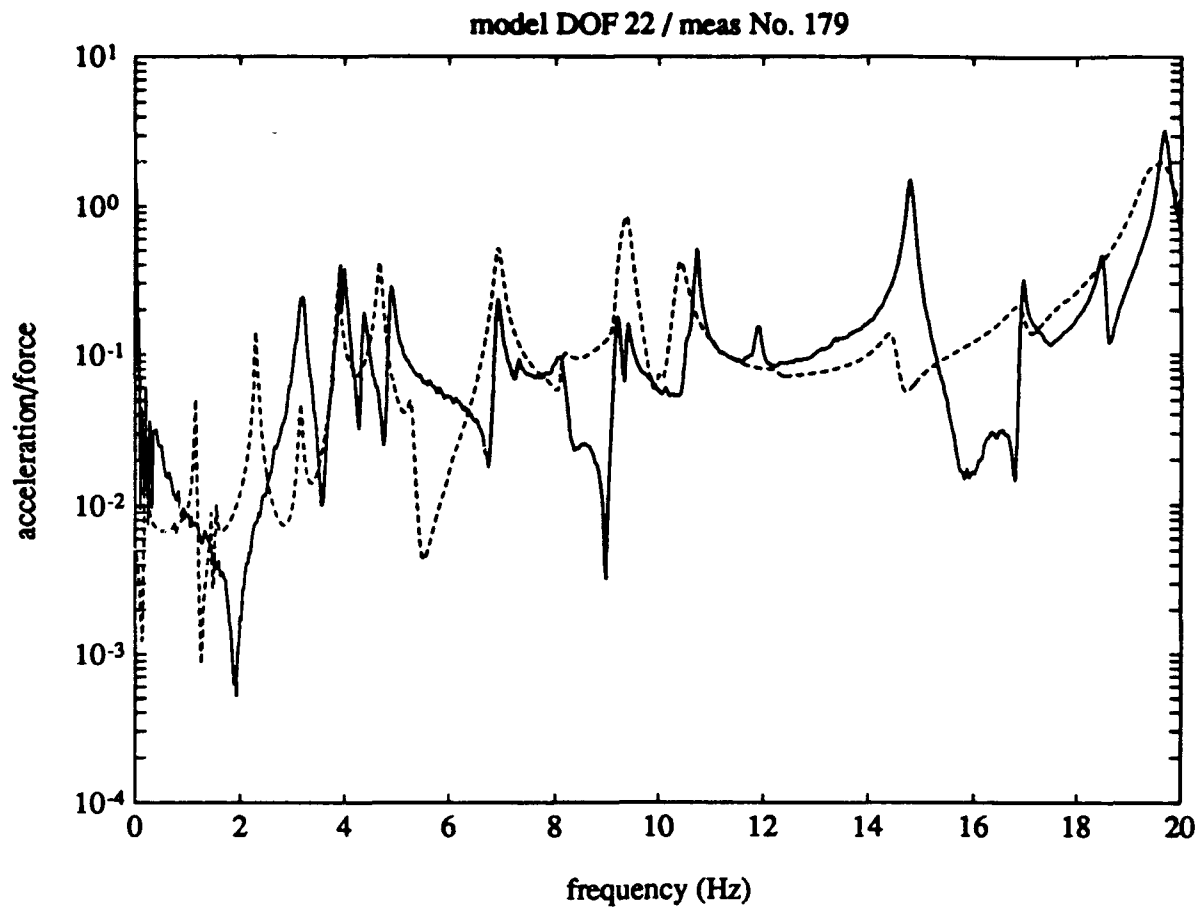


model DOF 20 / meas No. 171

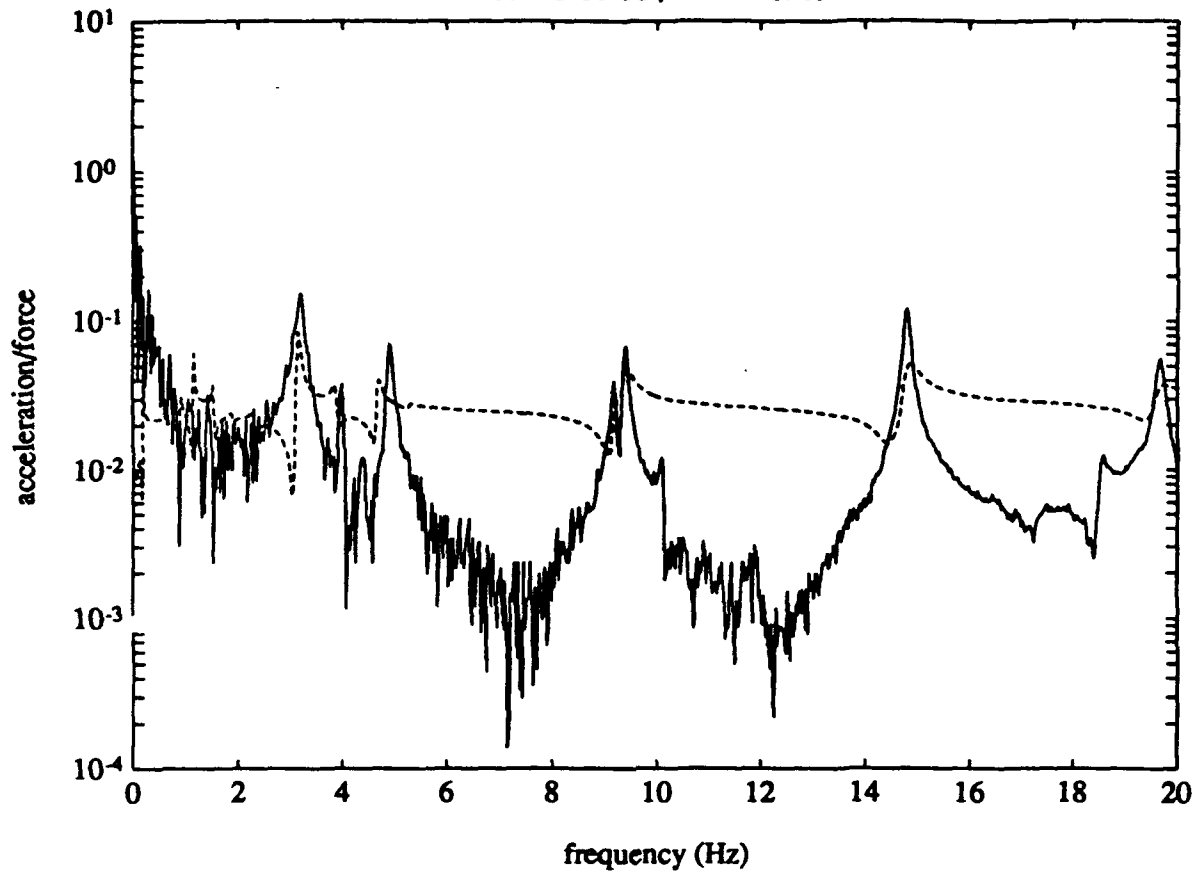


model DOF 21 / meas No. 180

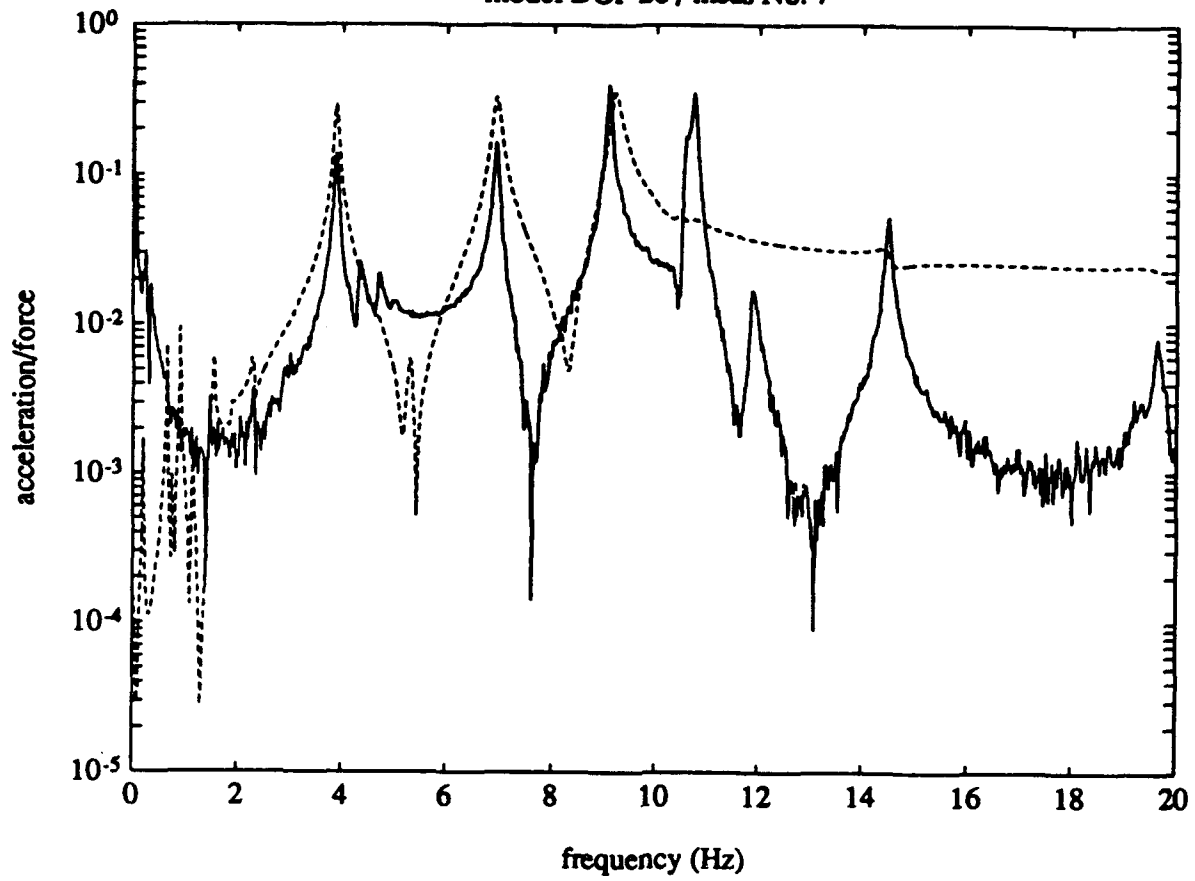




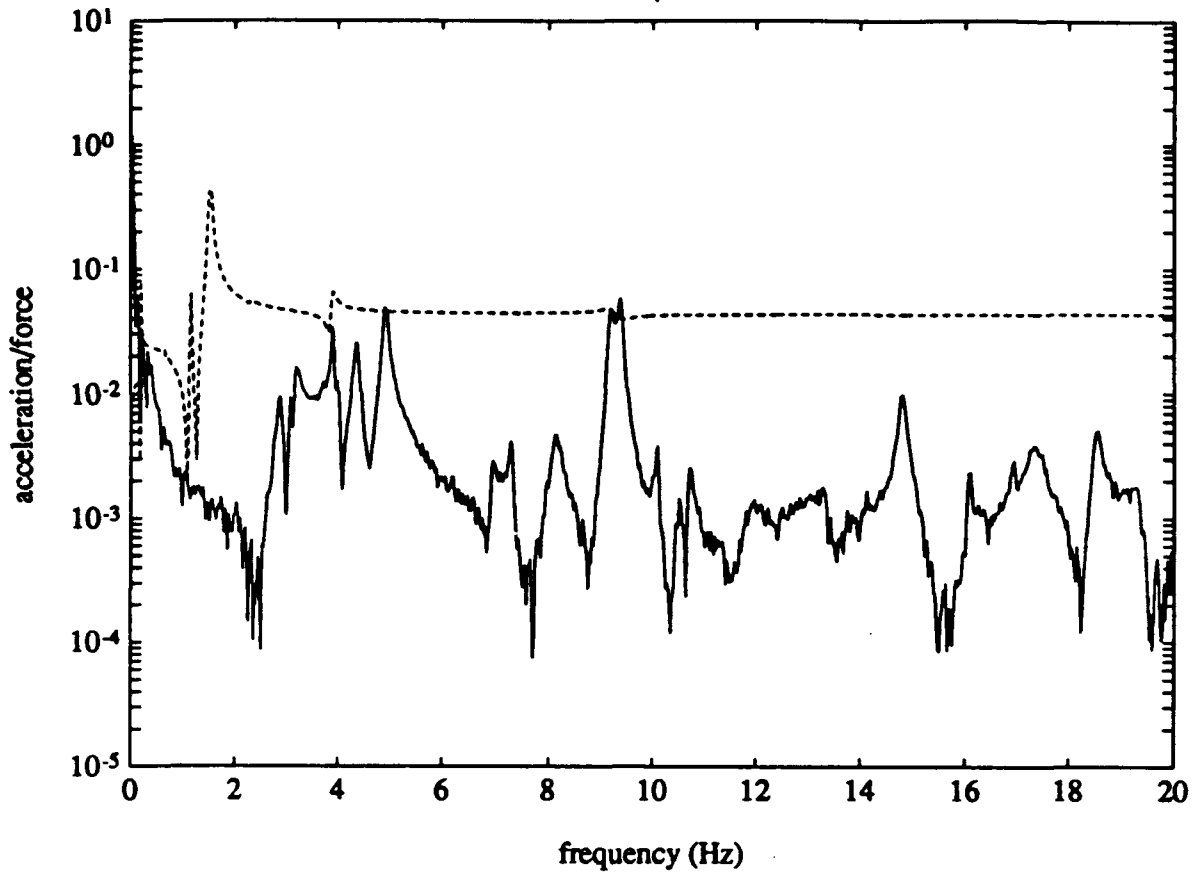
model DOP 25 / meas No. 152

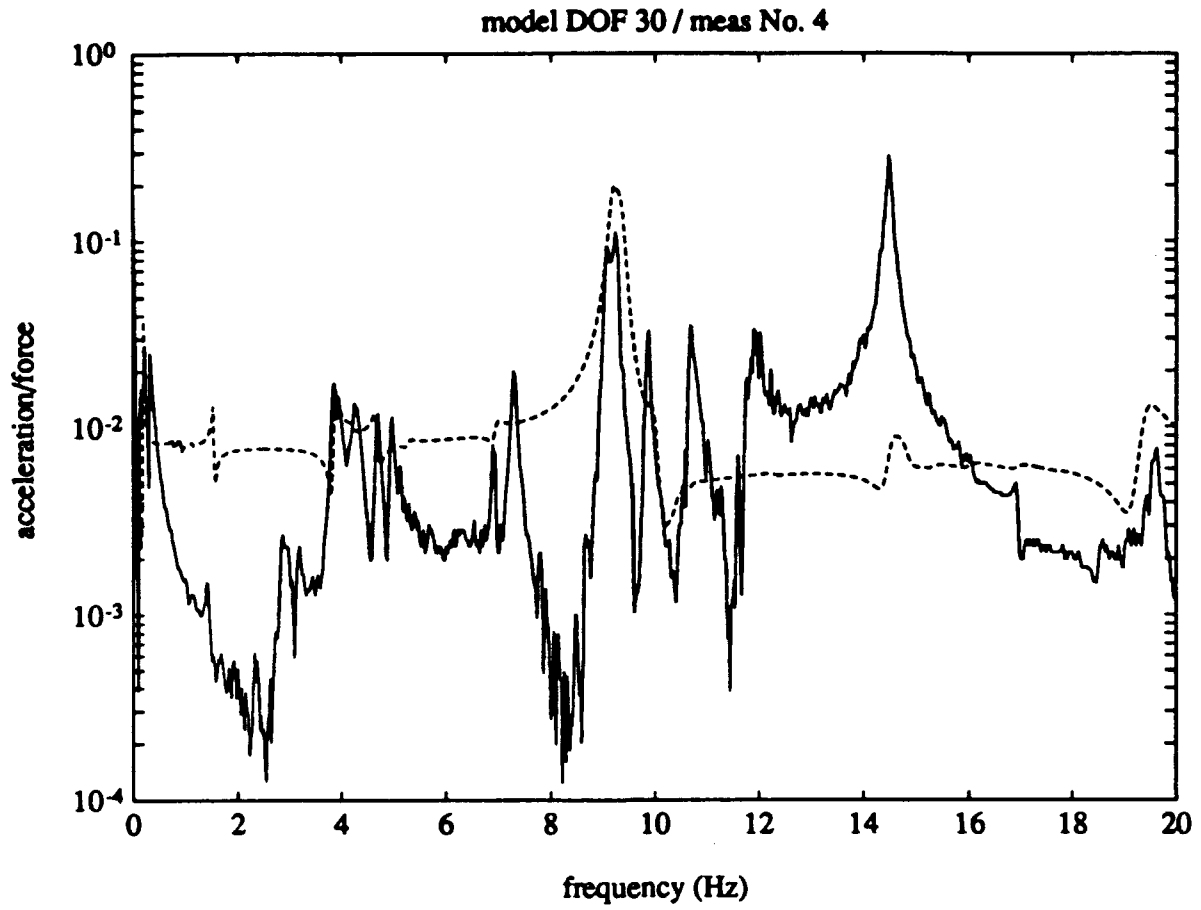


model DOF 26 / meas No. 7

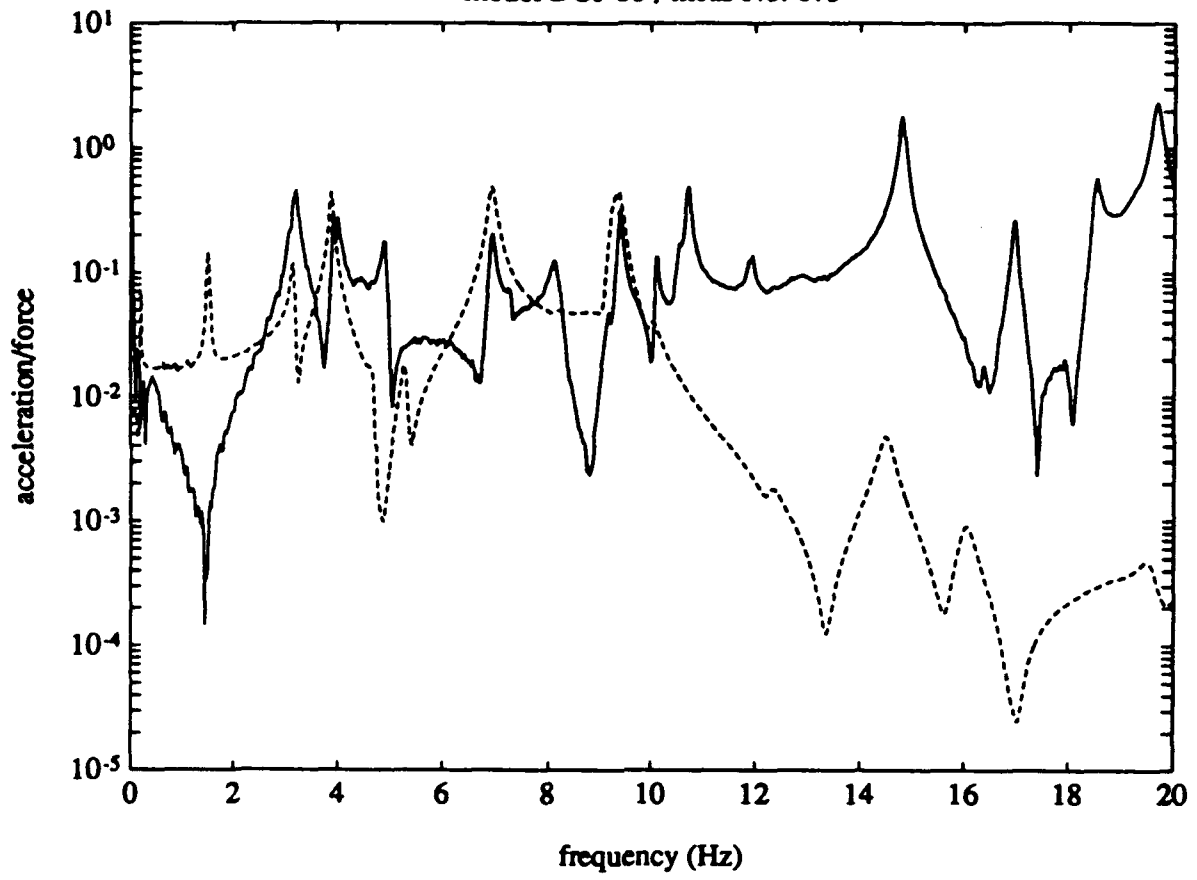


model DOF 29 / meas No. 151

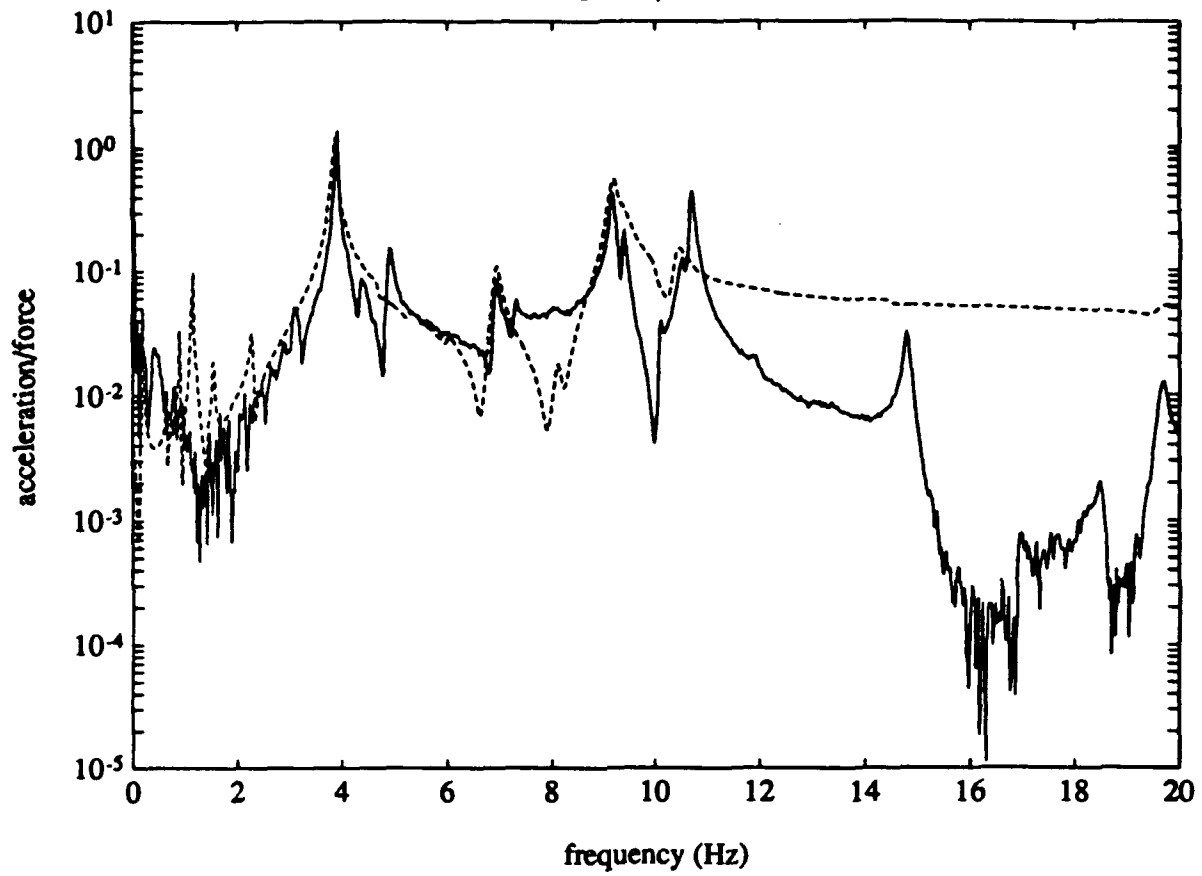




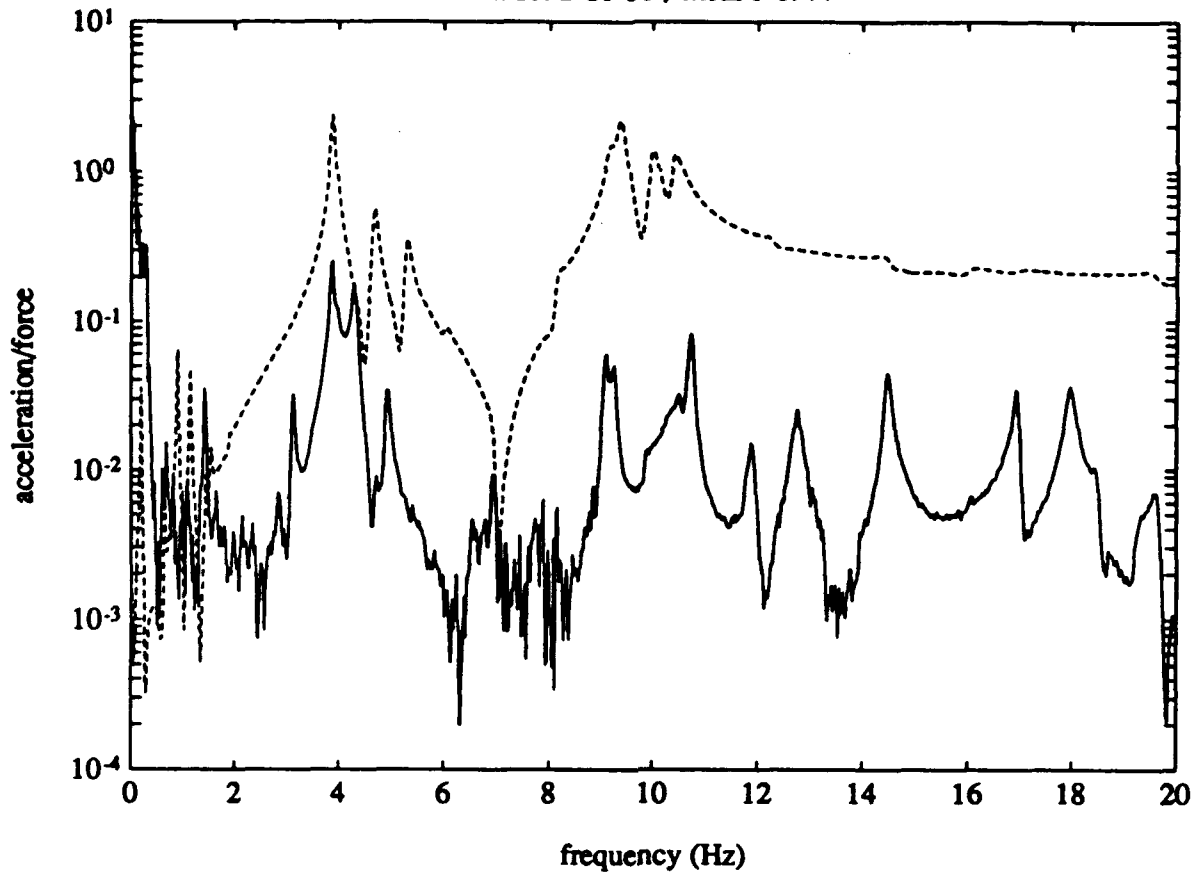
model DOF 33 / meas No. 175

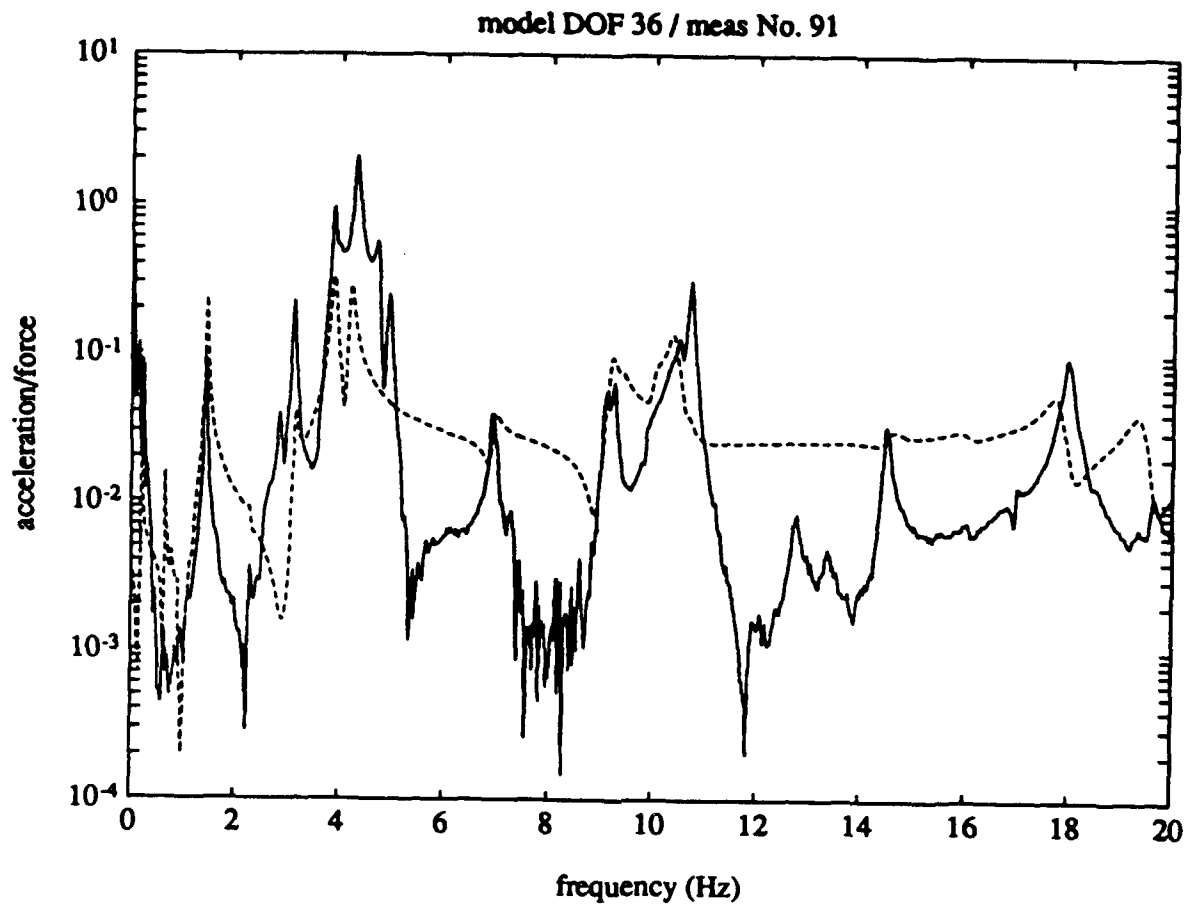


model DOF 34 / meas No. 176

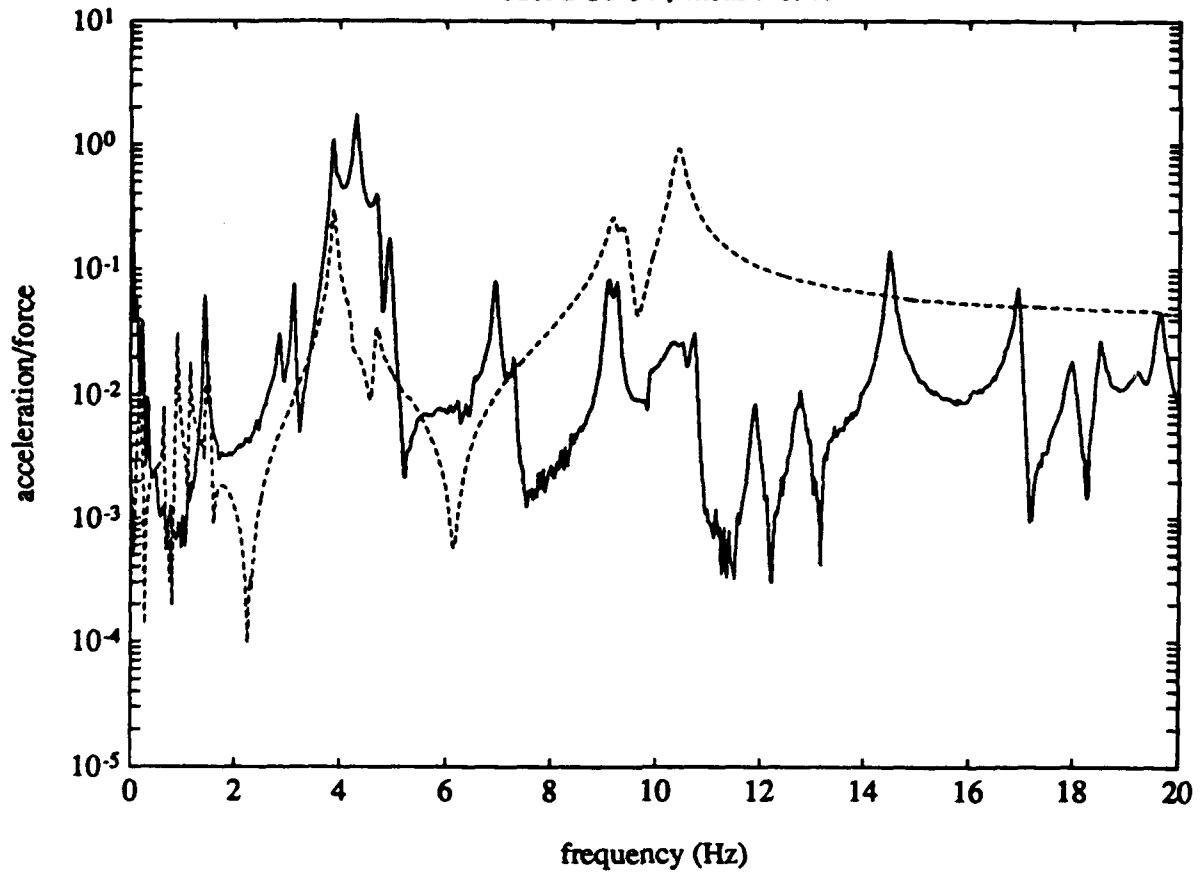


model DOF 35 / meas No. 77

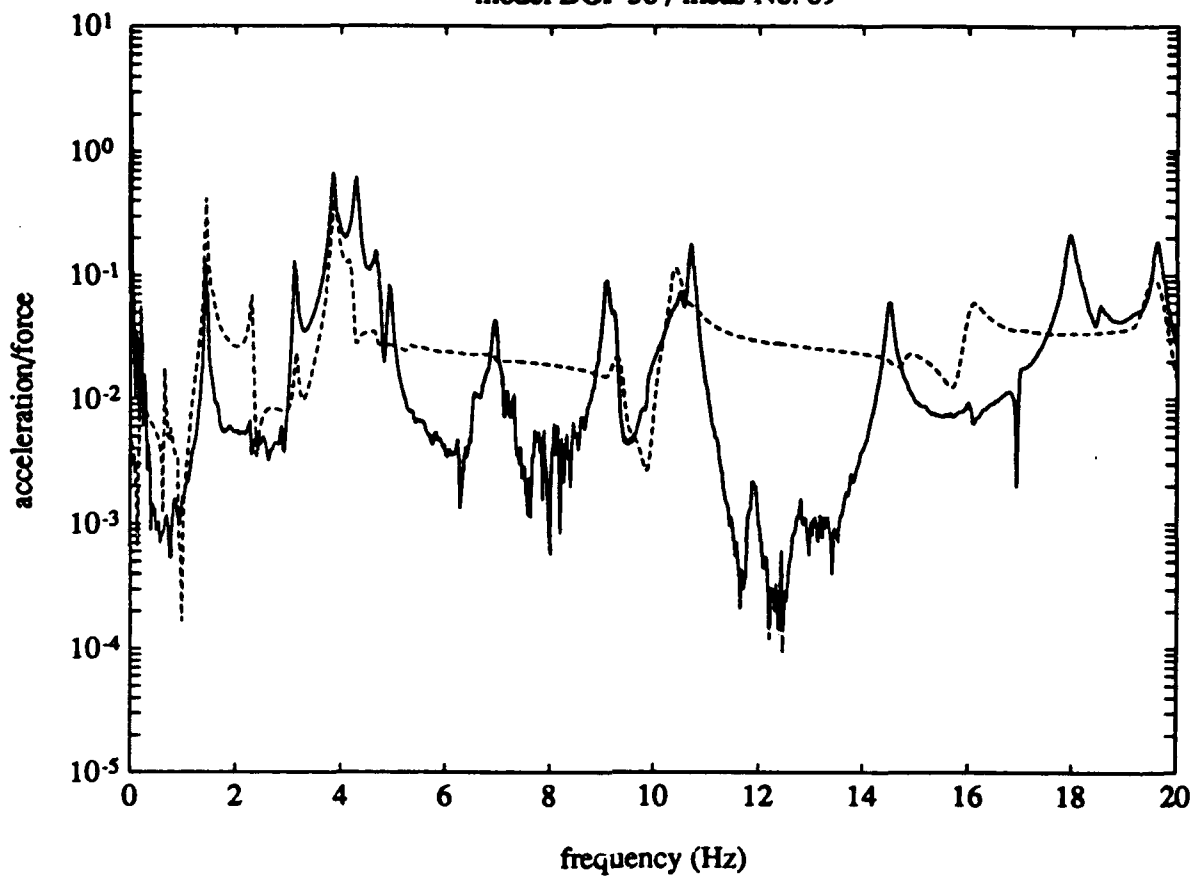




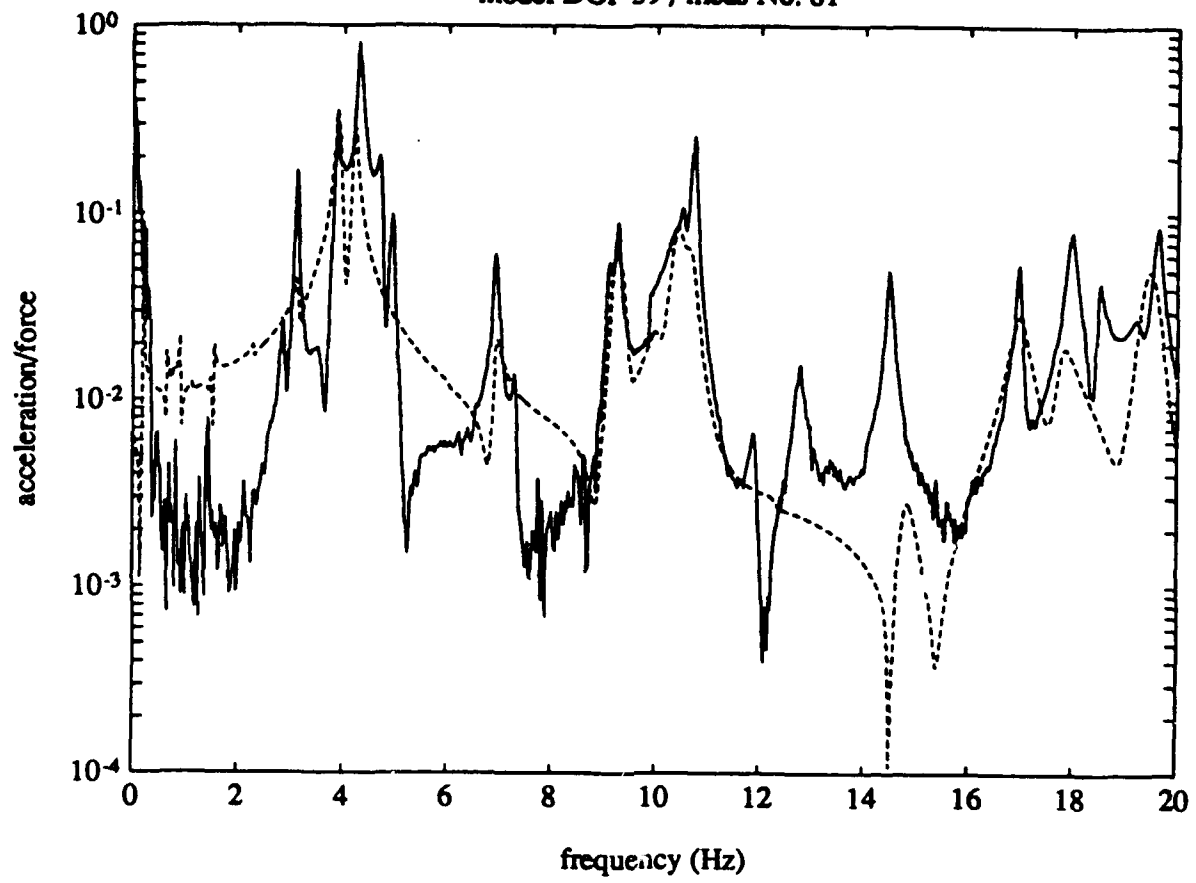
model DOF 37 / meas No. 79



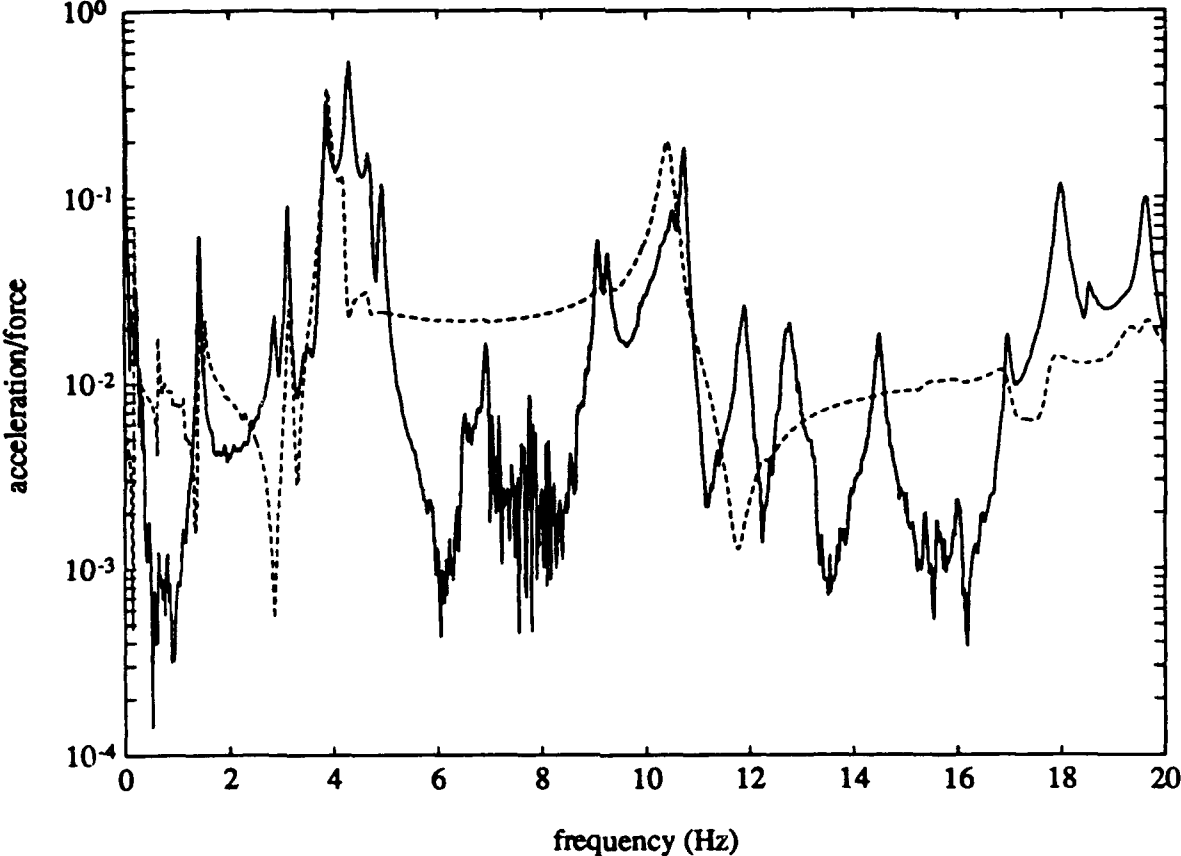
model DOF 38 / meas No. 89



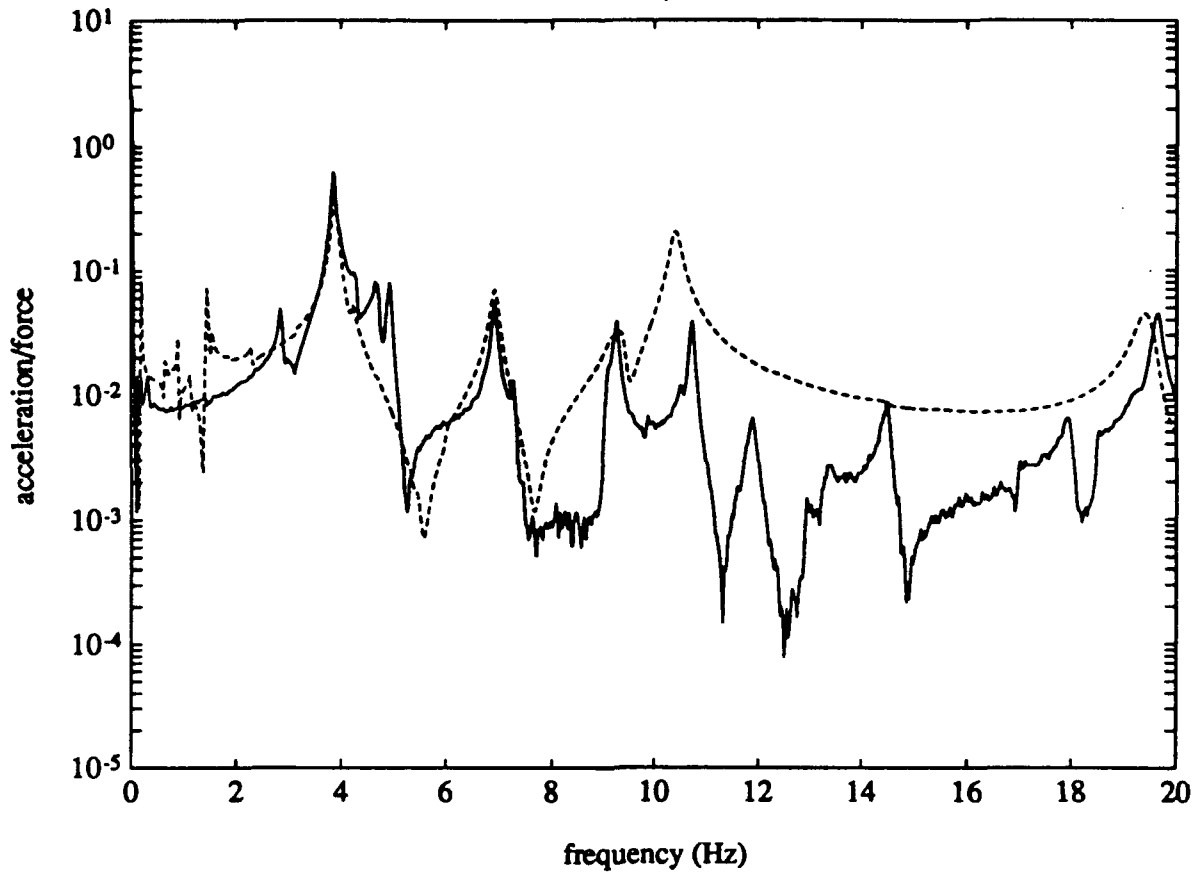
model DOF 39 / meas No. 81



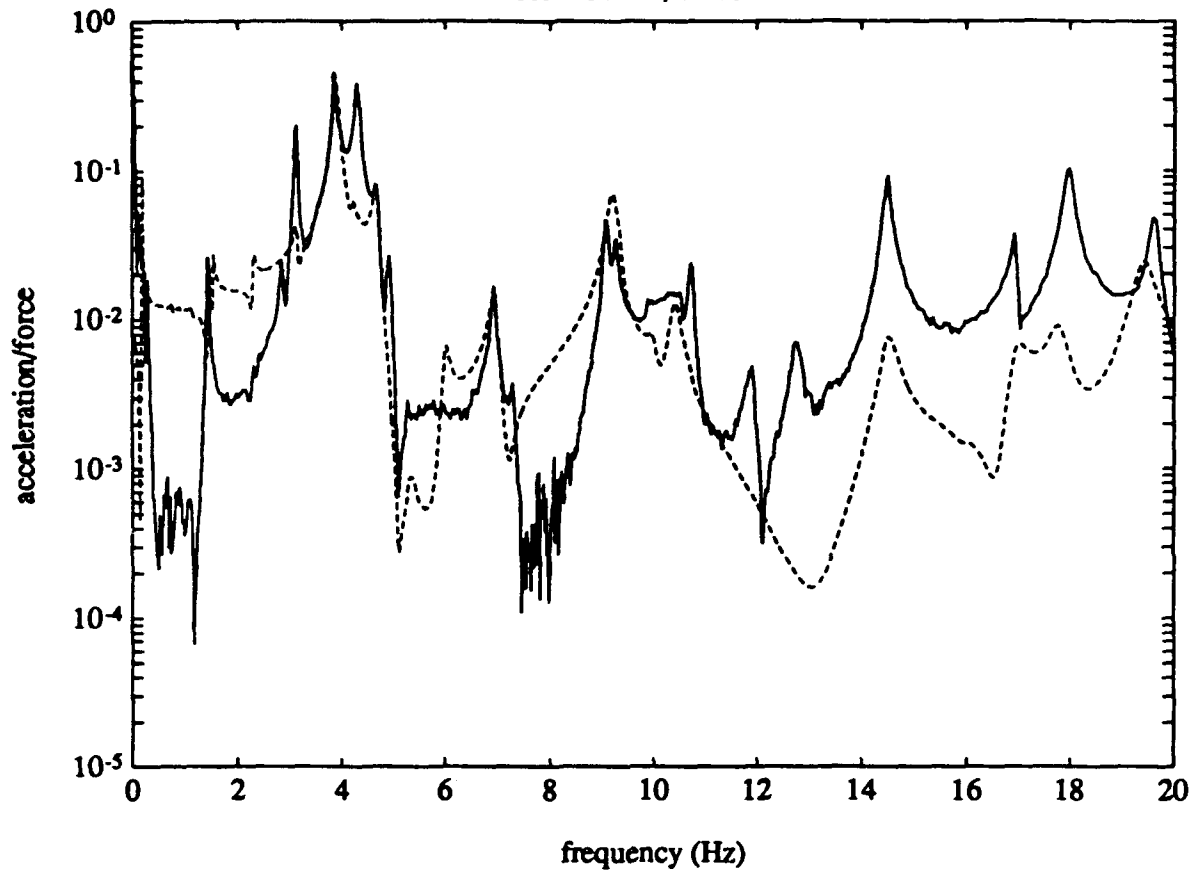
model DOF 40 / meas No. 87



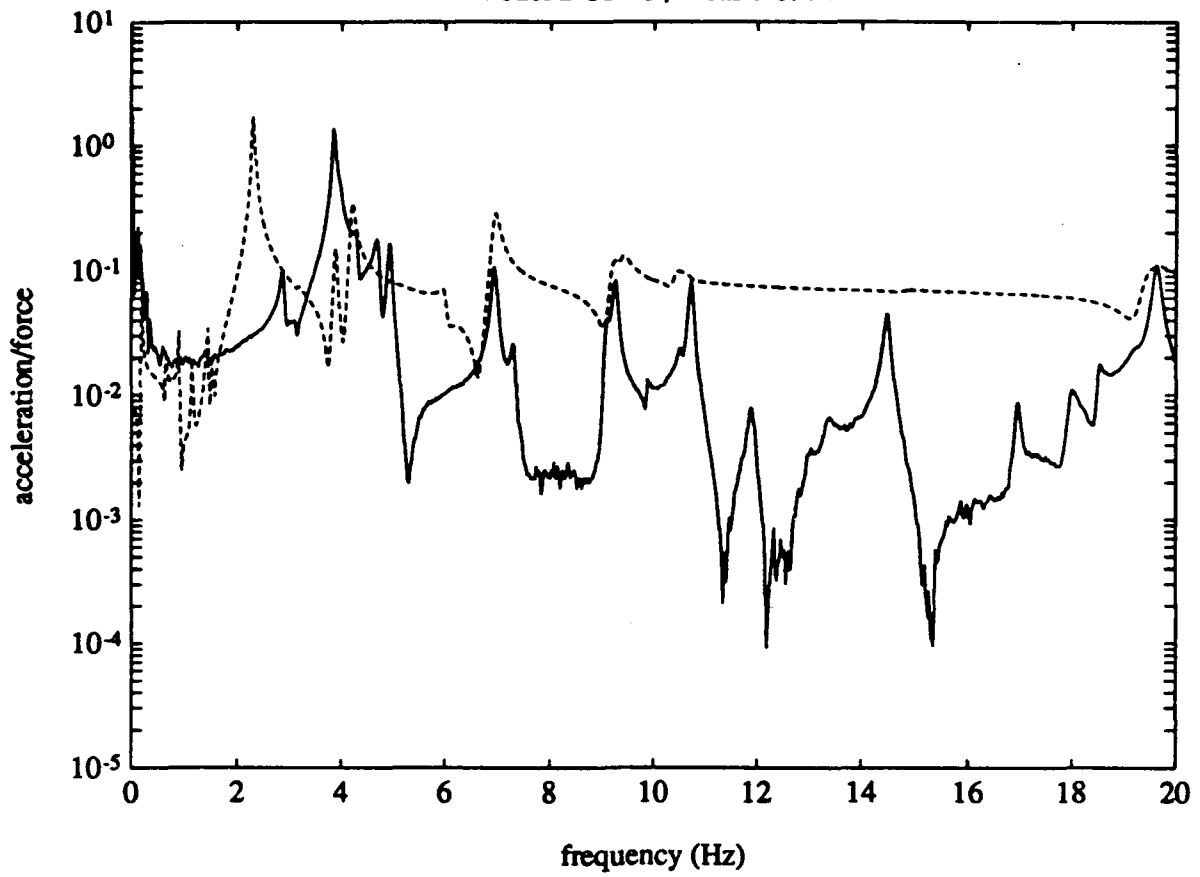
model DOF 41 / meas No. 86



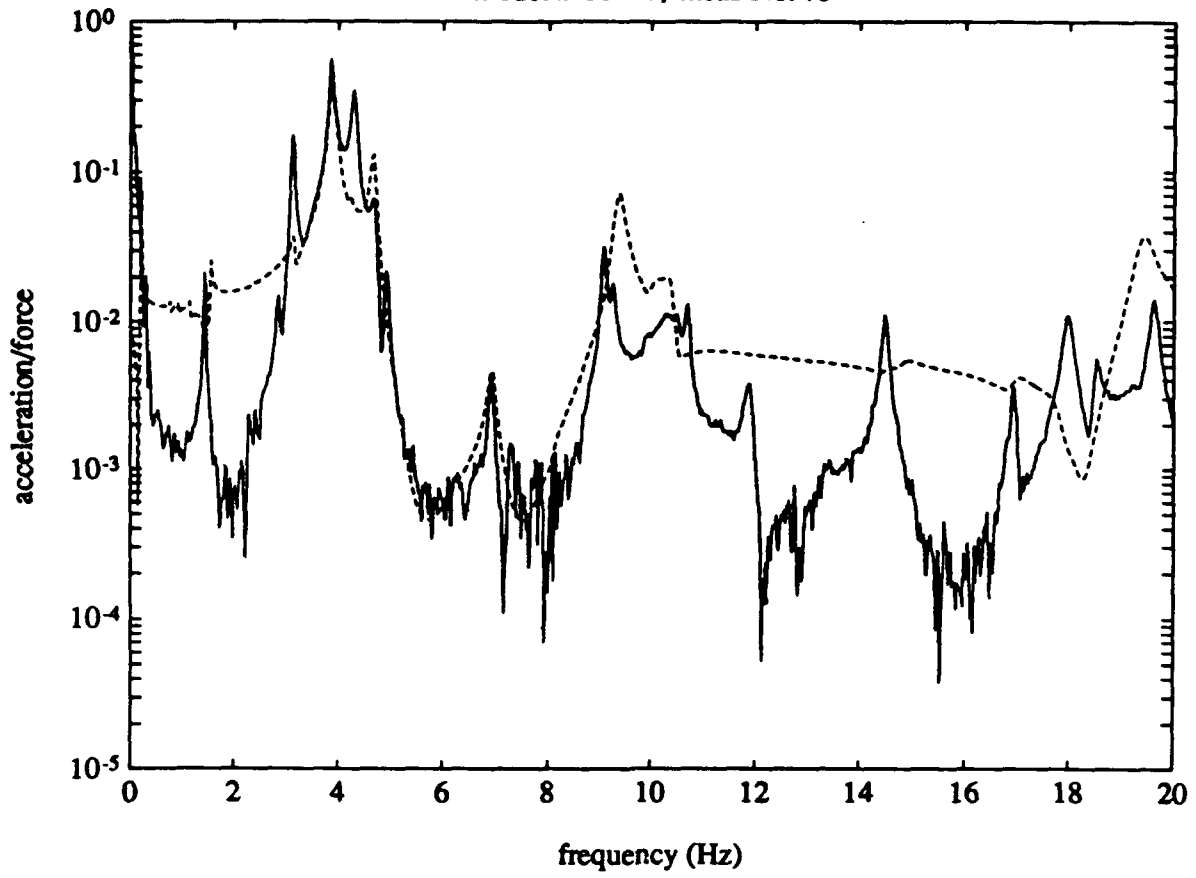
model DOF 42 / meas No. 85



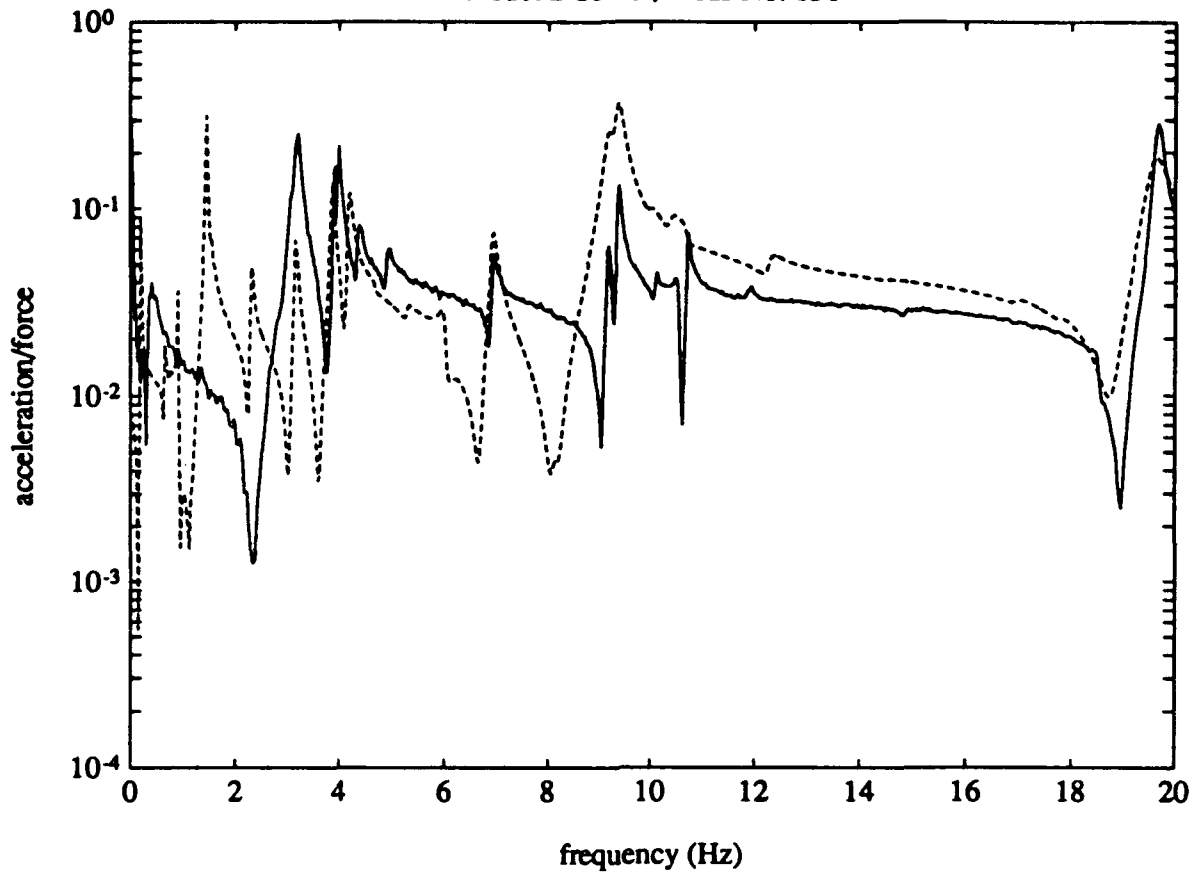
model DOF 43 / meas No. 74



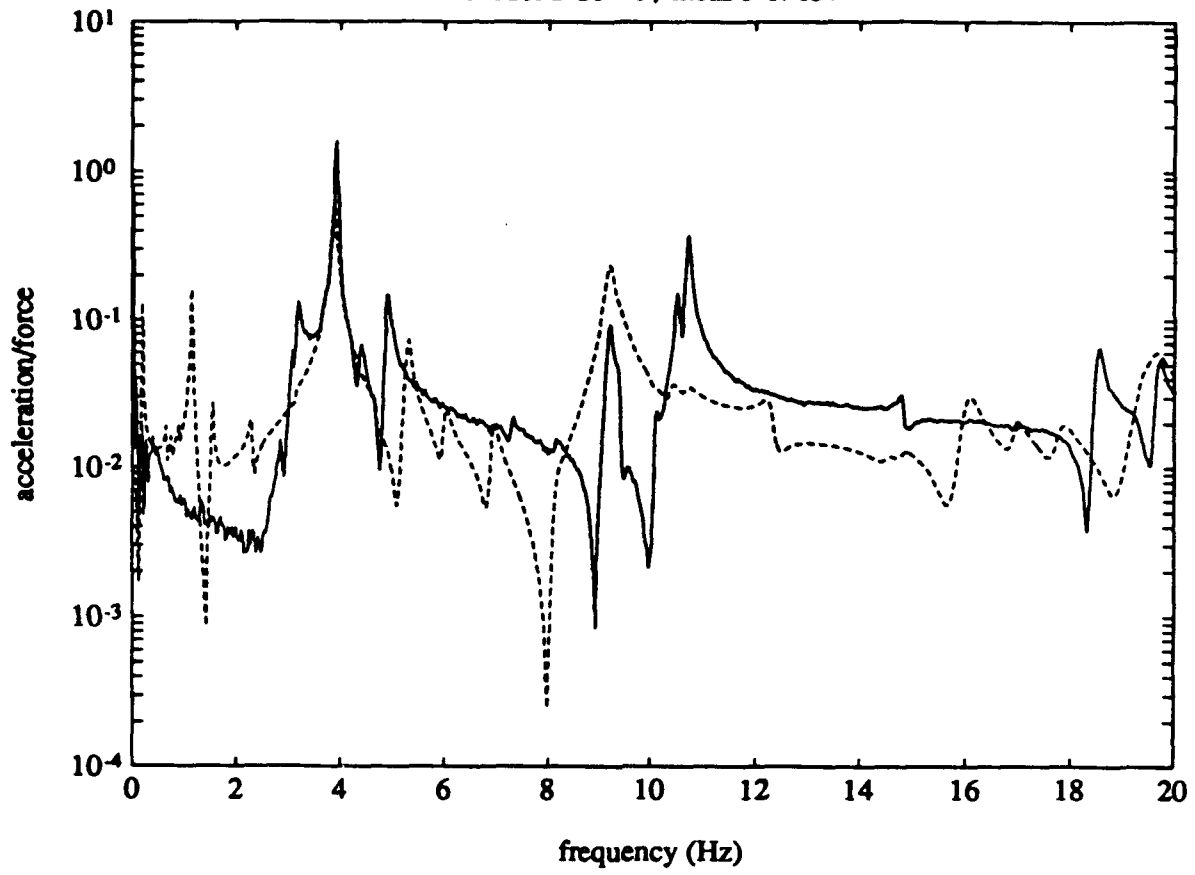
model DOF 44 / meas No. 73



model DOF 45 / meas No. 156



model DOF 46 / meas No. 157



Vita

Scott E. George was born on 15 July 1963 in Baltimore, MD. After graduating from Guilford High School in Rockford, Illinois in May 1981, he attended the University of Illinois at Urbana-Champaign on an Air Force ROTC scholarship. He graduated in May 1986 with a Bachelor of Science degree in Aeronautical and Astronautical Engineering. His first assignment was to the Ballistic Missile Office at Norton AFB, CA where he served as a Financial Manager, and then as Inertial Measurement Unit Lead Project Manager in the Peacekeeper ICBM System Program Office. In May 1990, he entered the School of Engineering, Air Force Institute of Technology, Wright-Patterson AFB, Ohio to pursue a Master of Science degree in Astronautical Engineering.

Permanent Address:

1416 Randall Dr.
Rockford, IL 61108